

Distribution Agreement

In presenting this thesis or dissertation as a partial fulfillment of the requirements for an advanced degree from Emory University, I hereby grant to Emory University and its agents the non-exclusive license to archive, make accessible, and display my thesis or dissertation in whole or in part in all forms of media, now or hereafter known, including display on the world wide web. I understand that I may select some access restrictions as part of the online submission of this thesis or dissertation. I retain all ownership rights to the copyright of the thesis or dissertation. I also retain the right to use in future works (such as articles or books) all or part of this thesis or dissertation.

Signature:

Sarah K. Suci

Date

The Ciliary Protein Arl13b Regulates Axon Guidance in the Developing Mouse Hindbrain

By

Sarah K. Suci

Doctor of Philosophy

Graduate Division of Biological and Biomedical Sciences
Genetics and Molecular Biology

Tamara Caspary, Ph.D.
Advisor

Gary Bassell, Ph.D.
Committee Member

David Weinshenker, Ph.D.
Committee Member

Ken Moberg, Ph.D.
Committee Member

Andrew Escayg, Ph.D.
Committee Member

Accepted:

Lisa A. Tedesco, Ph.D.
Dean of the James T. Laney School of Graduate Studies

Date

The Ciliary Protein Arl13b Regulates Axon Guidance in the Developing Mouse Hindbrain

By

Sarah K. Suci

B.S., Auburn University, 2014

Advisor: Tamara Caspary, Ph.D.

An abstract of

a dissertation submitted to the Faculty of the

James T. Laney School of Graduate Studies of Emory University

in partial fulfillment of the requirements for the degree of

Doctor of Philosophy

in the Graduate Division of Biological and Biomedical Sciences

Genetics and Molecular Biology

2020

Abstract

The Ciliary Protein Arl13b Regulates Axon Guidance in the Developing Mouse Hindbrain

By Sarah K. Suci

This dissertation covers questions of how localization of a protein known to be associated within the privileged environment of the primary cilium affects signaling and signal transduction. The focus of my work is a regulatory GTPase called ARL13B, a protein that is well known to enrich within the primary cilium. ARL13B has well-established roles in Sonic Hedgehog (Shh) signaling, a pathway that is critical for development which requires the primary cilium to regulate cell fate and proliferation. In mouse, *Arl13b*-deletion results in Shh-dependent defects in cell fate and proliferation. Recessive point mutations in *ARL13B* result in the ciliopathy Joubert Syndrome (JS), which presents with developmental delays, intellectual disability, and hypotonia and is diagnosed by the hindbrain malformation the molar tooth sign. This hindbrain defect is caused by a small, underdeveloped cerebellum and midline crossing failure of the superior cerebellar peduncles (SCPs), a projection neuron-based white matter tract that projects from the cerebellum across the midline of the brain into the opposite hemisphere thalamus. Transcription-dependent Shh signaling regulates cerebellar proliferation, so the small cerebellum is explainable by *ARL13B* mutations resulting in reduced Shh signaling. However, the mechanism by which cilia-associated proteins such as ARL13B impact the regulation of axon guidance remains unclear.

A potential mechanism resides in the additional, distinct role of Shh signaling that still requires the obligate transducer SMO, however, is transcription-independent. Transcription-independent Shh signaling regulates both commissural axon guidance in the neural tube and fibroblast migration towards Shh. Since *ARL13B* mutations result in axon guidance defects in JS, I investigated whether dysregulated Shh signaling is linked to the failure of SCPs to cross the midline of the brain. Consistent with this, my data shows SCPs lacking SMO or ARL13B display axon guidance defects in the mouse brain. I examined SCP projections in two additional *Arl13b* alleles: a cilia-excluded variant, *Arl13b*^{V358A} and a JS-causing mutation, *Arl13b*^{R79Q}. Both ARL13B variants were sufficient for SCP guidance, indicating that ARL13B functions outside the cilium to regulate projection neuron guidance. To better understand the relationship of *Arl13b* and transcription-independent Shh signaling I examined fibroblasts. Fibroblasts lacking SMO or ARL13B display decreased migration toward Shh. Interestingly, fibroblasts lacking cilia, or expressing a non-ciliary SMO mutant, show increased migration toward Shh. These results suggest that there may be a previously unknown, non-ciliary role for these cilia-associated proteins in the regulation of transcription-independent Shh signaling. Taken together, my data indicate that the mechanism of ARL13B action differs depending on whether signaling takes place within or outside of the primary cilium.

The Ciliary Protein Arl13b Regulates Axon Guidance in the Developing Mouse Hindbrain

By

Sarah K. Suci

B.S., Auburn University, 2014

Advisor: Tamara Caspary, Ph.D.

A dissertation submitted to the Faculty of the
James T. Laney School of Graduate Studies of Emory University
in partial fulfillment of the requirements for the degree of
Doctor of Philosophy
in the Graduate Division of Biological and Biomedical Sciences
Genetics and Molecular Biology

2020

Acknowledgements

I dedicate this dissertation to the people in my life who always believed this would happen, no matter how much I insisted I didn't know if I could do it. To my daddo who was always there to give me a pep talk or be my warden when I needed it. To my momma who always listens and knows when I need a pink drink. To my brother Dan for his humor and for being an example of success. To the Suciu/ Killen family, thank you for always supporting me and distracting me with happiness up in Glen Arbor. I love our family, and our funny little cousin gang. Special shoutout to my inspiration, Dr. Dan Suciu, for being an amazing grandpa as well as the first Suciu PhD. To my grammy Abele, thank you for all our German Christmases and for your love. To my Jackadore, I will always love you and think of you. Mona-Lisa, you're a distracting monster and I love you too.

To my beloved Auburn Mellons, ya'll are wild. I never would have survived college without you guys. Thanks for all the games, the New Year's celebrations, and the Lord of the Rings marathons. To Jemal, you are my oldest friend and I would not be the person I am if you had never thrown that ball of mud at me. Thanks for always coming back into my life. To Wendy, you are the sister I needed during so many hard moments along my journey. Thank you for always believing I could make it (with some help). Also, for teaching me how to be an adult human (in progress).

To my GMBeers, there are no words. You guys have been my light during all the dark times. I cannot imagine starting grad school with any other cohort than mine. Crystal, Chris, Bobbert, George, Binta, Anna, and Alyse: thanks for all the laughs, for watching me give bad presentations, and for all our cute cohort pictures. Alyssa, Doug, Bri, Tay, Jesse, and Sam: thanks for joining the program and for being a part of our group for silliness and day drinking. To Crystal, you are my day one (even though I don't super remember it) and you are my best friend and you inspire me. I can't wait to watch you run the world. To our travels, for with you guys I have seen the world and known what it is to truly have an adventure.

To my lab, past and present members. Alyssa thank you for always expecting the best from me. Tim, Ed, and Robby, you guys are the older brothers I never asked for. Thanks for keeping me humble for and taking jokes as hilariously as you give them. To Sarah and Laura, you are such an inspiration to me. Thank you for never giving up and for all your successes. I hope to be like you someday. To Cubes and Ollie, go get 'em kids. I'd also like to thank Pokemon Go for its powers of distraction and the many coffee runs it provided.

To the PIs that did not have to help me but chose to anyway, thank you to Rick Kahn and Michael Gambello. Our joint lab meetings provided so much help to my project over the years. To the PIs I chose to help me, my wonderful committee members David, Ken, Gary, and Andrew, thank you for your support, and for your belief that I could accomplish this. David, special thanks to your lab and Kirsten for guiding me through stereotaxic surgeries so that I could research my interests and so my dad could tell his friends that I am a brain surgeon.

To my mentor Tamara, I want to truly thank you. Without your coaching I would have never pushed myself as I have. Your mentorship gave rise to a body of work in which for the first time in my life I believed I could rise above acceptable to touch excellence. I appreciate and will always carry all that you've taught me over the years. After this experience, I believe in myself. Thank you for our time together.

Abbreviations

- AP – anterior-posterior
- BBS – Bardet-Biedl syndrome
- CGNP – cerebellar granule neuron precursor
- DV – dorsal-ventral
- E – embryonic day
- EGL – external germinal layer
- EtOH – ethanol
- FBS – fetal bovine serum
- IF - immunofluorescence
- IFT – intraflagellar transport
- IGL – internal granular layer
- GAP – GTPase activating protein
- GEF – guanine nucleotide exchange factor
- GliA – Gli activator
- GliR – Gli repressor
- GPCR – G-protein coupled receptor
- GTP – guanosine nucleotide triphosphate
- JS(RD) – Joubert Syndrome (and Related Disorders)
- MEF – mouse embryonic fibroblast
- MKS – Meckel-Gruber syndrome
- ML – medial-lateral
- O/N – overnight
- P – postnatal day
- PBS – phosphate buffered saline
- PCL – Purkinje cell layer
- PCP – Purkinje cell precursor
- PKD – polycystic kidney disease
- PDE – phosphodiesterase
- PFA – paraformaldehyde
- Ptch1 – Patched
- Shh – Sonic hedgehog
- Smo – Smoothed
- SuFu – Suppressor of Fused

Table of Contents

Chapter 1 Arl13b, Cilia, and Shh Signaling	1
1.1 Introduction	2
1.2 Overview of cilia	5
1.2.1 Cilia structure and trafficking	5
1.2.2 Cilia are required for neurodevelopment	10
1.2.3 Ciliary signaling takes place within the privileged environment of the primary cilium	11
1.3 Overview of Shh	12
1.3.1 The critical developmental pathway Shh signaling functions within as well as outside the cilium	12
1.3.2 The cilia-associated GTPase Arl13b regulates transcription-dependent and -independent Shh signaling	19
1.4 Roles of cilia, Shh signaling, and Arl13b during development	22
1.4.1 Neural cell fate specification requires signal transduction via the primary cilium	22
1.4.2 Neural cell proliferation requires Shh signal transduction via the primary cilium	26
1.4.3 Interneuron and neuron migration require the primary cilium	29
1.4.4 Neuronal axon guidance requires cilia-associated proteins and signaling pathways	31
1.5 Joubert Syndrome overview	36
1.5.1 Joubert Syndrome characteristics and diagnosis	36
1.5.2 Genetic complexity of Joubert Syndrome	38
1.6 The evolving connection of cilia to neuronal mechanisms of human disease	39
1.7 Dissertation roadmap	41
Chapter 2 Materials & Methods	43
2.1 Mice	44
2.2 Western blots	45
2.3 Fibroblast migration assays	46
2.4 Dissection and culture of embryonic spinal cord	47
2.5 Diffusion tensor imaging (DTI)	49
2.6 Tract tracing injections and analysis	53
2.7 CLARITY and tissue clearing	56
2.8 Analysis of cerebellar hemisphere and vermis size	57
Chapter 3 Measuring cell response to Shh as an attractive cue	59
3.1 Abstract	60
3.2 Introduction	60
3.3 Results	65
3.3.1 Lentiviral infection in MEFs drives expression of Arl13b constructs	65
3.3.2 Fibroblast migration assays are inconsistent	68
3.3.3 Commissural axon dissection and culture	73
3.4 Discussion	74
Chapter 4 Visualizations of SCP guidance	76
4.1 Abstract	77

4.2 Introduction	77
4.3 Results	83
4.3.1 Deletion of Smo results in a larger Corpus callosum tract	83
4.3.2 Deletion of Arl13b or Smo results in lessened SCP FA at decussation	85
4.3.3 Deletion of Smo results in a larger SCP tract	89
4.3.4 Anterograde injections indicate SCPs lacking Smo or Arl13b failed to project dorsally	91
4.3.5 Decussation in SCPs lacking Smo or Arl13b is disorganized	92
4.3.6 Clarity imaging is a promising method to image SCPs in whole brain with appropriate injected tracer	95
4.3.7 SCP retrograde decussation characterization	96
4.3.8 SMO is required for normal SCP projection to the dorsal thalamus	101
4.3.9 ARL13B is required for normal SCP projection to the dorsal thalamus	106
4.3.10 ARL13B does not function from within cilia to mediate SCP guidance	106
4.3.11 SCP projection in mice expressing a Joubert-causing allele, Arl13bR79Q	110
4.4 Discussion	112
Chapter 5 Perspective	117
5.1 Introduction	118
5.2 Preliminary results indicate Arl13b plays a critical role in cerebellar development	119
5.2.1 Arl13b may function as a GTPase to regulate cerebellar vermis size	119
5.2.2 Global cerebellar hypoplasia in mice lacking Ar13b in all neurons	122
5.2.3 Arl13b functions from within cilia to regulate cerebellar vermis size	124
5.2.4 Cilia are required to regulate cerebellar development	126
5.2.5 Summary	126
5.3 Perspective	127
5.4 Connecting cilia to axons via shared microtubule-based structures and modifications	130
5.5 Future Directions	135
References	137

List of Figures and Tables

Figure 1.1 The primary cilium is a signaling appendage of the cell involved in several developmental processes	4
Figure 1.2 The structure, composition, and trafficking of the primary cilium	7
Figure 1.3 The developmental signaling pathway Shh has two mechanistic arms	13
Figure 1.4 Transcription-dependent Shh signaling is interpreted by the cilium	14
Figure 1.5 Transcription-independent Shh signaling regulates fibroblast migration via cytoskeletal rearrangements at the leading edge	17
Figure 1.6 Transcription-independent Shh signaling regulates axon guidance via cytoskeletal rearrangements at the growth cone	18
Figure 1.7 Arl13b is a cilia-associated GTPase that includes a Arf-like GTPase domain, as well as a novel C-terminus	21
Figure 1.8 The cilium is required to transduce Shh signal and specify ventral neural tube cell fates	24
Figure 1.9 Shh is required for proliferation of granule neuron precursors in the cerebellum	28
Figure 1.10 Distinct cilia-dependent transcription response to Shh distinguishes axon pathfinding	35
Figure 1.11 The Joubert Syndrome diagnostic criteria, the molar tooth sign, is made up of cerebellar hypoplasia of the vermis and a guidance defect in the superior cerebellar peduncles	37
Figure 2.1 Spinal cord dissection steps	48
Figure 2.2 TDE clearing	57
Table 3.1 Summary of Mariani results from Arl13bhnn MEFs	63
Figure 3.1 Illustration of fibroblast migration assay	65
Figure 3.2 Description of integrated density-based normalization factors for total protein amount in western blots	67
Figure 3.3 Quantification of Arl13b constructs in transfection Arl13bhnn MEFs	67
Figure 3.4 Arl13bhnn Migration to 1% FCS (performed in Amsterdam)	69
Figure 3.5 Arl13bhnn Migration to 1:2000 Purmorphomine (performed in Amsterdam)	70
Figure 3.6 Arl13bhnn+GFP Only Individual Runs (performed at Emory)	71
Figure 3.7 Arl13bhnn+WTArl13b-GFP Individual Runs (performed at Emory)	72
Figure 3.8 Migration averages of Arl13bhnn+GFP Only versus Arl13bhnn+WTArl13b-GFP	73
Figure 4.1 Visual description of fractional anisotropy reported in DTI	83
Figure 4.2 Voxel size of Corpus Callosum (CC) masks via DTI	85
Figure 4.3 Initial results of fractional anisotropy (FA) of SCPs at the midline via DTI	87
Figure 4.4 Bins of fractional anisotropy of SCPs at the midline via DTI	87
Figure 4.5 Fractional anisotropy of control SCPs at the midline changed when DTI re-analyzed	89
Figure 4.6 SCPs lacking Smo are larger and more diffuse via voxel size in DTI	91
Figure 4.7 Anterograde SCP trace analysis of sections containing decussating SCPs	94
Figure 4.8 Anterograde SCP trace analysis of total axon length	95
Figure 4.9 Following SCPs in the horizontal plane via CLARITY imaging	96
Figure 4.10 SCP decussation characteristics	97
Figure 4.11 SCP decussation characterization of Arl13b or Smo conditional deletion	98
Figure 4.12 SCP decussation characterization of Arl13bR79Q GTPase and JS mutant	99

Figure 4.13 SCP decussation characterization of Arl13bV358A cilia-excluded mutant	100
Figure 4.14 Height of SCP decussation fibers crossing the midline	101
Figure 4.15 SCPs lacking Arl13b or Smo fail to project to the dorsal thalamus	103
Figure 4.16 Total injection results of Arl13bfl/+; Smofl/+ heterozygous controls	104
Figure 4.17 Total injection results of Arl13bNex-Cre and SmoNex-Cre mutants	105
Figure 4.18 SCPs expressing cilia-excluded ARL13BV358A project normally to both the dorsal and ventral thalamus	107
Figure 4.19 Total injection results of Arl13bV358A	108
Figure 4.20 SCPs expressing JS allele Arl13bR79Q project normally to both the dorsal and ventral thalamus	110
Figure 4.21 Total injection results of Arl13bR79Q	111
Figure 5.1 Expression of JSRD-causing allele Arl13bR79Q results in small cerebellar vermis	121
Figure 5.2 Pan-neuronal deletion of Arl13b result in small cerebellum	123
Figure 5.3 Expression of cilia-excluded Arl13bV358A results in small cerebellar vermis	125
Table 5.1 Summary of dissertation results	128
Figure 5.4 The mechanism of Arl13b regulation in development differs depending on both cilia localization and cellular context	129
Figure 5.5 The ciliary axoneme and the axon are microtubule projections that share regulation via post-translational modifications of tubulin	132

CHAPTER 1

ARL13B, CILIA, AND SHH SIGNALING

Parts of this chapter are published in:

Suciu, S.K., and Caspary, T. (2020) Cilia, neural development and disease. *Seminars in Cell & Developmental Biology*

1.1 Introduction

The primary cilium, a small microtubule-based signaling appendage of the cell once thought to be merely vestigial, has in the past few years been recognized as a critical center of developmental signaling (Ingham and McMahon 2001). Signaling effectors can meet and interact in the privileged environment of the cilium resulting in signal transduction. Cilia are present on nearly every vertebrate cell type (Wheatley, Wang, and Strugnell 1996). More and more developmental processes are being linked to the primary cilium or are linked to proteins that are themselves associated with the cilium (Bisgrove and Yost 2006). My dissertation will cover the basics of cilia biology and signaling, processes of development that are linked to the primary cilium, and how those processes can be impacted in human disease. In particular, ciliopathies, a subset of human disease caused by mutations in genes linked to cilia, will be explored as phenotypic outcomes can be indicative of processes that are misregulated in disease context. Ciliopathies often display neuropathy, but one disease in particular, the ciliopathy Joubert Syndrome, is unique as patients display clear defects in neuron targeting and guidance towards projection sites (Poretti et al. 2011b). The ultimate question I attempt to address in this dissertation revolves around whether the critical, cilia-associated signaling pathway, Sonic Hedgehog (Shh), links the multiple phenotypes in the ciliopathy Joubert Syndrome. While proteins associated with the primary cilium often function in cilia, there are instances of cilia-associated proteins functioning outside of or independently of the cilium (Petrulia et al. 2012; Casalou et al. 2014). Furthermore, Shh signaling itself has a cilia-independent mechanism and functions and thus, in this dissertation I will cover my work that explores the relationship between cilia-associated protein function and regulation in the context of cilia localization (Bijlsma et al. 2007; Charron et al. 2003; Yam et al. 2009).

The primary cilium is associated with the developmental processes of cell fate specification, cell proliferation, cell differentiation, cell migration, and is implicated in axon guidance of commissural neurons in the neural tube (**Figure 1.1**) (Chiang et al. 1996; Kenney and Rowitch 2000; Komada 2012; Bijlsma et al. 2007; Charron et al. 2003). Axon guidance is of particular interest; the axon is the microtubule-based projection off the neuron which is guided to synaptic targets via signaling at the growth cone, the tip of the axon located far from the soma. Because cilia-associated proteins are involved in regulation of axon guidance at the growth cone, the central question of my thesis asks how or if cilia are regulating this developmental process, or if regulation is done by cilia-associated proteins working outside of the cilium. This question can be emphasized via the ciliopathy Joubert Syndrome (JS). JS is caused by mutations in over 35 different cilia-associated genes, and yet all patients display axon guidance defects, a process that takes place at the distal growth cone (Parisi 2019; Poretti et al. 2011b). This implies a few potential scenarios; it may be that the cilium, the central localization of these proteins, is involved in the regulation of axon guidance. Alternatively, the cilia-associated factors could all regulate axon guidance outside the cilium at the growth cone. However, this could also imply that ciliary signaling is somehow permissive to axon guidance.

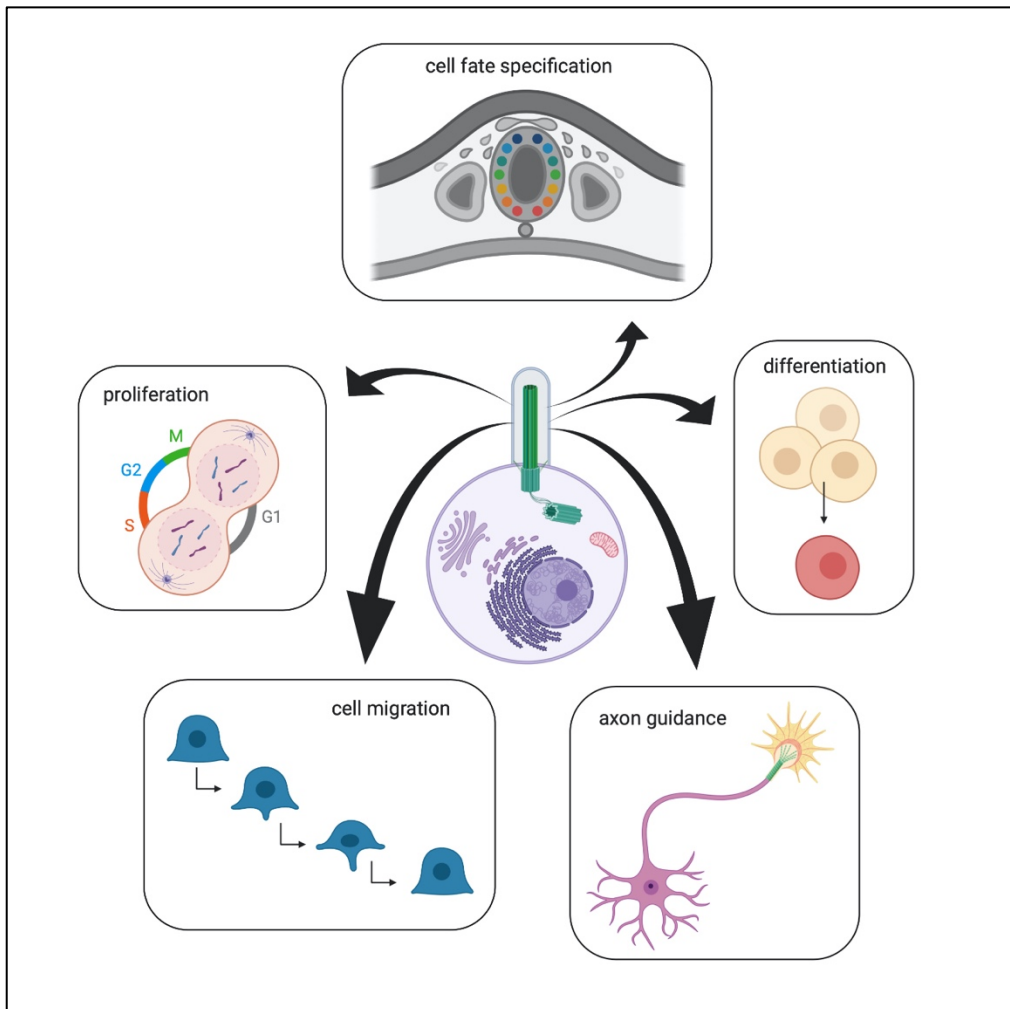


Figure 1.1 The primary cilium is a signaling appendage of the cell involved in several developmental processes. These processes include cell fate specification in the embryonic spinal cord (the neural tube), cell differentiation, neuron axon guidance, cell migration, and cell proliferation.

Shh signaling requires the primary cilium for transcriptional regulation and can also act in commissural axon guidance (Charron et al. 2003; Caspary, Larkins, and Anderson 2007). Shh signaling can either take place in the cilium to regulate target gene transcription, or outside the cilium in the growth cone to regulate axon guidance (Caspary, Larkins, and Anderson 2007; Yam et al. 2009). Small cilia-associate GTPase ARL13B is well-established to regulated transcription-dependent Shh signaling (Caspary, Larkins, and Anderson 2007). Furthermore,

ARL13B is one of the 35 cilia-associated genes that when mutated causes JS (Cantagrel, Silhavy, Bielas, Swistun, Marsh, Bertrand, Audollent, Attie-Bitach, Holden, Dobyns, Traver, Al-Gazali, Ali, Lindner, Caspary, Otto, Hildebrandt, Glass, Logan, Johnson, Bennett, Brancati, International Joubert Syndrome Related Disorders Study, et al. 2008). Thus, *ARL13B* is the central protein of interest in my dissertation work. From studying *ARL13B* localization, its regulation of Shh signaling mechanisms, and outcomes of *Arll3b* mutations on developmental processes, I aim here to answer the question of how cilia localization impacts *ARL13B* function during development.

To set up this work, I will begin with an introduction chapter that will cover the relevant topics of the field. I will start with an overview of cilia biology, Shh signaling, and *ARL13B* function followed by in-depth exploration of the roles of cilia in development. I will then cover Joubert Syndrome and the evolving connection of cilia to neuronal mechanisms of human disease, before ending with a roadmap of areas I explore in my dissertation work and how my research relates to and expands the field's understanding of the role of cilia and cilia-associated proteins in neural development.

1.2 Overview of cilia

1.2.1 Cilia structure and trafficking

The primary cilium is a non-motile signaling appendage of the cell. The cilium is often thought of as a signaling antennae, and is visualized as a small, hair-like structure projecting off of the cellular membrane. In this section I will cover the basics of cilia biology (**Figure 1.2**). The primary cilium is built from microtubules associated into tubulin doublets. In motile cilia, there is a pair of inner doublets that use dynein arms to

generate cilia beating (Ishikawa 2017). In primary cilia, which are immotile, there is no inner doublet, only the 9 outer doublets (Satir and Christensen 2007). Alpha and beta tubulin monomers form polymers to build protofilaments, which are arranged in A and B tubules to form the 9 doublets spread around the perimeter of the structure (Mandelkow and Mandelkow 1994). These microtubule doublets provide the structure of the cilium and provide the tracks for a critical transport process, intraflagellar transport (IFT). IFT uses kinesin and dynein motors to traffic proteins and microtubule building blocks into and subsequently out of the cell, a process necessary for cilia maintenance and signaling (Rosenbaum and Witman 2002; Taschner and Lorentzen 2016). These motors move along the axoneme, and so the microtubules forming the axoneme and their modifications are critical for IFT. The microtubule doublets originate from the basal body, the anchor of the cilium positioned at the base of the cilium within the soma. The basal body is a modified centriole, which is coopted from the mitotic spindle in the previous cell cycle (Kobayashi and Dynlacht 2011). The mother centriole forms the basal body to serve as an anchor for the ciliary axoneme with the daughter centriole attached in the soma. The basal body includes a complex of BBS proteins denoted the BBsome (Nachury et al. 2007). At the point of attachment between the basal body and the ciliary axoneme is the transition zone, an area that serves to gate and regulate entrance and exit of IFT trafficking. The transition zone includes transition fibers to anchor the basal body, Y-linkers that connect the axoneme to the membrane, as well as an accumulation of proteins at the ciliary membrane that form the ciliary necklace (Garcia-Gonzalo and Reiter 2017). Together, the transition zone gates IFT as well as membrane diffusion into and out of the cilium during trafficking.

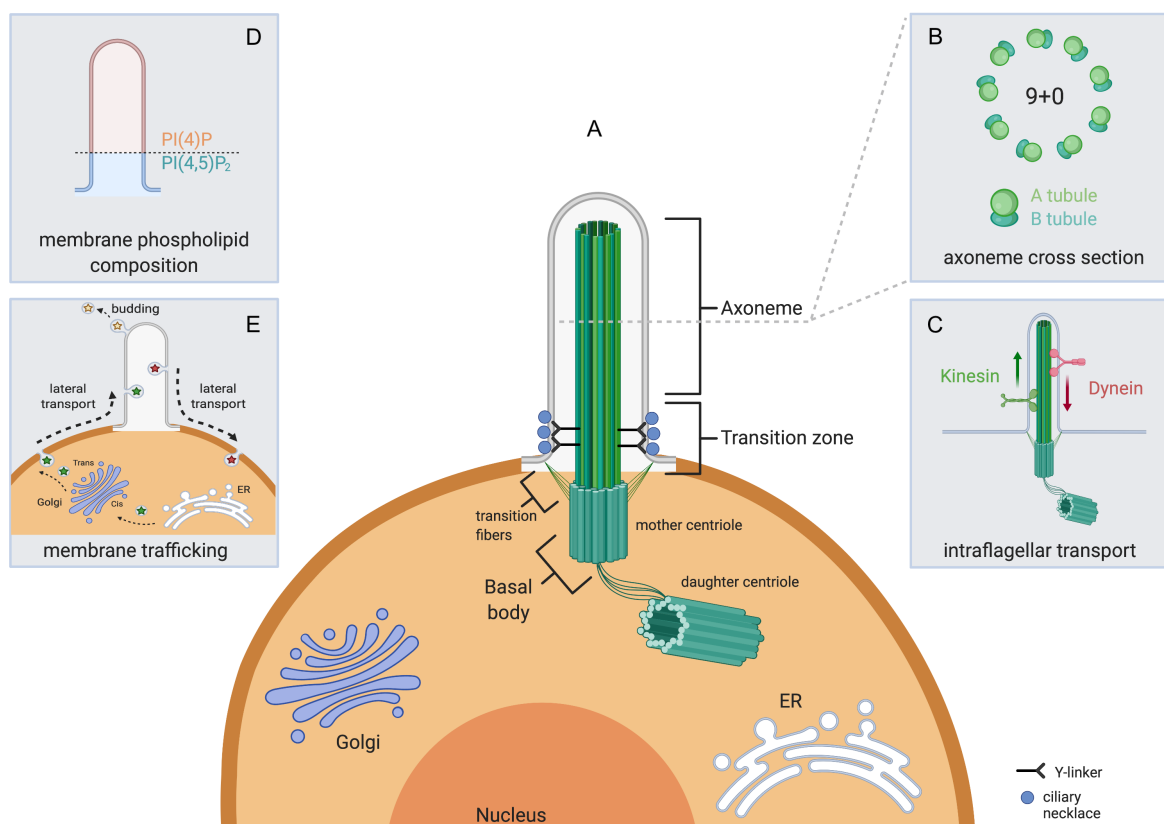


Figure 1.2 The structure, composition, and trafficking of the primary cilium. (A) The primary cilium is anchored to the plasma membrane by the basal body, made from the mother centriole. The basal body is held in place by transition fibers at the transition zone. The transition zone is also comprised of Y-linkers and proteins that form the ciliary necklace. After the transition zone, the cilium is built and maintained via a microtubule-based axoneme backbone. (B) The ciliary axoneme is made up of a 9+0 arrangement of microtubule doublets. These doublets are comprised of an A tubule and a B tubule. (C) The axoneme is used for ciliary trafficking via intraflagellar transport (IFT). In IFT, kinesin motors travel anterograde to bring materials into the ciliary compartment. Dynein motors travel retrograde along the axoneme for out-trafficking. (D) While the ciliary membrane is contiguous with the plasma membrane, the cilium is compartmentalized and exclusive. This allows for membrane lipid composition of phosphoinositides to differ between the plasma membrane made up of PI(4,5)P₂ and PI(4)P while the ciliary membrane is composed of PI(4)P. (E) In addition to IFT ciliary trafficking can occur via membrane vesicles and lateral diffusion. Vesicles targeted to cilia involve proteins generated in the ER that have gone through the Golgi apparatus for modifications and ciliary sorting. These vesicles can drop membrane proteins for lateral diffusion or endocytose into the ciliary membrane at the ciliary pocket. Out-trafficking of ciliary components can be through lateral transport, exocytosis, or even budding to allow for cell-cell communication.

The ciliary membrane is particularly interesting, as it is contiguous with the cell's plasma membrane but also exclusive, with the boundary between them at the base of the cilium in the ciliary pocket. Y-linkers and proteins within the ciliary necklace prevent aberrant lateral diffusion of membrane associated proteins and lipids into the ciliary membrane. Instead, trafficking of membrane components occurs through specialized vesicular transport. Protein synthesis begins within the endoplasmic reticulum (ER) and the resulting proteins are trafficked to the cis Golgi for sorting and modifications (Nachury, Seeley, and Jin 2010). Cilia membrane proteins are targeted to cilia via vesicular targeting or lateral transport along the membrane. Trans Golgi vesicles include cilia transport markers to allow endo or exocytosis at the clathrin-coated pits in the ciliary pocket regulated by basal body component the BBSome while lateral transport through the transition zone is mediated by small GTPases (Pedersen, Mogensen, and Christensen 2016; Nachury et al. 2007; Kim et al. 2014). To remove membrane-associated particles from the cilium, vesicles exit via BBSome and are subsequently broken down or recycled. Because the ciliary membrane is exclusive, it can be specialized. In fact, the phosphoinositide (PIPs) composition of the ciliary membrane is distinct from that of the plasma membrane; the plasma membrane is predominantly PI(4,5)P₂ and PI(4)P while the ciliary membrane is composed mostly of PI(4)P (Hammond et al. 2012; Hammond, Machner, and Balla 2014; Garcia-Gonzalo et al. 2015). Ciliary PIPs are regulated by INPP5E, a cilia-associated phosphoinositide 5-phosphatase which removes the 5' phosphate from PI(4,5)P₂ and PI(4)P to maintain ciliary PI(4)P. Disruption of INPP5E results in the ciliary membrane being enriched for PI(4,5)P₂ and PI(4)P, which results in defects in signal transduction (Garcia-Gonzalo et al. 2015). The ciliary membrane is also capable of budding, both to maintain the ciliary membrane and to send out signals extracellularly. Budding involves pinching off a portion of the ciliary

membrane to form an ectosome (Wang et al. 2014). These ectosomes carry ciliary proteins, membrane proteins, signaling components or enzymes to allow for cell-cell communication (Wang and Barr 2018).

The primary cilium is built as the cell exits the mitosis cycle, with the centrosome moving and adapting to become the basal body. Maintenance of the cilium represents a delicate tug of war between the constant assembly and disassembly of ultrastructures, with the emphasis on building and stabilization during cilia construction. These processes of concurrent building and breakdown of the cilium will continue throughout its existence, until the cell reenters the cell cycle at which point the microtubule turnover in the cilium will shift to favor breakdown (Avasthi and Marshall 2013). IFT takes place along the microtubule tracks that form the axoneme. Anterograde IFT is regulated by kinesin motors moving and carrying cargo along the A tubule while retrograde IFT is regulated by dynein motors along the B tubule of the axoneme (Rosenbaum and Witman 2002; Taschner and Lorentzen 2016). The motors themselves will be dropped at the site of cargo destination and subsequently recycled for further use. Loss of anterograde IFT results in loss of cilia, as critical ciliary components are not trafficked in (Chiang et al. 1996). Loss of retrograde IFT signaling causes cilia to display an abnormal bulbous tip as proteins that entered the cilium are unable to be trafficked out (Qin et al. 2011; Pazour, Wilkerson, and Witman 1998). Signaling factors are often trafficked in and out of cilia for activation, or to interact with other ciliary effectors (Mukhopadhyay et al. 2017). Thus, loss of IFT can result in loss or aberrant ciliary signaling and signal transduction.

1.2.2 Cilia are required for neurodevelopment

In mice, complete loss of cilia is incompatible with life (Cortellino et al. 2009). Furthermore, null mutations in some cilia-associated genes can also be incompatible with life (Casparly, Larkins, and Anderson 2007; Zhang, Ramalho-Santos, and McMahon 2001). When cilia or cilia-associated proteins are mutated, it can give rise to a wide range of phenotypes in human disease. This category of disease is known as ciliopathies and affect multiple organ systems. Polycystic Kidney Disease (PKD) is a most common ciliopathy with a prevalence of approximately 1:10,000, likely reflecting the fact that kidney function relies on ciliary function (Bergmann et al. 2018). Typical phenotypes of ciliopathies include kidney and liver abnormalities, polydactyly, cleft palate, and in some instances neuropathy (Waters and Beales 2011). In fact, among the multitude of symptoms exhibited in ciliopathy patients, perhaps the most enigmatic is intellectual disability (Valente et al. 2014; Guo et al. 2015). This is mainly due to the complexity of brain circuitry, which reflects the culmination of neural development. Fully developed neural circuitry includes sensory neurons that integrate environmental and internal signals from the periphery to transmit to the central nervous system (CNS), motor neurons that transmit signals from the CNS to effector cells, and interneurons that connect neural networks. Additionally, astrocytes provide nutrients to the brain, oligodendrocytes envelope the axons with the myelin sheath necessary for efficient synapse transduction, and microglia act as the immune system. In ciliopathy patients with intellectual disability any of these cells may be affected as all of these neuronal and glial cell types, including their precursors, build a microtubule-based primary cilium. Ciliopathy patients exhibit additional phenotypes reflecting abnormal neural development such as cerebellar hypoplasia and retinal disease (Hildebrandt, Benzing, and Katsanis 2011). In these cases, we have clear clues to how cilia dysfunction misregulates specific

steps in neural development. Human disease states are hugely informative in revealing the roles of cilia during neural development and these clinical data are complemented by animal studies that uncover the mechanisms through which cilia function during neural development. As many cilia genes are essential for mammalian embryonic survival, the patient alleles tend to be hypomorphic alleles while animal studies often analyze severe loss of function or null alleles. While the link between cilia and axon guidance is clear from the phenotypes of ciliopathies such as Joubert syndrome or Kallmann syndrome, the mechanistic links are just beginning to be uncovered (Engle 2010). Joubert Syndrome, the ciliopathy of greatest interest to my dissertation work will be further covered in its own section (“Joubert Syndrome Overview”).

1.2.3 Ciliary signaling takes place within the privileged environment of the primary cilium.

In response to signal, signaling molecules are trafficked in and out of the cilium to interact with effectors (Mukhopadhyay et al. 2017). The best studied cilia-dependent pathway is Shh signaling (covered in the following “Overview of Shh section”). This pathway is critical for development, and several developmental processes are associated with Shh, the cilium, and ciliary factors. These include cell fate specification, cell proliferation, cell migration, and axon guidance in the neural tube (covered in the following “Roles of cilia, Shh signaling, and Arl13b during development section”) (Chiang et al. 1996; Kenney and Rowitch 2000; Komada 2012; Bijlsma et al. 2007; Charron et al. 2003).

1.3 Overview of Shh

1.3.1 The critical developmental pathway Shh signaling functions within as well as outside the cilium

Shh signaling is a particularly interesting developmental signaling pathway because it has two, distinct, mechanistic arms (**Figure 1.3**). The first arm is sometime called canonical because it was discovered first, and but refers to Shh signal transduction in a transcription-dependent manner (Falkenstein and Vokes 2014). This transcription-dependent arm of the pathway requires the primary cilium likely because so many pathway components are dynamically in and out of the cilia in response to Shh ligand stimulation. PTCH1, the receptor for Shh, is enriched in cilia until Shh is present and binds PTCH1 (Rohatgi, Milenkovic, and Scott 2007). That interaction relieves the inhibition of the pathway's obligate transducer Smoothed (SMO) (Corbit et al. 2005a). This results in activation of Gli transcription factors which will go on to transcribe Shh target genes (**Figure 1.4**) (Wen et al. 2010; Corbit et al. 2005b). In contrast, in the absence of Shh ligand, SMO inhibition results in processing Gli to a transcriptional repressor, which turns off target gene transcription (Haycraft et al. 2005; Rohatgi, Milenkovic, and Scott 2007). Thus, the amount of Shh ligand determines the ratio of Gli activator to repressor resulting in varying expression of target genes (Motoyama et al. 2003; Persson et al. 2002). Transcription-dependent Shh is critical to regulate cell fate specification in the neural tube and cellular proliferation in the cerebellar precursor cells.

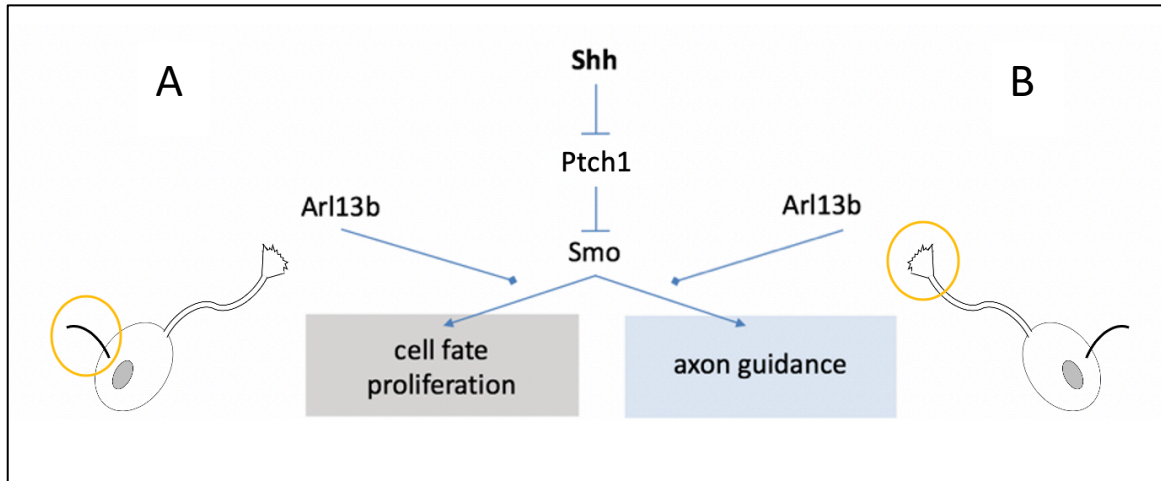


Figure 1.3 The developmental signaling pathway Shh has two mechanistic arms. Both arms of the pathway involve Shh ligand binding receptor PTCH1 leading to activation of pathway obligate transducer SMO. (A) One arm takes place within the cilium, where Shh regulates cell fate specification in the neural tube and cell proliferation in cerebellar neuron precursors. Shh signaling interpreted by the cilium elicits cell response via a transcription-dependent mechanism. (B) The other arm takes place outside of the cilium, where Shh ligand acts as a guidance cue in a transcription-independent mechanism. In commissural neurons Shh can act as either an attractive or repulsive axon guidance cue at the growth cone, the tip of the projecting axon. Shh can also act as a chemoattractant to induce fibroblast migration at the cell leading edge. Cilia-associated GTPase ARL13B is required for signal transduction in both the transcription-dependent and -independent arms of the Shh signaling pathway.

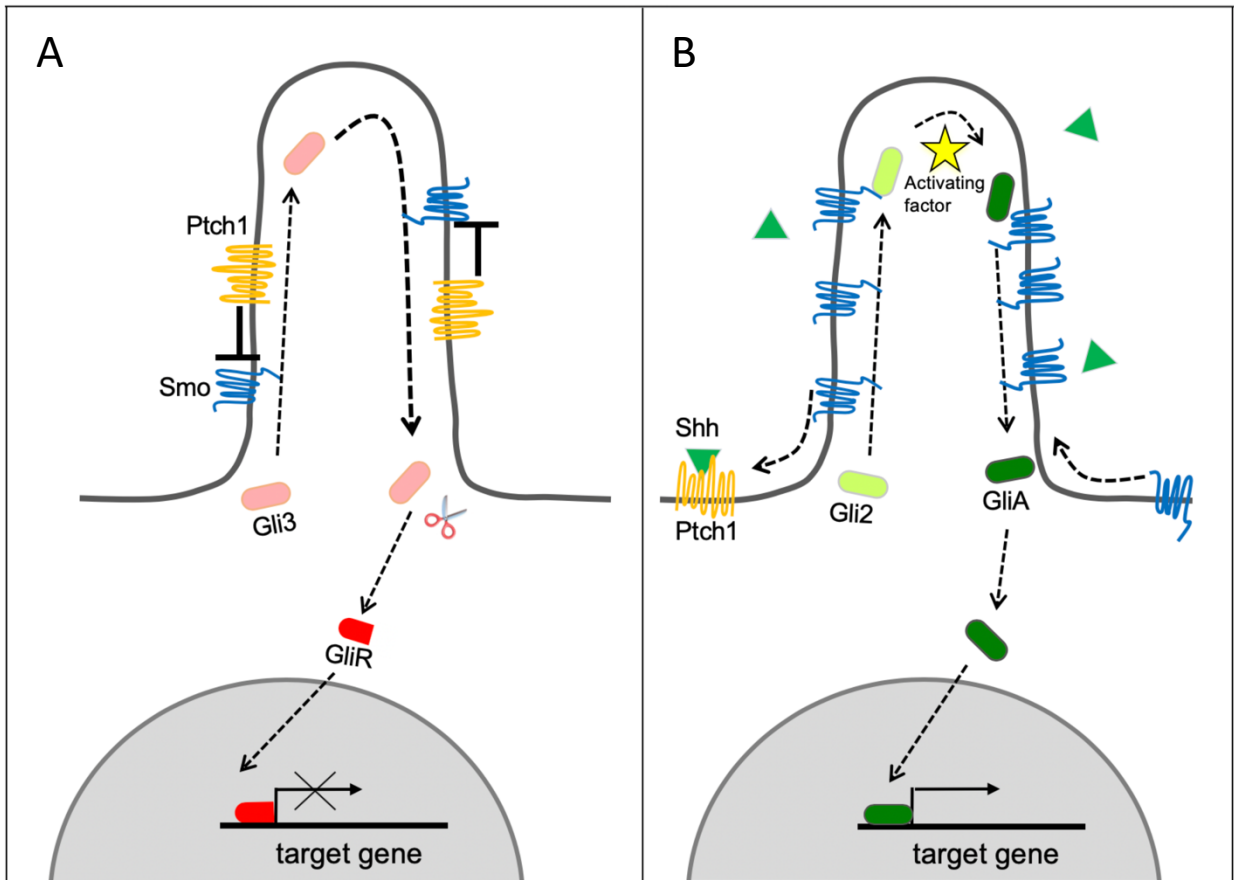


Figure 1.4 Transcription-dependent Shh signaling is interpreted by the cilium. (A) Shh signaling in the cilium results in either activation or repression of target genes. In the absence of Shh ligand, Shh receptor PTCH1 inhibits the pathway's obligate transducer SMO, resulting in Gli3 cleavage and formation of Gli repressor (GliR) which will repress Shh target gene transcription in the nucleus. (B) When Shh ligand is present, Shh will bind to its receptor PTCH1 and relieve inhibition of pathway obligate transducer SMO. SMO activation results in activation of Gli2 to form Gli activator (GliA) which will move to the nucleus and activate transcription of Shh target genes.

In contrast, the other mechanistic arm of the pathway is transcription independent which means the Gli proteins are not required (Bijlsma et al. 2007; Yam et al. 2009). Transcription-independent Shh acts as a fibroblast chemoattractant and as an axon guidance cue for neurons (Bijlsma et al. 2007; Charron et al. 2003; Yam et al. 2009). Fibroblast migration is the process by which fibroblasts project out their lamellipodia, a protrusion of the plasma membrane, towards chemoattractant signals and pull the cell body towards that signal at the leading edge (**Figure 1.5**). In this pathway, a concentration gradient of Shh ligand is intercepted by pathway obligate transducer SMO coupled with G_i protein. This binding leads to activation of Rho family small GTPases and results in oxidation of arachidonic acid metabolites to form leukotrienes. Leukotrienes go on to stabilize actin and cause the cytoskeletal rearrangements at the leading edge to form a lamellipodia and initiate migration toward the Shh signal. Of note, Shh-dependent chemotaxis in fibroblasts occurs even in cells completely lacking cilia, or in cells expressing a cilia-excluded variant of SMO (Bijlsma, Damhofer, and Roelink 2012; Bijlsma et al. 2008). Furthermore, transcription-independent Shh signaling can regulate axon guidance. During neural tube development, commissural neurons that require targeting of the axon to synaptic end points builds neural circuitry. In this context, Shh acts as a guidance cue to stabilize microtubules in the direction of Shh signal at the neural tube floor plate, thus turning the axons towards that signal (**Figure 1.6**) (Lepelletier et al. 2017). This takes place in the tip of the axon, the growth cone, distant from the cell body and nucleus. Several key Shh effectors localize to the growth cone, including the Shh receptor, PTCH1, and obligate transducer, SMO. In commissural axon guidance Src family kinases are activated in the growth cone via a SMO-dependent

mechanism, resulting in phosphorylation of zipcode binding protein 1 (ZBP1) (Okada et al. 2006; Yam et al. 2009; Fabre, Shimogori, and Charron 2010; Lepelletier et al. 2017). ZBP1, previously binding and inhibiting actin mRNA, then releases the mRNA for local translation and resulting cytoskeletal rearrangements turn the growth cone towards Shh expressed at the neural tube midline while post-crossing commissural axons are repulsed to further direct them towards synaptic targets (Fabre, Shimogori, and Charron 2010; Domanitskaya et al. 2010; Yam et al. 2012; Lepelletier et al. 2017). In addition to SMO and Src kinases, the rapid cytoskeletal rearrangements in axons requires leukotriene synthesis (Bijlsma et al. 2007; Bijlsma et al. 2008; Yam et al. 2009; Bijlsma, Damhofer, and Roelink 2012)

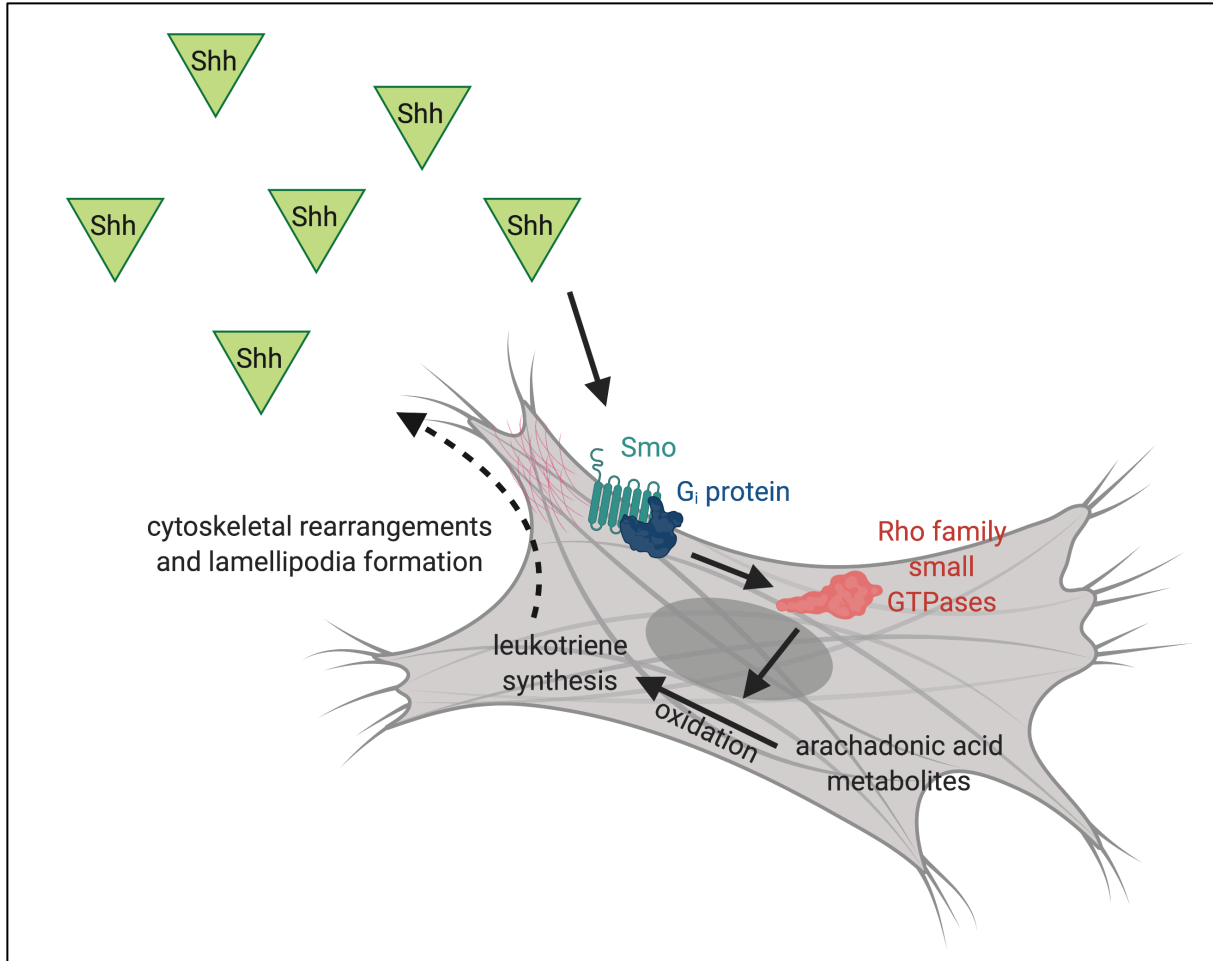


Figure 1.5 Transcription-independent Shh signaling regulates fibroblast migration via cytoskeletal rearrangements at the leading edge. Fibroblasts will respond to a gradient of Shh as a chemoattractant. In fibroblast migration, Shh obligate transducer SMO coupled with G_i protein acts as the Shh receptor. Signal transduction results in activation of Rho family small GTPases as well as arachidonic acid metabolite oxidation to form leukotrienes. Leukotriene synthesis results in cytoskeletal rearrangements at the fibroblast leading edge to stabilize actin at the site of signal, allowing the cell to form a lamellipodia and move towards chemoattractant Shh.

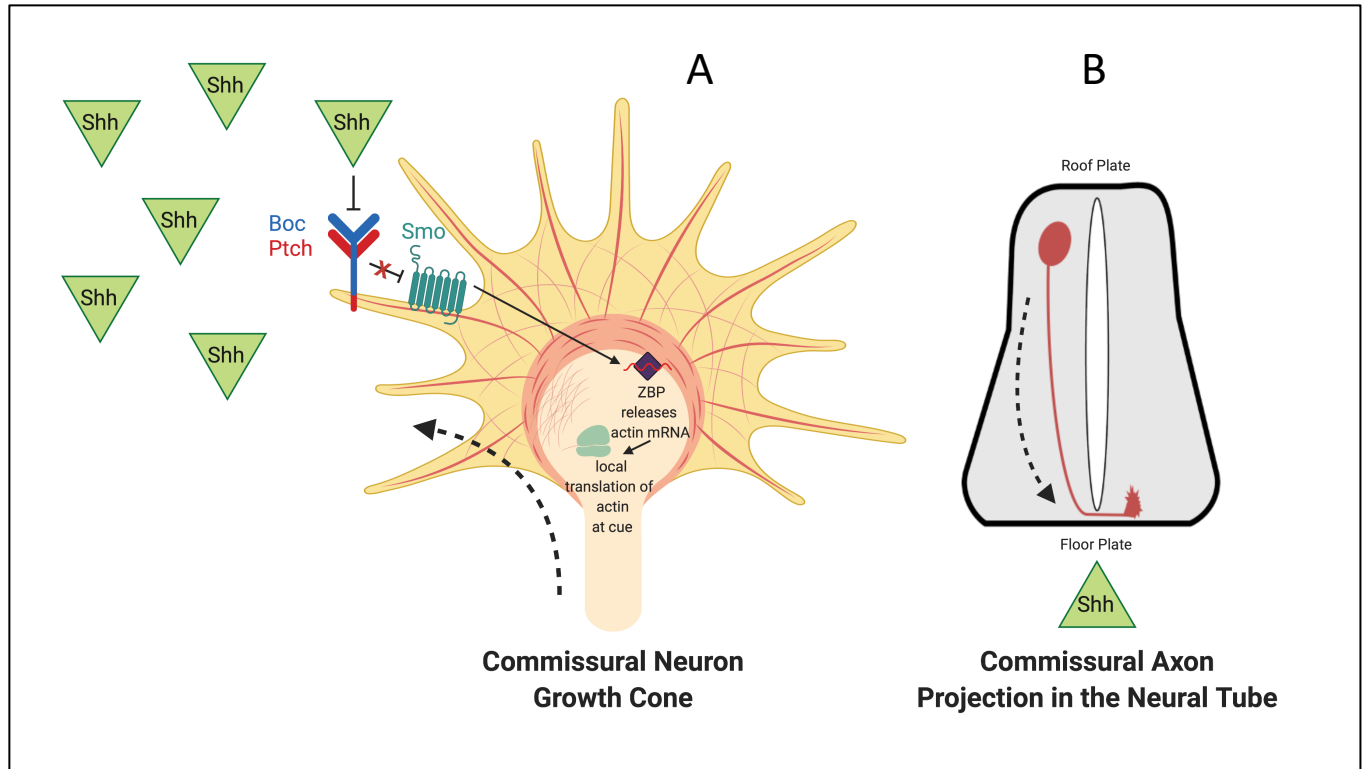


Figure 1.6 Transcription-independent Shh signaling regulates axon guidance via cytoskeletal rearrangements at the growth cone. (A) Commissural neurons respond to Shh as a guidance cue. As in other mechanisms of Shh signaling, transduction requires activation of obligate transducer SMO. In axon guidance, Shh binds to receptors PTCH1 and BOC at the growth cone, the tip of the projecting axon. Shh binding to receptors relieves inhibition of SMO and allows for phosphorylation of Src family kinases. This leads to release of actin mRNA trafficked to the growth cone and held by zipcode binding protein 1 (ZBP1). When ZBP1 releases actin mRNA at the site of Shh interception, local translation of actin occurs at the cue. This stabilizes the growth cone in the direction of Shh signal and allows the growth cone to turn towards that signal. (B) *In vivo*, commissural neurons are born at the roof plate of the neural tube, the embryonic spinal cord. Shh signal is located at the neural tube floorplate, where it acts as an attractant cue to guide commissural axons to the floorplate and to cross the midline.

1.3.2 The cilia-associated GTPase *Arl13b* regulates transcription-dependent and -independent *Shh* signaling

ADP-ribosylation factor-like 13b (ARL13B) is a regulatory GTPase that is involved in regulating the Shh signaling pathway in both transcription-dependent and -independent mechanistic arms of Shh regulation (Mariani et al. 2016; Ferent et al. 2019; Caspary, Larkins, and Anderson 2007). In transcription-dependent Shh signaling, *Arl13b*-deletion misregulates Gli activator production but not Gli repressor production (Caspary, Larkins, and Anderson 2007). The result is *Arl13b*-deletion mice display constitutive, low-level Shh response. In the transcription-independent Shh signaling, ARL13B is required for axon guidance and fibroblast migration (Ferent et al. 2019; Mariani et al. 2016). Fascinatingly, cilia themselves are not required for fibroblast migration, but when ARL13B is excluded from cilia fibroblast migration is halted, indicating that ARL13B function in fibroblast migration is dependent on the cilium or some ciliary factor(s) (Mariani et al. 2016). However, ARL13B localizes outside the cilium in circular dorsal ruffles, a plasma membrane structure involved in cell motility, early endosomes and in the site of axon guidance the growth cone (Barral et al. 2012; Casalou et al. 2014; Hoon, Wong, and Koh 2012; Petralia et al. 2012; Ferent et al. 2019). This idea that ARL13B may not just function from within the cilium, even in the context of Shh signaling, can lead us to new understandings of potential cilia-independent function of cilia-associated proteins.

The Arl family of small GTPases is known for its homology to the Arf and Arf-like family, and so *Arl13b* displays similar sequences. The GTPase N-terminal Arf domain of *Arl13b* includes Switch 1 and Switch 2 loops to bind GTPase effectors as well

as four nucleotide-binding motifs (Joneson et al., 1996; Kuai and Kahn, 2000). However, ARL13B deviates from homology in the second nucleotide-binding motif with the loss of a conserved glutamate known in Arfs to regulate GTP hydrolysis. A further discrepancy between the Arl family and Arfs resides in an Arf-conserved N-terminal glycine that allows for membrane binding (Donaldson and Jackson, 2011). ARL13B is one of several Arl GTPases to lack this glycine, however, the protein still localizes to the membrane via an N-terminal palmitoylation motif (Cevik et al. 2013). This motif is further required for ARL13B localization to the ciliary membrane, where it is targeted via a C-terminal VxP-containing cilia localization signal (CiLS) (Sun et al. 2004; Higginbotham et al. 2012b). Other cilia-associated proteins show homology to the ARL13B CiLS, including rhodopsin and polycystins (Deretic et al., 2005; Geng et al., 2006; Ward et al., 2011).

Mutations in *Arl13b* cause developmental defects in zebrafish and mutations in the *C. elegans* gene *arl-13*, homologous to *Arl13b*, disrupt cilia structure and ciliary protein trafficking (Zhu et al. 2020; Duldulao et al., 2009; Sun et al., 2004; Cevik et al., 2010; Li et al., 2010; Warburton-Pitt et al., 2014). Total loss of *Arl13b* is embryonic lethal in mammals (Casparly et al., 2007). Furthermore, mutations in *ARL13B* cause the ciliopathy Joubert Syndrome (**Figure 1.7**). These mutations are typically found in the GTPase domain and are often hypomorphic point mutations, as loss of *Arl13b* function is embryonic lethal. ARL13B, for its function in both mechanistic arms of the Shh signaling pathway (both ciliary transcription-dependent and non-ciliary transcription-independent) is a fascinating example of how a protein thought to be completely localized to the primary cilium may not function in there in all mechanisms of regulation. Furthermore, because *ARL13B* is implicated in the human ciliopathy Joubert

Syndrome (JS), there is great interest in dissecting apart the different functions and functional locations of ARL13B during development.

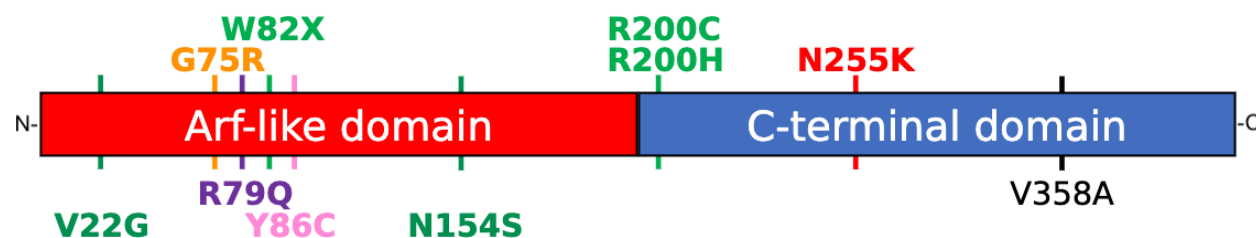


Figure 1.7 ARL13B is a cilia-associated GTPase that includes an Arf-like GTPase domain, as well as a novel C-terminus. Mutations in both the GTPase and C-terminal domain resulting in the ciliopathy Joubert Syndrome. The novel C-terminus of ARL13B includes a cilia localization sequence such that ARL13B will be trafficked to and is visualized localized in cilia. This sequence was mutated in *Arl13b*^{V358A} to exclude ARL13B from cilia.

There are many ways in which *ARL13B* mutations are implicated in JS. ARL13B as a GTPase has different conformations upon binding GDP or GTP, and thus multiple effector proteins with which it can interact (Miertzschke et al. 2014; Pasqualato, Renault, and Cherfils 2002). For example, ARL13B can function as a guanine exchange factor (GEF) for ARL3, another JS-implicated GTPase (Gotthardt et al. 2015; Ivanova et al. 2017). Furthermore, ARL13B is a critical component of trafficking the inositol phosphatase INPP5E to cilia, and mutations in INPP5E are also implicated in causing JS (Bielas et al. 2009). *ARL13B* has several point mutations that cause JS. G75R, R79Q, V22G, W82X, N154S and Y86C are all JS-causing mutations within *ARL13B*'S GTPase domain while R200C, R200H, and N255k are JS-causing point mutations within *ARL13B*'S novel C-terminus.(Cantagrel, Silhavy, Bielas, Swistun, Marsh, Bertrand,

Audollent, Attie-Bitach, Holden, Dobyms, Traver, Al-Gazali, Ali, Lindner, Caspary, Otto, Hildebrandt, Glass, Logan, Johnson, Bennett, Brancati, International Joubert Syndrome Related Disorders Study, et al. 2008; Thomas et al. 2015; Shaheen et al. 2016; Bachmann-Gagescu et al. 2015; Rafiullah et al. 2017). Other proteins mutated to cause JS affect ciliary targeting, leading to abnormal ciliary traffic, which could explain the defective signaling that results in the molar tooth sign (Srour et al. 2012; Arts et al. 2007; Hopp et al. 2011; Garcia-Gonzalo et al. 2011; Roberson et al. 2015; Delous et al. 2007). Interestingly, the *ARL13B* JS-causing mutations R79Q, Y86C, and R200C do not disrupt GTP binding to ARL13B or GTP hydrolysis, however, all three mutations disrupt ARL13B function as a GEF for ARL3 (Ivanova et al. 2017).

1.4 Roles of cilia, Shh signaling, and Arl13b during development

1.4.1 Neural cell fate specification requires signal transduction via the primary cilium

Neural development starts during embryogenesis when the neurectoderm is induced and folds into the neural tube. The anterior neural tube forms the brain and the posterior neural tube becomes the spinal cord. Within the dorsal-ventral axis of the spinal cord, cell fates are specified by a combination of signaling pathways. Wnt and Bone Morphogenic Protein (BMP) signaling from the surface ectoderm overlying the dorsal neural tube, retinoic acid signaling from the paraxial mesoderm and Sonic hedgehog (Shh) from the notochord, a structure just ventral to the neural tube, are all important players (Jessell 2000). Shh signaling is the best understood and is required to specify all ventral neural cell fates (Chiang et al. 1996). The highest level of Shh activity is at the ventral midline of the neural tube and specifies the floor plate, a secondary signaling center, that is induced to also express Shh ligand. Shh activity decreases at successive

dorsal positions in the neural tube; distinct amounts of Shh activity result in the expression of specific combinations of transcription factors which determine the different ventral neural cells fates (**Figure 1.8**) (Briscoe and Ericson 1999). In the course of a forward genetic mouse screen, Kathryn Anderson's group identified a mutant that lacked ventral neural cell fates due to a loss of cilia (Huangfu et al. 2003). This demonstrated that cilia are essential to specify neural cell fate and linked cilia and Shh signal transduction.

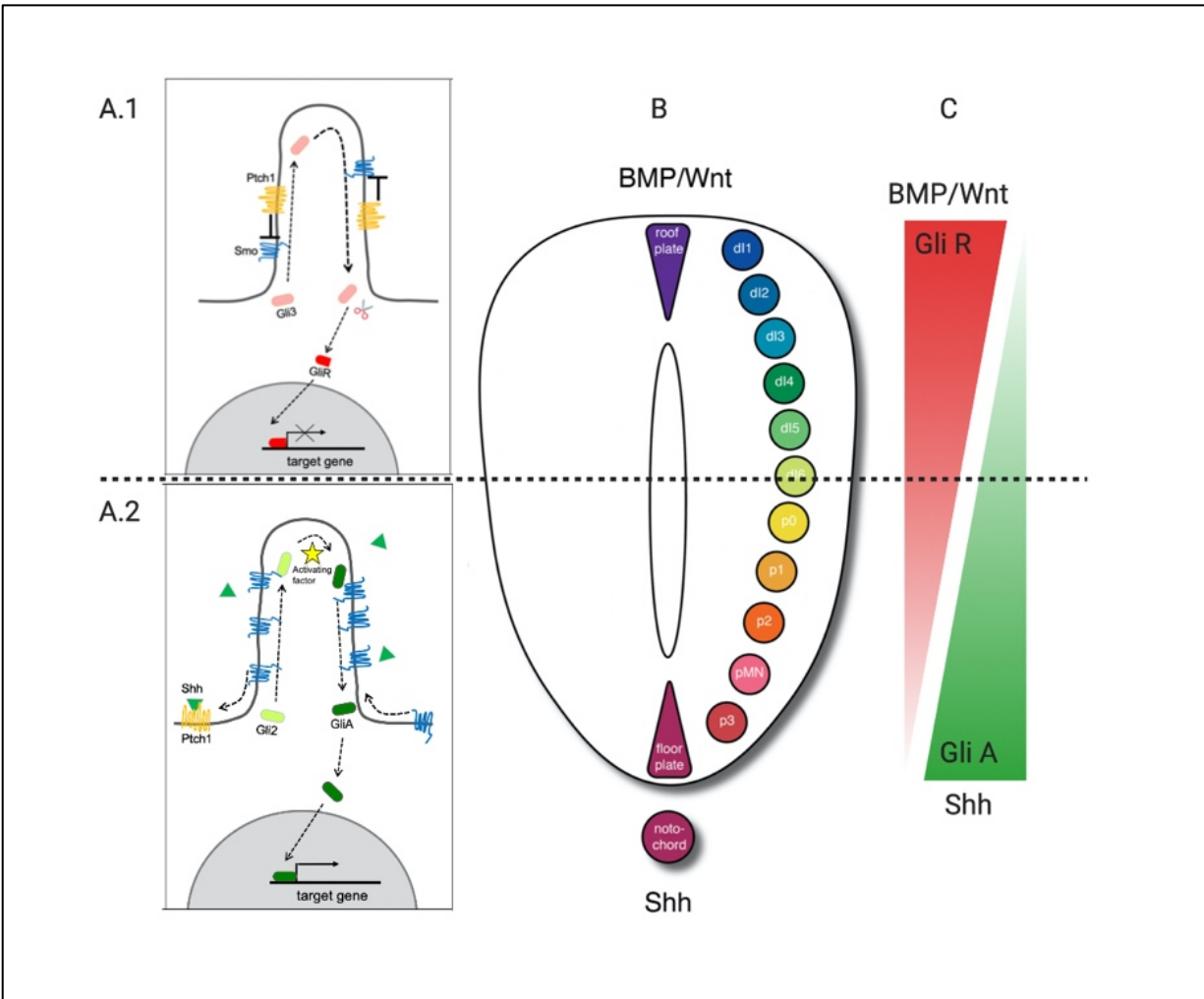


Figure 1.8 The cilium is required to transduce Shh signal and specify ventral neural tube cell fates. (A) Shh signaling components dynamically traffic within cilia. In the absence of Shh signal (A.1), receptor PTCH inhibits SMO leading to Gli repressor (GliR) production which represses target gene transcription. When Shh signal is present (A.2), it binds receptor PTCH and is endocytosed. SMO accumulates in the cilium and is activated leading to production of Gli activator (GliA) which, in turn turns on target genes. (B) Ventral neural tube cell fates (floorplate \rightarrow progenitor 0 (p0)) are defined by their position relative to the notochord which secretes Shh ligand. Dorsal cell fates are specified by signals including BMPs and Wnts. (C) Opposing GliA and GliR gradients along the neural tube dorsal-ventral axis are determined via the amount and duration a given cell is exposed to Shh ligand. The GliA/GliR ratio induces the expression of a specific set of transcription factors that determine the distinct ventral fates.

By understanding the trafficking events required to transduce Shh signaling, it is clear that the lack of ventral cell fates in a $Shh^{-/-}$ mutant is mechanistically distinct from the lack of ventral cell fates in mutants lacking cilia, such as $Ift172^{wim/wim}$. In the absence of Shh ligand ($Shh^{-/-}$ mutant), Gli protein is cleaved to a repressor form so ventral cell fates are not specified because the required transcription factors are actively repressed (Chiang et al. 1996). In contrast, in the absence of cilia ($Ift172^{wim/wim}$ mutant), Gli proteins cannot be trafficked to cilia so are not cleaved to a repressor form nor are they processed to an activator form- thus the transcription factors required for ventral cell fates are neither turned on nor repressed (Liu, Wang, and Niswander 2005; Huangfu and Anderson 2005). Similarly, mutants that lack retrograde intraflagellar transport and thus display bulbous cilia due to the block in traffic egress within the cilium also do not process or cleave Gli proteins and so do not specify ventral cell fates (Qin et al. 2011; Pazour, Wilkerson, and Witman 1998). The fact that mutations in proteins controlling intraflagellar anterograde or retrograde traffic in cilia both lead to an absence of ventral cell fate argue that it is their role within the cilium itself, and not a cellular function, that transduces the Shh pathway (Huangfu and Anderson 2005).

Other mutations in cilia-associated genes impact Gli proteins in distinct manners. Loss of GPR161, a ciliary GPCR, results in lack of Gli repressor formation consistent with it negatively regulating Shh signaling (Mukhopadhyay et al. 2013). In contrast, loss of ARL13B, a ciliary GTPase, results in normal Gli repressor formation and abnormal Gli activator processing (Caspary, Larkins, and Anderson 2007). ARL13B targets a phosphatase, INPP5E, to cilia (Humbert et al. 2012). Loss of INPP5E seems to control the kinetics of Gli repressor processing as neural patterning is initially abnormal but is

mostly restored over time (Constable et al. 2019). Gli3 acts predominantly as a repressor in the neural tube and *Inpp5e* mutants that also lack Gli3 do not restore patterning consistent with *Inpp5e* single mutants having delayed Gli repressor production (Constable et al. 2019; Persson et al. 2002).

The role of cilia is also evident in neural cell specification in the brain. Mice lacking DYNC2H1, a retrograde dynein motor, display intermingled cells in the telencephalon at the cortico-striatal border (May et al. 2005). This phenotype is also exhibited by *Ift88^{cbs/cbs}* mice carrying a hypomorphic mutation in *Ift88*, an anterograde IFT necessary for cilia (Willaredt et al. 2008). These phenotypes resemble what is observed in Gli3 mutants underscoring the fact that cilia disruption can lead to loss of Gli repressor (Besse et al. 2011). However, just as in the neural tube, distinct cilia mutants can uncouple the repressor and activator Gli functions. For example, mutations in the retrograde *Ift139*, *Ift139^{aln/aln}*, constitutively produce Gli activators and display loss of the boundary between the diencephalon and telencephalon along with loss of the dorsal cortex (Stottmann et al. 2009). These phenotypes highlight the intimate link between a variety of cilia associated proteins and processing of the Shh signal, especially related to the Gli transcription factors, during neural cell fate specification.

1.4.2 Neural cell proliferation requires Shh signal transduction via the primary cilium

Shh signaling plays critical roles in the brain via its proliferative function. As a mitogen, Shh activates cyclins that cause G1 cells to transition to S phase for DNA replication and cell division, thus proliferating the cell population (Kenney and Rowitch 2000). This is particularly relevant in Shh-dependent proliferation of cerebellar precursors, which give rise to the granule neurons (Wang and Zoghbi 2001). When there is insufficient proliferation, the cerebellum is

hypoplastic (Nguyen et al. 2018). Alternatively, when proliferation persists, it gives rise to medulloblastoma, the most common pediatric tumor in North America (Ellison et al. 2011; Stevens et al. 1991a). Furthermore, Shh-dependent proliferation is important in adult neural stem cells to balance between active and quiescent populations and prevent exhaustion of the stem cell pool.

During cerebellar development, Shh ligand is secreted from the Purkinje layer causing proliferation of the ciliated external germinal layer (Dahmane and Ruiz i Altaba 1999; Wechsler-Reya and Scott 1999) (**Figure 1.9**). Once the external germinal layer is sufficiently proliferated, it migrates internal to the Purkinje cell layer to complete cerebellar growth during postnatal cerebellar development. Failure of neurons to proliferate properly results in a hypoplastic, underdeveloped cerebellum. Indeed, mutants lacking cilia display hypoplasia and lack cerebellar folds (Chizhikov et al. 2007). Furthermore, zebrafish lacking *Arl13b*, a regulator of Shh signaling, display cerebellar development defects (Zhu et al. 2020). Proper control of proliferation in the cerebellum must be tightly regulated so that it is promoted for a period of time and subsequently turned off to prevent overproliferation and cancer. Cerebellar progenitor overproliferation results in medulloblastoma, the most common pediatric malignant brain tumor in North America (Stevens et al. 1991b). As true during cerebellar development, cilia promote such Shh-dependent proliferation. One class of mutations in medulloblastoma involve activation of SHH via loss of *PTCH1* or activating *SMO* mutations (Raffel et al. 1997; Hallahan et al. 2004). In such contexts, loss of cilia suppresses medulloblastoma progression (Han et al. 2009). However, in cases where the Shh pathway is activated due to activating mutations in *GLI*, the presence of cilia lessens the disease severity because

Gli repressor is still produced and dampens the Gli activator (Wong et al. 2009). Thus, depending on where in the pathway Shh signaling is activated, cilia play opposing roles in Shh-dependent medulloblastoma.

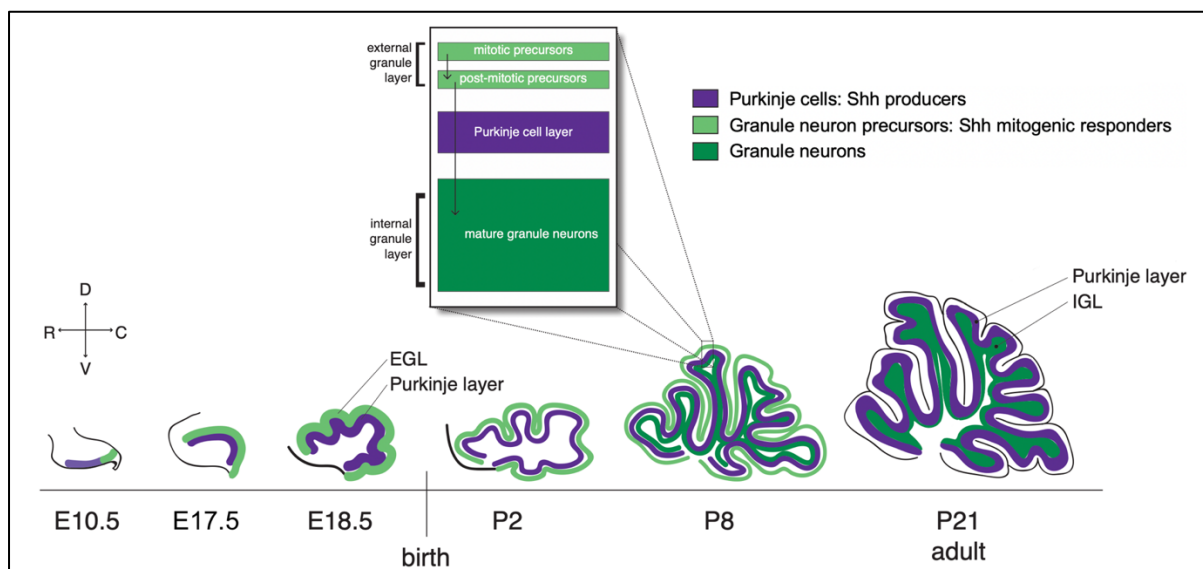


Figure 1.9 Shh is required for proliferation of granule neuron precursors in the cerebellum. Cerebellar development occurs during embryonic and postnatal stages. Ciliated granule neuron precursor (GNP) cells (green) form the external granule layer (EGL) and respond to Shh produced by the Purkinje cells (purple) to proliferate. Once proliferation is complete, the GNPs migrate beneath the Purkinje cell layer forming the internal granule layer (IGL) where they mature to granule neurons (dark green). Cerebellar granule neurons are the most abundant neuron in the brain due to this proliferation step.

In adulthood, neural stem cells within the brain's subventricular zone and hippocampal subgranular zone are necessary for adult plasticity and regeneration after injury (Bond, Ming, and Song 2015; Pastrana, Cheng, and Doetsch 2009). Loss of these neural stem cell populations diminish learning and memory recall in adults along with decreased traumatic brain injury recovery. The stem cell population is either quiescent, slowly dividing to maintain the population, or activated, rapidly proliferating prior to differentiating into glial or neuronal cell

fates to be integrated into neural circuitry (Bonaguidi et al. 2011). In the subventricular layer, epidermal growth factor stimulates Shh to regulate proliferation of both quiescent and activated neural stem cells (Daynac et al. 2016). If Shh is blocked, the cells proliferate less leading to an insufficient stem cell population and inappropriate transition from quiescent cells to active cells (Komada 2012; Martínez et al. 2013). Conversely, upon Shh upregulation in adult neural stem cells, quiescent neural stem cells over-proliferate leading to precursor depletion (Daynac et al. 2016).

1.4.3 Interneuron and neuron migration require the primary cilium

Once interneurons are specified, they need to migrate to their appropriate location as the brain develops. Cell migration occurs through regulation of microtubules and actin rearrangements to polarize cells, allowing them to extend their plasma membrane and move towards attractive signals and retract away from repulsive signals. Abnormal migration leads to multiple diseases. When interneuron migration is dysregulated, it can cause Lissencephaly Type I which displays an absence of brain folds (Reiner and Sapir 1998). The lissencephaly protein, LIS1, localizes within mammalian motile cilia (Pedersen et al. 2007). Migration dysregulation can also result in periventricular heterotopia where neurons aberrantly accumulate in the brain's ventricles (Sheen 2012). Mutations that cause heterotopia, such as mutations in microtubule associated protein, *EML1*, can result in improper cilia formation in radial glia, the cells that form the scaffold required for proper cortical architecture (Uzquiano et al. 2019).

Mouse mutants reveal a role of cilia in migration of GABAergic interneurons in the ventral forebrain. These interneurons begin their migration in a tangential pattern and

switch to a radial path before colonizing the cortical plate. Higginbotham et al demonstrated that conditional deletion of cilia-associated ARL13B protein results in aberrant accumulation in migratory interneurons at the pallial-subpallial boundary (Higginbotham et al. 2012a). Live imaging showed cilia extending in all directions and the migrating interneurons lacking somal translocation consistent with abnormal migration. Baudoin et al used a distinct *Cre* line to delete either *Ift88* or *Kif3a* in the migrating interneurons and found few cells that switched out of the tangential stream to the radial one. They also found the migration of the interneurons could be altered by pharmacological agents that manipulated Shh signaling (Baudoin et al. 2012). Live cell imaging showed that the Shh migration guidance cue is interpreted by the interneuron's cilium. These studies demonstrate the important role of cilia in immature interneuron migration. Interestingly, deletion of *Arl13b* in post-migratory interneurons did not affect their postnatal differentiation (Higginbotham et al. 2012a).

Earlier in cortical development, polarized radial glia cells form scaffolding along which neurons migrate towards their post-mitotic positions. Radial glia are polarized with their cilia located on their apical side. Once the polarized cells have been established, they will divide either symmetrically to replenish the population or asymmetrically to form one neuron daughter cell with a glial or intermediate precursor daughter cell (Farkas and Huttner 2008). The glial cells will go on to form the scaffolding that neurons will use as a guide towards the correct migration destination. Ciliary signaling plays an important role in radial glia polarity. In radial glia with aberrant cilia signal transduction, such as those lacking ARL13B, the apical-basal polarity of the glial scaffold is reversed (Higginbotham et al. 2013). The role of ARL13B is limited to the polarization of the radial glia; it is not necessary to maintain that polarity or for subsequent scaffold establishment. However, during this critical time of establishing radial glia polarity,

disruption prevents the following neurons from migrating to their proper place in the cortex, as the scaffolding they use to find their place has been compromised (Higginbotham et al. 2013).

1.4.4 Neuronal axon guidance requires cilia-associated proteins and signaling pathways

Neurons must form circuits with other neurons to function so properly positioning projections is crucial to form connections. Axon guidance requires the integration of extracellular signals that guide the growth cone at the axon's distal tip. Such extracellular signals cause dynamic shifts in actin and microtubule-based structures within the growth cone. Attractive cues will stabilize and promote building of cytoskeletal architecture, whereas repulsive cues will cause disassembly. There are numerous human diseases of dysregulated axon guidance, including corpus callosum dysgenesis, Kallmann Syndrome, palsy, and Joubert Syndrome (Lee and Gleeson 2010). These diseases, caused by incorrect axon guidance and therefore improper neural circuitry, are often associated with intellectual disability or motor coordination defects. Among these diseases are clear ciliopathies suggesting that cilia-associated genes may play roles in axon guidance. In fact, at least 35 distinct cilia-associated genes cause the ciliopathy Joubert syndrome (Parisi 2019). This is particularly of interest, as the axon and particularly the growth cone are a significant distance from the cell body and therefore the cilium. This leads to the question of whether it is the cilium regulating these developmental processes or potentially cilia-associated factors that may not be functioning within the cilium during specific processes of developmental regulation.

Several mouse models of cilia-associated genes reveal axon guidance defects. When the Bardet-Biedl associated gene, *Bbs3*, is deleted, olfactory axon targeting is impaired (Tadenev et al. 2011). Genetic ablation of cilia via *Ift88* deletion in olfactory sensory neurons leads to abnormal axon targeting to the olfactory bulb (Green et al. 2018). Deletion of *Arl13b* or *Inpp5e* in projection neurons leads to abnormal targeting of cerebellar tracks to the thalamus (Guo et al. 2019). The data that cilia-associated proteins regulate axon guidance are a bit surprising as cilia project from the soma of the cell whereas the growth cone is at the tip of the axon, which can be a great distance away. Thus, the mechanism connecting cilia and axons is of great interest. One mechanism for cilia related axon guidance involves Shh signaling. As described, Shh from the neural tube floorplate attracts dorsal commissural axons to project to the ventral midline (Charron et al. 2003). Shh at the growth cone is interpreted by the receptor PTCH, co-receptor BOC and the pathway's obligate transducer SMO (Petralia et al. 2012; Okada et al. 2006). Instead of regulating Gli and transcription, Smo regulates the phosphorylation of Src family kinases which signals to control the local translation of actin (Okada et al. 2006; Yam et al. 2009; Lepelletier et al. 2017). *Arl13b* deletion results in aberrant Shh-dependent commissural axon pathfinding in the neural tube, linking a cilia protein to a non-ciliary process (Ferent et al. 2019).

ARL13B is one of the cilia-associated genes implicated in Joubert syndrome (Cantagrel, Silhavy, Bielas, Swistun, Marsh, Bertrand, Audollent, Attie-Bitach, Holden, Dobyns, Traver, Al-Gazali, Ali, Lindner, Caspary, Otto, Hildebrandt, Glass, Logan, Johnson, Bennett, Brancati, International Joubert Syndrome Related Disorders Study, et al. 2008). Interestingly, *ARL13B* need not be in the cilium to mediate its function in Shh-mediated axon guidance in commissural neurons of the neural tube (Ferent et al. 2019). It remains unclear whether additional ciliary

proteins function outside the cilium in axon guidance. Lepelletier et al. exposed cultured commissural axon projections to Shh signal, cut the axon away from the soma and observed normal growth cone turning towards the Shh cue (Lepelletier et al. 2017). This could be interpreted as the factors that mediate growth cone turning are in the axon which would predict that the 35+ cilia-associated proteins affected in Joubert syndrome may be found at the growth cone. However, it is not clear whether factors were transported to the axon prior to the axon being cut. In fact, other experiments manipulated ARL13B and INPP5E expression within cilia and concluded that they act from within cilia to control axonal targeting (Guo et al. 2019). In these experiments, the guidance cue being studied was not defined. Thus, the underlying mechanistic connection of cilia and axon guidance remains an open question in the field. Furthermore, recent evidence points to a role for cilia in neurite projection. Before an axon can be guided towards its synaptic target it must first initiate the building of the microtubule-based axon, which starts as a neurite projection. Work from Raman Das' group indicates that the cell must build a cilium in order for neurite projection to initiate (Toro-Tapia and Das 2020). The exact role of the cilium preceding neurite projection is unclear. It may indicate that cilia-associated proteins require a cilium to be present to be activated, or potentially this is merely a checkpoint step to ensure appropriate timing of projection in neuron development. In either case, this example highlights the complicated relationship between the cilium and proteins associated with the cilium that seem to function in pathways that do not require the presence of a cilium.

Activation of signaling pathways in the primary cilium can alter axon microtubule dynamics and dramatically impact the growth cone response to cytoskeletal remodeling

guidance cues (Guo et al. 2019). In the optic chiasm, two populations of ciliated retinal ganglion cells (RGCs) respond distinctly to Shh depending on the Shh activity level at specification. Contralateral RGCs are specified under high Shh activity whereas ipsilateral RGCs are induced under low Shh activity. Thus, contralateral RGCs predominantly produce Gli activator which induces target genes including Shh. Contralateral RGCs project from the retina first to the midline of the optic chiasm and are then guided across the midline. As they ramp up Shh mRNA production, contralateral RGCs transport Shh mRNA anterograde along the axon to release Shh signal from the axon shaft at the optic chiasm, a process that is SMO-dependent (Peng et al. 2018). The release of Shh from the contralateral RGCs predates projection of the ipsilateral RGC population. The ipsilateral RGC population projects axons to the optic chiasm and, without crossing the midline, into the optic tract of their own hemisphere. Due to ipsilateral RGCs being born under low Shh conditions, Gli activation is lowered to the level that induces transcription of Shh receptor *Boc*, not present in the high Shh contralateral population (Sanchez-Arrones et al. 2013). BOC in the ipsilateral RGC growth cone encounters Shh left behind by the contralateral RGCs at the optic chiasm and responds to Shh as a repulsing cue (Fabre, Shimogori, and Charron 2010). Through the transcription-independent Shh guidance pathway, the growth cone will depolymerize in the direction of Shh, thus preventing midline crossing of the ipsilateral population and allowing for proper projection (**Figure 1.10**). Thus, ciliary interpretation of signals can influence what effectors are trafficked to the growth cone and thereby how the growth cone will respond to guidance cues.

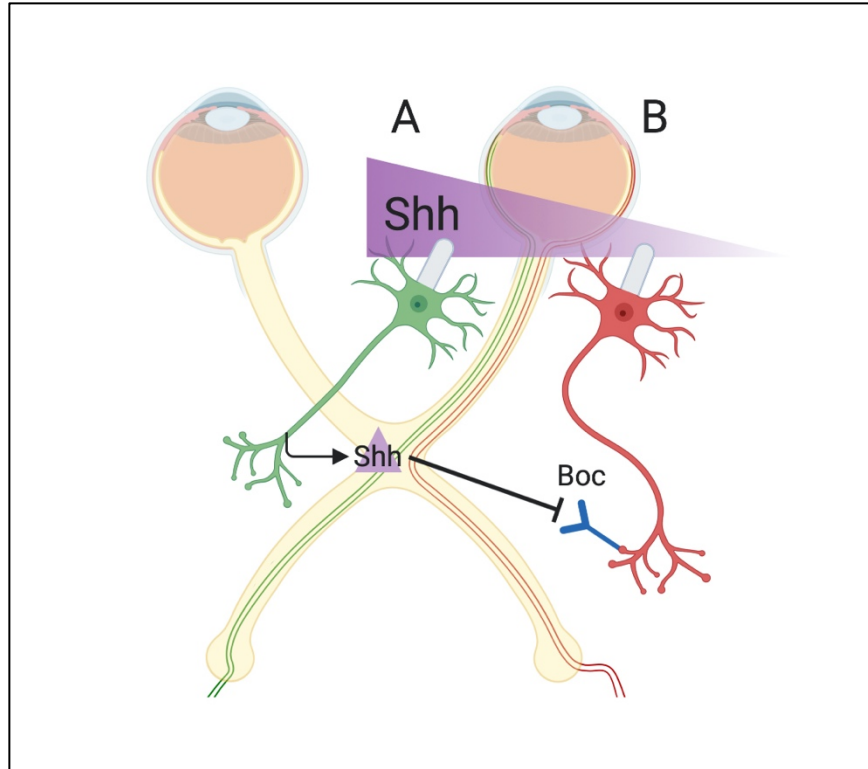


Figure 1.10 Distinct cilia-dependent transcription response to Shh distinguishes axon pathfinding. (A) Contralateral (green) retinal ganglion cells (RGCs) are specified due to high Shh activity (purple gradient) and produce Gli activator that induces Shh mRNA for transport into the axon. Contralateral RGC axons project across the midline of the optic chiasm where they release Shh signal. (B) Ipsilateral (red) RGCs are specified due to low Shh activity, resulting in Gli activator levels that turn on expression of Shh receptor, BOC. BOC is trafficked to the growth cone where it encounters Shh at the optic chiasm midline from the contralateral population. BOC interprets Shh as a repulsive cue so projects from the optic chiasm without crossing the midline.

1.5 Joubert Syndrome Overview

1.5.1 Joubert Syndrome characteristics and diagnosis

Joubert syndrome and related disorders (JSRD or JS) are congenital disorders caused by mutations in over 35 different cilia-associated genes (Parisi 2019). As it is caused by mutations in genes associated with the cilium, JS is classified as a ciliopathy. These mutations are autosomal recessive and result in developmental delays and intellectual disability, as well as craniofacial defects, polydactyl, and abnormal respiratory rhythms, such that JS patients often suffer and can die from apnea (Parisi et al. 2007). JS is published to have prevalence between 1:80,000 to 1:100,000 (Brancati, Dallapiccola, and Valente 2010). JS is diagnosed by a hindbrain malformation identified through MRI shaped like a molar tooth, and thus denoted the molar tooth sign (MTS) (**Figure 1.11**). While the etiology of the MTS is not known, from MRI it is clear that JS patients have axon guidance and decussation defects in the brain white matter tract superior cerebellar peduncles as well as hypoplasia or underdevelopment of the cerebellar vermis (Poretti et al. 2007; Yachnis and Rorke 1999). The superior cerebellar peduncles project from deep cerebellar nuclei out to the midline of the brain where they decussate or cross the midline before projecting to the contralateral thalamus. In fact, hindbrain nuclei are known to be linked to breathing problems, potentially underlying respiratory defects and apnea in patients who display the MTS (Onimaru, Kumagawa, and Homma 2006). Outside the MTS, JS patients also display decussation defects in the optic chiasm and the pyramidal tracts in the spine (Sanchez-Arrones et al. 2013; Fabre, Shimogori, and Charron 2010). While axon guidance issues are sometimes found in ciliopathies, JS is unique due to several clear instances of guidance defects (Guo et al. 2015).

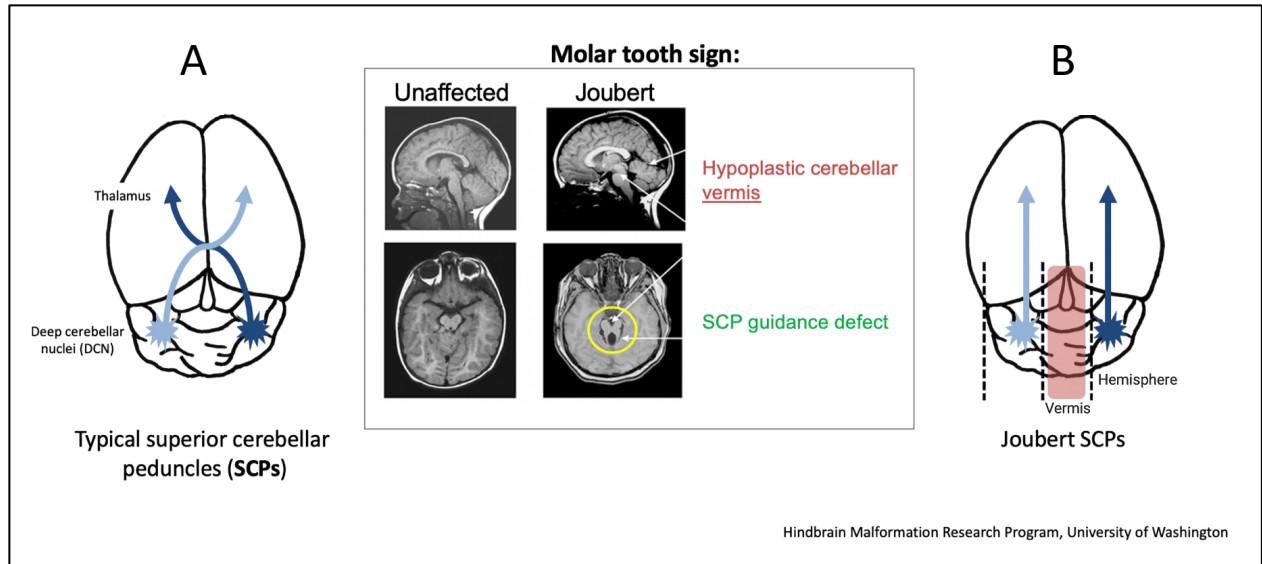


Figure 1.11 The Joubert Syndrome diagnostic criteria, the molar tooth sign, is made up of cerebellar hypoplasia of the vermis and a guidance defect in the superior cerebellar peduncles. (A) The superior cerebellar peduncles (SCPs) are a white matter tract that originate in the cerebellum. These deep cerebellar nuclei (DCN) project their axons out of the cerebellum into the cortex, where they will decussate or cross the midline of the brain before targeting projection to the thalamus of the hemisphere opposite the nuclei. (B) In Joubert syndrome, the SCPs fail to decussate, and project instead out of the cerebellum and into the thalamus of the same hemisphere. In addition to the SCP guidance defect, Joubert patients display hypoplasia, or underdevelopment of a particular region of the cerebellum. The cerebellum consists of a vermis at the midline and is bordered by two cerebellar hemispheres. In Joubert, patients display cerebellar vermis hypoplasia, with unaffected cerebellar hemispheres. The combination of SCP decussation failure and cerebellar vermis hypoplasia result in the hindbrain malformation molar tooth sign (yellow circle) shaped like a tooth when visualized in horizontal MRI imaging.

The MTS can be broken down to the cerebellar vermis hypoplasia and SCP guidance defects with a deepened interpeduncular fossa, or in terms of developmental processes: aberrant cell proliferation and axon guidance (Poretti et al. 2011b). A potential connection between these two pathways is the developmental signaling pathway Shh. Shh can regulate cerebellar proliferation as a mitogenic cue via a transcription-dependent mechanism and can act as a guidance cue for axon projection via a transcription-independent mechanism (Charron et al. 2003; Kenney and Rowitch 2000). Decreased

Shh could underly the cerebellar hypoplasia in the MTS (Kenney and Rowitch 2000; Dahmane and Ruiz i Altaba 1999; Wechsler-Reya and Scott 1999). Shh is a known axon guidance cue in commissural neurons and so it is possible that Shh is a cue involved in SCP guidance, none of which are currently known (Charron et al. 2003). Decussation of the optic chiasm is Shh-dependent so the defects in decussation shown by JS patients is consistent with abnormal Shh signaling underlying multiple aspects of JS (Fabre, Shimogori, and Charron 2010). Thus, I set out to assess ARL13B function the mouse brain with an emphasis in SCP guidance in order to determine whether Shh is a mechanistic link for the phenotypes of JS.

1.5.2 Genetic complexity of Joubert Syndrome

JS can be caused by mutations in any of 35 different cilia-associated factors (Parisi 2019). As cilia-associated genes, their respective proteins localize to the cilium or to ciliary structures such as the centrosome (Parisi 2019). As these proteins are ciliary, they are often involved with similar pathways or can even be interregulated. A prime example of this comes from my protein of interest ARL13B. Ciliopathies are well established to be genetically complex. Joubert Syndrome patients with different *ARL13B* mutations display distinct phenotypes among patients, such as obesity reported in the *ARL13B*^{Y86C} mutation and occipital encephaloceles in a family expressing *ARL13B*^{R79Q} (Cantagrel, Silhavy, Bielas, Swistun, Marsh, Bertrand, Audollent, Attie-Bitach, Holden, Dobyns, Traver, Al-Gazali, Ali, Lindner, Caspary, Otto, Hildebrandt, Glass, Logan, Johnson, Bennett, Brancati, International Joubert Syndrome Related Disorders Study, et al. 2008; Thomas et al. 2015). This is exemplified by related individuals carrying the same mutation with distinct phenotypic outcomes and even diagnoses. For example, JSRD-causing mutations in *TMEM67* (R208X) and *TMEM216* (R73H) can also

cause the more severe disease Meckel-Gruber syndrome (Valente et al. 2010; Otto et al. 2009; Consugar et al. 2007). Understanding the genetic modifiers underlying the phenotypic variation will be key to understanding disease etiology as will understanding when and how relevant pathways interact. In mouse models of the JSRD- and Meckel-Gruber Syndrome-linked gene *Tmem67* two phenotypic categories emerged: one with cerebellar malformations resembling JSRD and another with more severe CNS defects reminiscent of Meckel-Gruber syndrome (Abdelhamed et al. 2013). The two categories correlated with cilia retention, with the severe Meckel-Gruber-like phenotype in animals lacking cilia. Furthermore, the two groups impacted Hh and Wnt signaling differently pointing to both being critical (Abdelhamed et al. 2019). However, it is not a question of whether cilia are present. Another JSRD mouse model, *Talpid3*, lacks cilia yet displays a JSRD-like small cerebellar vermis (Bashford and Subramanian 2019). Thus, mouse models are incredibly informative yet point to the enormous complexity underlying the MTS.

1.6 The evolving connection of cilia to neuronal mechanisms of human disease

Despite being underappreciated by many neuroscientists, the cilium is required for many of the essential developmental processes leading to a mature nervous system. Dysfunction in any one step, or combination of steps, could underlie the intellectual disability found in many ciliopathy patients, particularly JS. Therefore, it is critically important to better understand the many functions of cilia in neural development. In addition to the roles in specification, proliferation, migration and axon guidance, cilia impact dendrites as well. Dendrite extension and connection is critical to build a synapse

and connect neurons to each other. In fact, in mouse models loss of cilia or cilia-associated proteins dramatically alters dendritic arbors and neuronal connectivity (Guadiana et al. 2013; Kumamoto et al. 2012). Understanding the mechanisms underlying the connection between cilia and dendrites will likely illuminate how circuitry is disrupted in cilia-associated neuropathies.

Cilia are critical for additional developmental processes, some of which are important for proper neural development. For example, *Ift172^{slb/slb}* mutants lack cilia in the E7.0 embryonic node, a critical signaling center for both anterior-posterior and left-right axis specification. These embryos fail to form anterior mesoderm which normally induces FGF8 at the midbrain-hindbrain boundary and is needed for growth in the telencephalon (Gorivodsky et al. 2009). Thus, critical roles of cilia-dependent signaling in diverse tissues at different timepoints may underlie the ultimate observed phenotype. This also underscores the challenges in pinpointing the disrupted process that is causal of intellectual disability.

While ciliopathy-related intellectual disability may represent multiple processes gone awry, other symptoms of ciliopathy-related neuropathies likely reflect functional dysfunction of cilia. For example, obesity is associated with Bardet-Biedl syndrome (BBS) (Guo and Rahmouni 2011). In mouse models, animals with neuronal cilia loss during adulthood develop obesity (Davenport et al. 2007). While the mechanisms behind this phenotype are not yet fully understood, it is clear that the signaling controlling satiety is misregulated in BBS patients. Furthermore, ciliary signaling has been implicated in the regulation of satiety (Vaisse, Reiter, and Berbari 2017). BBS patients also display photoreceptor dysfunction resulting in retinal degeneration starting in childhood (Beales et al. 1999). Photoreceptors are ciliated and mutations in cilia genes, particularly regarding microtubule transport mechanisms, result in retinal

degeneration (Chang et al. 2006). This example in particular highlights the necessity of microtubules and their modifications for continued neuronal function post-development.

Cilia are clearly fundamental to multiple aspects of neurodevelopment and function. As there are many ciliopathies that exhibit neurodevelopmental issues and neuropathies, the mechanistic connections of cilia-associated proteins and a functional nervous system will continue to grow in scope. Ciliopathies are rare diseases and as such, benefit greatly from whole exome and whole genome sequencing to identify players. We expect that complementary animal models will continue to aid the field as it pushes towards understanding the underlying mechanisms that grow the brain and wire neural circuitry.

1.7 Dissertation roadmap

From reviewing the field's understanding of the roles of cilia in distinct aspects of neurodevelopment, several questions begin to arise. Among these is the central connection of Joubert Syndrome, wherein a mutation in any one of the Joubert 35 cilia-associated genes always results in instances of axon guidance defects to form the molar tooth sign (Parisi 2019; Poretti et al. 2011b). Critically, the primary cilium remains at the cell body while the axon is incredibly dynamic, with the growth cone responding rapidly to external cues in a manner that makes cilia-dependent regulation of this process unlikely. However, this does not discount the idea that cilia-associated proteins are shown to localize and have function outside of the cilium leading to the central questions of my thesis; 1) does localization of cilia-associated ARL13B impact its function or regulatory mechanism? and, 2) can abnormal transcription-dependent and -independent Shh signaling explain the phenotypes displayed in Joubert Syndrome? My data will cover the

methods used to answer this question, including *in vitro* cell migration assays in fibroblasts, MRI imaging of mutated brains, and finally culminate with the data I have accrued through SCP tract tracing of *in vivo* mouse alleles. These models include deletion of *Arll3b* or *Smo* specifically in projection neurons; a JS patient allele, *Arll3b^{R79Q}*, which disrupts ARL13B GEF activity for ARL3; and an engineered mutation, *Arll3b^{V358A}*, which mutates the cilia localization sequence, excluding ARL13B from cilia without affecting its known biochemical function.

CHAPTER 2
MATERIALS AND METHODS

2.1 Mice

All mice were cared for in accordance with NIH guidelines and Emory University's Institutional Animal Care and Use Committee (IACUC). Lines used were *Nex-Cre* (*Neurod6^{tm1(cre)Kan}*)-C3H/HeJ [MGI:2668659](Schwab et al. 2000), *Brn4-Cre* (*Tg(Pou3f4-cre)32Cren*)-C3H/HeJ [MGI:2158470](Ahn et al. 2001), *Smo^{fllox}* (*Smo^{tm2AMC}*)-C3H/HeJ [MGI:2176256](Long et al. 2001), *Arll3b^{fllox}* (*Arll3b^{tm1Tc}*)-C3H/HeJ [MGI:4948239], *Arll3b^{V358A}*-C57Bl/6J (*Arll3b^{em1Tc}*) [MGI:6256969](Ferent et al. 2019), and *Arll3b^{R79Q}*-C57Bl/6J (*Arll3b^{em2Tc}*) [MGI:6279301]. Note that *Arll3b^A* is the deletion allele resulting from germline deletion of the conditional *Arll3b^{fllox}* allele. Genotyping was as previously described (Gigante et al. 2020; Goebbels et al. 2006; Heydemann, Nguyen, and Crenshaw Iii 2001; Nolan-Stevaux et al. 2009; Su et al. 2012a).

To generate the R79Q mutation in *Arll3b*, a CRISPR gRNA (ATTATTATGCTGAATCCTATGG) targeting exon 3 of the *Arll3b* locus along with a donor oligo (5'-GTTCCAAGTTACCATCTTTGACTTAGGAGGTGGAAAAAGAATTCAGGGCCATATGGAAGAATTATTATGCTGAATCCTATGGGGTAATATTTGTTGTGGATTCCAGTGATGAGGAGAGAAT-3'; underlined bases are engineered) were designed to generate a G-to-A change creating the R79Q point mutation as well as A-to-C and T-to-A silent changes to create a NdeI restriction site that could be used for genotyping (Millipore Sigma). The gRNA (50 ng/ul), oligo donor (50 ng/ul) and CRISPR protein (100 ng/ul) were injected into 1-cell C57Bl/6J zygotes and subsequently transplanted at the 2-cell stage into C57Bl/6J pseudopregnant females by the Emory Transgenic and Gene Targeting Core. Genomic DNA from toes was amplified via PCR using primers (5'-TCACTTGCAACAGAGCATCC-3') and (5'-

ACAGCTCTGCCCGTGTTTAC-3') located upstream and downstream of the donor oligo breakpoints; products were sequenced with the forward (first) primer. A single founder animal heterozygous for both the R79Q mutation and NdeI restriction site was identified with no additional editing. Subsequent allele-specific genotyping of progeny was performed on ear punch or yolk sac using the following primers: Fwd-wt primer: 5'-GGAGGTGGAAAAAGAATaCg-3'; Fwd-mut primer: 5'-gctctatggctgGGAGGTGGAAAAAGAATTga-3'; Rev primer: 5'-AGTGCTAAGACACCCGAGGA-3'. PCR bands at 142bp (wild type) and/or 154bp (mutant) were produced, due to the addition of 12 non-templated bases to the 5' end of the Fwd-mut primer (lowercase). Note the 3' ends of the two forward primers differed in the base that codes for the R to Q change (final nucleotide of the primer) and includes a "wobble" base (lowercase) to provide allele-specific amplification after the first round of PCR (Gaudet et al. 2009).

2.2 Western blots

MEFs were washed in PBS, detached with 0.25% trypsin, resuspended in MEF media, and centrifuged to form pellets. Cell pellets were either lysed immediately or frozen at -80°C until lysis. Cell lysis was performed using modified RIPA buffer plus SIGMAFAST protease inhibitors (S8820). Modified RIPA buffer is 50 mM sodium-Tris, pH 7.4, 150 mM NaCl, 2% (vol/vol) NP-40, 0.5% (wt/vol) deoxycholate, 0.1% (wt/vol) SDS, and 1 mM DTT. Lysates were clarified by centrifugation at 20,000 × g at 4°C for 45 min. A 20-µg amount of protein was separated on 10% Bio-Rad Mini-PROTEAN TGX Stain-Free Precast Gels (4568034). Gels were imaged after activation using the

Bio-Rad ChemiDoc Touch Imaging System and transferred to a 0.2- μ m nitrocellulose membrane using the Bio-Rad Trans-Blot Turbo Transfer System with the Bio-Rad defined High Molecular Weight setting. Blots were imaged again to ensure proper transfer before being blocked for 30 min with Pierce Superblock T20 (PBS; 37516). Primary antibodies were diluted in T20, and blots were incubated in primary antibody overnight at 4°C.

Blots were rinsed three times for 5 min each in Tris-buffered saline plus Triton X-100 (TBST) and incubated with secondary antibodies diluted in 5% (wt/vol) milk in TBST for 1 h at room temperature. Blots were rinsed three times for 10 min each in TBST before a 5-min incubation in Amersham ECL Prime Western Blotting Detection Reagent (GE Healthcare; RPN2232V1). Blots were then imaged for chemiluminescence using the ChemiDoc Touch Imaging System. All analysis of Western blots was done using Bio-Rad ImageLab software. Bands were normalized to an unprobed control protein as measured on the stain-free gel as a loading control. Protein bands of interest were normalized to a loading control protein as measured on the stain-free gel.

2.3 Fibroblast migration assays

MEF migration assays were performed using the FluoroBlok Transwell system (BD Falcon) as in (Bijlsma, Damhofer, and Roelink 2012). Before beginning the migration assay, MEFs were washed with PBS and incubated with 10 μ M CellTracker Green in serum-free DMEM for 1 hour (dye was pre-equilibrated in serum-free DMEM for one hour before use). Cells were detached using 5 mM EDTA in PBS, resuspended and washed in serum-free DMEM, and transferred to a Transwell insert (8 μ m pore size) in 100 μ L of medium at a concentration of 50,000 cells/well. The lower portion of the Transwell plate contained 600 μ L of control or

attractant (0.1 $\mu\text{g/mL}$ rShhN or 2 μM purmorphamine) medium. During migration, the plate reader measured fluorescence in the lower portion of the Transwell plate once every 2 minutes for ~ 3 hours.

To analyze migration data, several corrections were applied. Background fluorescence was controlled by subtracting the average value of plate reads from a blank well (containing medium but no cells) over the course of the entire experiment from each individual plate read for the cell-containing wells. Non-specific migration of each cell line was controlled by subtracting the average fluorescence of cells migrating toward control medium from each individual plate read for the corresponding cells in the attractant condition. Finally, migration curves for each cell line were made more directly comparable by setting the starting point of each normalized migration curve to zero. This was done by subtracting a normalizing value from every point on the migration curve such that the value of the first point on the curve was equal to zero. Pooling data was done using these normalized curves expressed relative to the Arl13b^{WT}-GFP control from each experiment, or relative to the GFP-only control.

2.4 Dissection and culture of embryonic spinal cord

E11.5 pregnant dams were euthanized via cervical dislocation. embryos were dissected into cold L-15 medium. Embryos were placed and the head and posterior region was cut away head and posterior region at the angles shown in **Figure 2.1a**. Two sets of forceps were used; one to hold the embryo in place and one to peel off the skin covering the back of the embryo starting in between the "holding" forceps. Tissue to one side of the spinal cord was punctured with closed "free" forceps, as close to the spinal cord as

possible. the forceps were slowly opened to tear the tissue, detaching the dorsal root ganglia. Starting from the anterior end, a hook-shaped tungsten needle was used to carefully open the spinal cord by dragging the needle along the midline then to detach the tissue from both sides of the embryo. The spinal cord was detached from the disrupted tissue using a scooping motion with the forceps. The meninges and the spinal cord are visualized as two "sheets" of tissue apposed onto each other. The separation of the two layers was identified near the hindbrain, both layers held by forceps, and slowly peeled away from each other in a smooth, constant movement (Figure 2.1j). The spinal cord was then moved to to a Petri dish containing L-15 + 10% HiHS on ice and the wide anterior portion was cut away. Tungsten needles were used to cut out lateral strips at 1/5th the width of half the spinal cord and transferred to a 15 mL plastic tube containing L-15 + 10% HiHS on ice (Figure 2.1l, right).

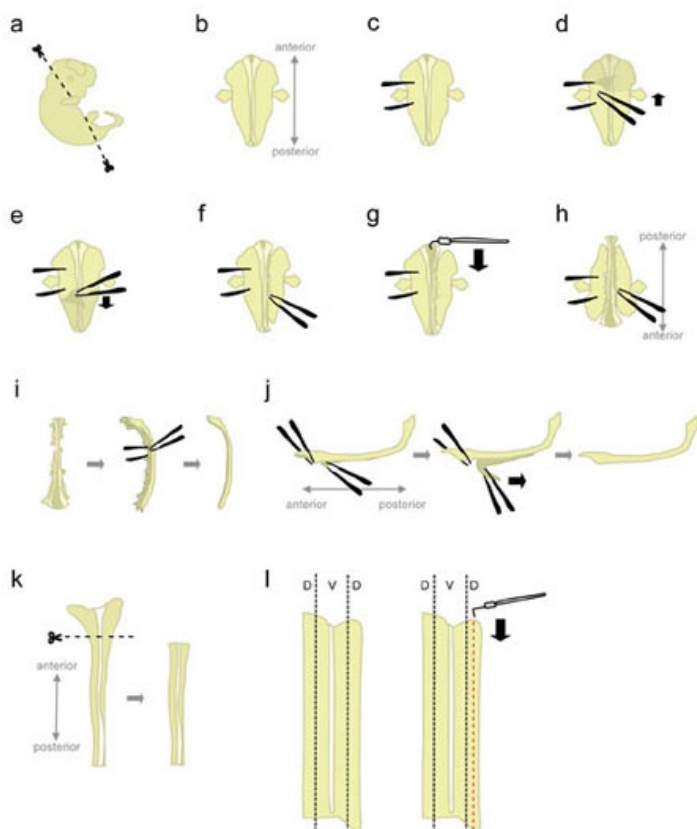


Figure 2.1: Spinal cord dissection steps. D=Dorsal, V=Ventral.

Glass coverslips were coated with a small dome of 100 ug/mL 1x PLL solution for 1.75-2 hrs prior to plating and washed in water, preventing drying out. Dosal strips were washed in cold HBSS (Ca²⁺/Mg²⁺-free) using pipettes then transferred to 37 °C HBSS with 0.15% trypsin and incubated for 7 minutes. DNase and MgSO₄ were added to concentrations of 150U/mL and 0.15% respectively. Tissue fragments were twice centrifuged and washed in warm HBSS. Cells were dissociated via mechanical disruption pipetting with decreasing diameter glass Pasteur pipettes (fire-polished via Bunsen burner). Cell suspension was counted in a haemocytometer using trypan blue marker and plated at ~75,000 cells/well in neurobasal plating media (12.7 mL Neurobasal, 1.3 mL Heat-inactivated FBS, 130 µL L-glutamine, 65.0 µL Penicillin/Streptomycin antibiotics). After 18 hours the media is changed to Neurobasal Growth Media (49.0 mL Neurobasal, 500 µL L-glutamine 250 µL Penicillin/Streptomycin antibiotics [1:200] 1 mL B27), with subsequent changes every two days.

2.5 Diffusion Tensor Imaging (DTI)

DTI scans were performed by the Emory MRI core and headed up by Jeakuen Park. Scans were completed in ex-vivo whole brain tissue, that had been perfused, drop fixed, and embedded in agarose. Scans were delivered through the core server, and interpreted locally using terminal-run FSLView, a 2D and 3D brain volume viewer. Through FSLView, the T1 scan is initially analyzed. The T1 scan, or typical anatomical image is used to locate the SCPs within the brain, and then region of interest (ROI) masks can be drawn. ROI masks are drawn with 3D aspects of the brain in mind, with each pixel (visualized in the 2D space in the scan image) representing a 3D “voxel” in the scan.

Voxels are used as 3D pixels such that as you move through the T1 scan dorsal to ventral, you can capture the entirety of the tract. In fact, it took about 6 horizontal slices of the scan in order to capture the SCPs. ROIs were made on the SCPs in voxels, and those ROIs were remade two more times. Thus, every brain scan had 3 separate ROI masks drawn for its T1 scan. The program will save the ROI mask made, and through interface can be applied to the V1 scan.

The V1 scan is the first eigen vector image. Eigen vectors represent the degree to which the measured movement through a white matter tract is medial/ lateral, rostral/ caudal, and dorsal/ ventral. The first Eigen vector, visualized in V1, is the primary direction of movement through a given white matter tract. From patient SCP DTI scans, we initially expected to see a loss of medial/ lateral movement and an increase in rostral/ caudal movement in the V1 at the point of SCP crossing. However, I was unable to determine any change in the direction of movement in the SCP midline. This is where directionality can be expanded through use of the other eigen vectors, V2 and V3. These secondary and tertiary directions of the tract, respectively, can be used with V1 to determine the fractional anisotropy, or directionality of the tract.

Fractional anisotropy is the degree to which the first eigen vector V1 (the direction of the movement measured most) wins out over the alternative vectors V2 and V3 (Alexander et al. 2007). As such, a high fractional anisotropy would arise from the first eigen vector being the direction strongly exhibited by the measured movement, and be closer to 1 than 0 (illustrated in **Figure 4.1**). A low fractional anisotropy would indicate the first eigen vector is the most exhibited direction, but not by very much, and so would be closer to 0 than 1. In this way, the overall directionality of a white matter tract can be established and to a degree, the organization or firmness of that directionality can be measured. However, it is not possible to distinguish decussation from tract “kissing” in DTI (Jbabdi and Johansen-Berg 2011). Kissing tracts indicate

that two sides of the tract project towards each other but fail to decussate. In this way, the tracts primary direction at the point of decussation would still read as medial/ lateral, although the tracts themselves do not cross over each other or decussate. This would result in a typical looking DTI scan, and thus the guidance defect would be masked. This caveat must be kept in mind while interpreting DTI data, and therefore what DTI can tell us about the tract is limited. The 3D voxel masks of the SCP ROI are used to get the FA of the region and were compared across genotypes. As three ROI masks were made per brain, the FA was averaged for relevant voxels and that FA average value can be combined with the FA of the other brains of that genotype.

However, resolution of the brain in DTI scans are quite variable, and thus normalization was attempted. Because the corpus callosum is a white matter tract with strong directionality, that is an FA close to one in the primary direction of medial/ lateral, it seemed an optimal white matter tract to measure and normalize against. As in the SCPs, 3 ROI masks were drawn over the corpus callosum in the T1 scan and the FA of the CC was averaged. Using the FA of the CC, I created a normalization method similar to that used in the western blot normalization (Chapter 3). I collected the FA of the corpus callosum for each brain, and then arbitrarily set the first measure at 1. To do this, the FA of brain one was divided by itself, thus equaling 1. Going forward, the FA of brain one was divided by all the other brain CC FAs, resulting in a ratio of the FA of brain two compared to brain one, and so on. If a brain sample had a higher FA value than brain one, the resulting normalization factor would be less than 1, such that the CC FA would be brought down to the level of brain one, and that same normalization factor would be applied to the FA measured in that brain's SCP. In contrast, if a brain sample

had a lower FA value than brain one, the normalization factor would be greater than one, bringing that CC FA up to the level of brain one and that normalization factor would be applied to the FA of the brain's SCP.

As described, ROI masks were drawn on the corpus callosum in an attempt to have an FA measure to use for normalization purposes across brains. However, I was later an author on our collaborators' paper that indicated loss of ARL13b has organization consequences for the CC with the tract expanded and less organized (aberrant CC fibers not in line with the tract, diffuse tract). Thus ultimately, this method was not used for normalization.

Mice were perfused with 50mLs of PBS followed by 30mLs of 4% PFA. Brains were kept in PFA overnight and subsequently embedded in agarose. Scans were obtained from Jeakeun Park at the 9.4 T Bruker BioSpec MRI machine located in Whitehead Biomedical research building room L05. To acquire FA data from the DTI scans, we used Unix to run FSLView version 3.2.0 on the Emory CSI/BITC server. Using the code flsview we opened the T1 file and moved to the Z plane where the dark pigment of the SCP voxels at the midline indicate the start of midline crossing. We then used the create mask option's pencil tool to color SCP voxels that were at the midline through all of the relevant Z planes, stopping when the light voxel pigment indicated we had reached the boundary of the tract. The mask was saved to the server and the command `getMeanValueMask` using the T1 mask on the FA file. This mean FA value was recorded. The process was repeated twice, such that three masks of the SCP voxels crossing the midline were made on each brain. The average of the mean FA values was recorded as the FA value for that brain.

2.6 Tract tracing injections and analysis

SCP projection was analyzed in my work using a precise stereotaxic injection procedure of a fluorescent dextran that is absorbed into myelinated axon tracts. The dye can be injected either at the proximal end of the axon at the cell body (anterograde diffusion) or at the distal end where the tract has terminated projection (retrograde diffusion). Through this method we can answer distinct questions. To inject tracer at the cell bodies of the DCN displays the axons' total projections. In this way, it could be observed where the SCP tract projects, if and at what rostral caudal point does it decussate, and the degree to which the directionality is followed by all axons within the tract. While my efforts towards these anterograde injections and their visualization through the brain clearing technique CLARITY will be discussed, the majority of my experiments were done in retrograde by injecting tracer into the terminal projection sites of the SCPs at the thalamus. Through retrograde tracing injections, the cell bodies that have axons projecting to that site will become illuminated, as the tracer follows the myelinated axon bundle towards the projections' source. By injecting a small amount of tracer in the SCP projection site in the thalamus of one hemisphere, we can prevent tracing both tracts of the SCPs and more carefully examine the nature of one hemisphere's tract. The location and density of the SCP decussation can also be seen in this type of injection by identifying traced axons in a bundle at the site of midline crossing.

A further implication of retrograde vs anterograde tract tracing involves how the tract can be visualized and imaged. Retrograde tract tracing injects the projection site to visualize the cell bodies, and in this way coronal sectioning of the brain makes sense. The tract will not be visible during any point where it projects rostral to caudal in coronal

sections, as sectioning through a line would appear as merely a dot in this orientation. However, the point of SCP decussation, where the tract moves medial/ laterally, is easy to visualize in coronal sections, as are the DCN cell bodies. However, coronal sectioning of an anterograde injection, is not useful, as the projection site would look like nothing more than dots, or perhaps a haze. Thus, horizontal sectioning was ultimately used to characterize these anterograde traces. This plane of visualization is not without its own caveats, where project rostral to caudal will now be visualized, any projection dorsal ventral would only appear as a dot. Furthermore, while the projection site of the SCPs is restricted to a small, easy-to-inject region of the thalamus, the origin of the tract is much more diffuse. The DCN are spread throughout the rostral-caudal axis of the cerebellum. The three populations of DCN; fastigial, interposed, and dentate, can all be identified through staining in multiple areas of the cerebellum, too spread out to accurately and effectively hit all of the cell bodies (Bohne et al. 2019). This caveat results in a lack of ability to identify the entirety of the tract in anterograde, though despite this caveat I was able to make some important conclusions via this method.

In particular, the limitations of the horizontal visualization plane went on to help me identify the SCP guidance defect in the absence of *Arl13b* or *Smo* and could be further reduced through the use of 3D visualization such as CLARITY (Treweek et al. 2015).

Tract tracing experiments were performed in accordance with the protocol approved by Emory University's Institutional Animal Care and Use Committee (IACUC). Male and female mice at P90 or older were used for tract tracing experiments. At least 3 mice of each genotypic group were analyzed in experiments. Mice were anesthetized with inhaled isoflurane and maintained under anesthesia throughout the procedure. 5mg/kg of Metacam Meloxicam diluted in Bacteriostatic saline were injected subcutaneously prior to incisions as an analgesic. Animals

were secured in a Stoelting stereotax (provided by the Weinshenker lab), and the scalp was cleaned with Prevacics (provided by DAR) and opened with bregma and lambda aligned to flatskull position. The stereotaxic arm was lowered to the mouse bregma skull landmark, then adjusted to the coordinates for the injection and a small hole was drilled using an Ideal Micro-Drill in the skull at these coordinates unilaterally. Stereotaxic coordinates were taken from “The Mouse Brain in Stereotaxic Coordinates” third edition by Franklin and Paxinos: cerebellar injections were targeted to the bregma (AP:-6.24, ML:+1.50, DV:-2.6, Angle:0°), dorsal thalamus injections were targeted to the bregma (AP:-0.70, ML:+1.13, DV:-3.28, Angle:0°) and ventral thalamus injections were targeted using coordinates to the bregma (AP:-0.70, ML:-3.11, DV:-4.69, Angle:25°) (Franklin and Paxinos 1997). Ventral injection targeting includes a 25° angle to avoid pulling dye through the dorsal thalamus upon needle removal. Then, a 5 ul Hamilton microsyringe was lowered to target and target was injected with lysine fixable dextran tetramethylrhodamine neuroanatomical tracer (fluoro-Ruby, 10,000 MW, ThermoFisher Scientific D1817). Animals received 0.05 - 0.5 ul injections of 10% dextran tetramethylrhodamine in sterile phosphate buffered saline (pH = 7.25) unilaterally at a rate of 0.1 ul/minute using a Stoelting Quintessential Stereotaxic Injector pump. The head wound was closed using VetBond tissue glue and mice were closely monitored for signs of distress during a 3-day recovery period (lack of nestlet tearing or eating/ defecation, hunched position).

Seven days post-procedure mice were perfused with 50mLs of PBS followed by 30mLs of 4% PFA. Brains were kept in PFA overnight and subsequently placed in 30% sucrose in 0.1M phosphate buffer (pH 7.3) for cryoprotection for at least 48 hours. Brains

were then embedded in Tissue-Tek OCT for coronal sectioning on a Leica CM1850 cryostat at 60 microns thick and processed through 70% ethanol dehydration and 0.1% sudan black autofluorescence quencher, rehydrated in PBS and DAPI nuclei staining was performed prior to fluorescence imaging. Images were taken on a Lionheart or Leica CTR6000 microscope at 5x using SimplePCI in overlapping areas to allow stitching and montaging of images to reveal the entirety of the brain section in Fiji or Photoshop. Pre-established exclusion criteria removed any sample for which the injection was not properly targeted. Surgical injection sites were assessed to ensure dye was present at the desired injection site. If the injection was off-target (determined by rostral-caudal landmarks as defined by “The Mouse Brain in Stereotaxic Coordinates” stereotaxic coordinate atlas) or dye at the injection site was not seen, samples were removed from analysis. Cerebellar images from injections were evaluated for DCN staining with assessor blinded to genotype. The number of injections that resulted in fluorescent DCN for each injection site (dorsal and ventral thalamus) were compared between genotypes using a two-sided Fisher’s exact test.

2.7 CLARITY and tissue clearing

CLARITY was performed using the method described in (Treweek et al. 2015) with additional reagents made as described in the CLARITY Wiki solutions page (<http://wiki.claritytechniques.org/index.php/Solutions>). Hydrogel monomer solution was prepared the day of perfusion and was injected into the heart during perfusions in lieu of 4% PFA. Tissues remained in clearing solution in light-protected tubes for 90 days and checked frequently for tissue clearing. 3D tissue imaging was performed using the Leica SP8 scope provided by the Emory University Integrated Cellular Imaging core.

Furthermore, a similar but much less intensive type of clearing using TDE was explored (Aoyagi et al. 2015). In this method, an alternative cryostat was used to section brains horizontally at 300 microns thick. This increase in thickness, compared to the 60-micron thickness of previous horizontal sections, would allow for greater visualization of the SCP tract as it would be less divided among horizontal sections. Upon introduction of sections to 10 minutes of 60% TDE, tissue became less opaque (**Figure 2.2**).

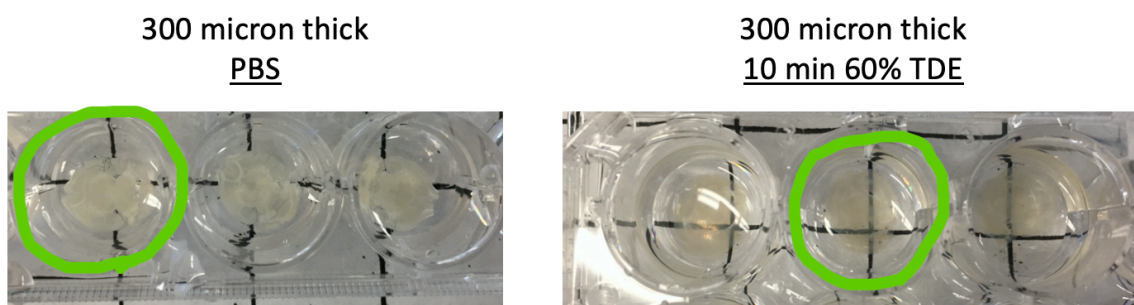


Figure 2.2 TDE clearing. Tissue in PBS remains opaque while tissue in 60% TDE becomes translucent.

2.8 Analysis of cerebellar hemisphere and vermis size

P21-P24 male and female mice were sacrificed and brains were harvested and fixed in 4% PFA for 24 hours. Three mouse brains were collected for each genotype. Brains were transferred to 30% sucrose in 0.1M phosphate buffer (pH 7.3) for 48 hours, embedded in OCT compound. Animals within genotypic groups were embedded to randomize examination of both left and right hemisphere. 60-micron sagittal cryosections were collected through either the left or right cerebellar hemisphere and the entire vermis. Sections were stained with DAPI and 4x images of each section were collected and tiled

(Lionheart with BioTek Gen5 software). For each image, the analyst was blinded to the genotype of the sample, the cerebellar sections were outlined, and the cerebellar area was measured in pixel area (Photoshop). The images were divided into hemisphere or vermis based on foliation, size and location. Mean area for each hemisphere or vermis sample was calculated and averaged within the genotypic groups.

CHAPTER 3

MEASURING CELL RESPONSE TO SHH AS AN ATTRACTIVE CUE

Parts of this chapter published in:

Mariani, L. E., M. F. Bijlsma, A. I. Ivanova, S. K. Suci, R. A. Kahn, and T. Caspary. 2016.

Arl13b regulates Shh signaling from both inside and outside the cilium, *Mol Biol Cell*.

3.1 Abstract

Fibroblast migration is a cellular process of movement that is associated with Shh as an attractive cue. Fibroblasts in culture will migrate towards Shh signal in a SMO-dependent mechanism that is transcription-independent. Cellular migration is regulated through Shh, however, in the absence of a cilium migration is increased compared to ciliated cells indicating Shh-dependent migration takes place outside the cilium. Previous graduate student Laura Mariani, PhD, showed that while a cilium is not required for fibroblast migration, migration will cease if ARL13B is excluded from the primary cilium. This indicates that ARL13B must either function within cilia for migration, or that ARL13B requires interaction with a cilia-localized effector to regulate migration. Here I describe Laura's results as well as my efforts to continue these studies through fibroblast migration assays. I found that fibroblast migration assays are inconsistent and explored the possibility of moving these analyses into cultured commissural neurons.

3.2 Introduction

Shh signaling uses a transcription-independent pathway to regulate Shh-dependent migration in fibroblasts. Through a transcription-independent mechanism, Shh acts as a chemoattractant for fibroblasts in culture (Bijlsma et al. 2007; Charron et al. 2003; Yam et al. 2009). Fibroblasts migrate towards a concentration gradient of Shh whereby induction of cytoskeletal rearrangements at the cell's leading edge move the fibroblast towards the Shh source (Bijlsma et al. 2007). The rapid cytoskeletal rearrangements for fibroblasts requires SMO and leukotriene synthesis (Bijlsma et al. 2007; Bijlsma et al. 2008; Yam et al. 2009; Bijlsma, Damhofer, and Roelink 2012). Furthermore, fibroblasts lacking ARL13B display decreased migration toward

Shh (Bijlsma et al. 2007; Mariani et al. 2016). Interestingly, fibroblasts lacking cilia, or expressing a non-ciliary SMO variant, show increased migration toward Shh (Bijlsma, Damhofer, and Roelink 2012). These results suggest a non-ciliary role for these cilia-associated proteins in the regulation of transcription-independent Shh signaling.

Building off of this background, Caspary Lab alumna Laura Mariani, PhD set out to investigate the effects of disease-causing and other mutations in *Arl13b* on cilia morphology and Shh signaling. Previous studies of ARL13B's function in Shh signaling relied on null or conditionally deleted alleles of *Arl13b* (Caspary, Larkins, and Anderson 2007; Horner and Caspary 2011; Larkins et al. 2011; Su et al. 2012b). Furthermore, these studies only examined transcriptional Shh signaling. Laura's goal was to analyze the effect of JS-causing and other point mutations on both transcription-dependent and transcription-independent Shh signaling, with the hope of defining the role of ARL13B in regulating Shh signaling in normal and disease states. To achieve this goal, she expressed ARL13B variants in mouse embryonic fibroblasts (MEFs) that lacked endogenous *Arl13b* and subjected them to a variety of assays investigating cilia, transcription-dependent Shh signaling (via Shh target gene expression), and transcription-independent Shh signaling (via Shh-dependent chemotaxis).

To study possible cilia-independent functions of ARL13B, Laura designed a mutation that would disrupt its cilia localization. ARL13B contains a cilia localization signal (CiLS) homologous to the VxP-containing CiLS motifs in rhodopsin, polycystin-1, and polycystin-2 (Deretic et al. 2005; Geng et al. 2006; Ward et al. 2011). Other studies have confirmed that this motif in ARL13B is required for its cilia localization (Cevik et al. 2013; Higginbotham et al. 2012b). To test the effects of excluding ARL13B from

cilia, she generated an *Arl13b*^{V358A} point mutation that disrupts the CiLS motif. Our collaborators find that ARL13B^{V358A} displays rates of GTP hydrolysis indistinguishable from wild-type ARL13B protein (Mariani et al. 2016). Furthermore, ARL13B is an ARL3 guanine exchange factor (GEF), and ARL13B and ARL13B^{V358A} show identical GEF activity for ARL3 (Gigante et al. 2020). Thus, ARL13B^{V358A} is biochemically active in known functions and is an ideal tool to examine ARL13B's role in transcription-independent Shh signaling. Previous studies identified JS patients with homozygous R79Q mutations in *ARL13B*, a point mutation that disrupts the GTPase domain of ARL13B, which Laura generated as *Arl13b*^{R79Q} (Cantagrel, Silhavy, Bielas, Swistun, Marsh, Bertrand, Audollent, Attie-Bitach, Holden, Dobyns, Traver, Al-Gazali, Ali, Lindner, Caspary, Otto, Hildebrandt, Glass, Logan, Johnson, Bennett, Brancati, International Joubert Syndrome Related Disorders Study, et al. 2008; Thomas et al. 2015). These variants were transfected into MEFs null for ARL13B, called *Arl13b*^{hmn} (Caspary, Larkins, and Anderson 2007).

Laura's data is summarized in **Table 3.1**. She found that while ARL13B^{V358A} and ARL13B^{R79Q} did not display aberrant ciliation rates, cilia expressing non-ciliary ARL13B^{V358A} were shorter than in controls. ARL13B is involved in tethering ciliary glutamylases, critical for axonemal microtubule stability, to the base of the cilium (He et al. 2018). Excluding ARL13B from cilia could potentially disrupt ciliary glutamylation, and therefore may explain the loss of ciliary length and stability in ARL13B^{V358A}. Thus, it is perhaps unsurprising that cells expressing cilia-excluded ARL13B^{V358A} display a length phenotype. Furthermore, ARL13B^{R79Q} cilia were shorter than controls, also possibly implicating a loss of ARL13B function in glutamylase tethering. However, despite not being localized to the cilium, ARL13B^{V358A} was sufficient for normal Shh-dependent SMO accumulation in the cilium, a process disrupted in the total absence

of ARL13B. Furthermore, ARL13B^{V358A} displayed no issues in transcription-dependent Shh signal output.

Arl13b variant (in hnn MEFs)	Mutation type	Cilia number	Cilia length	Smo in cilia	Shh migration
WT-GFP	N/A	Normal	Normal	Normal	Normal
GFP only	Null	Normal	<u>Short</u>	<u>Abnormal</u>	<u>Impaired</u>
R79Q-GFP	JS	<u>Varied</u>	<u>Short</u>	Normal	Normal
V358A-GFP	CiLS	Normal	<u>Short</u>	Normal	<u>Impaired</u>

Table 3.1 Summary of Mariani results from *Arl13b*^{hnn} MEFs. Results of experiments testing the effects of expressing ARL13B variants ARL13B^{R79Q} (GTPase domain mutation) and ARL13B^{V358A} (cilia localization mutation) in *Arl13*^{hnn} MEFs.

Laura observed that JS-causing ARL13B^{R79Q} variant had no significant effect on migration toward Shh compared to controls. However, the ciliary localization mutant ARL13B^{V358A} behaved similarly to *Arl13b*^{hnn} MEFs that lack ARL13B, and thus ARL13B needs to be localized to the cilium to regulate migration. Fibroblasts require both ARL13B and SMO in order to migrate towards Shh, however, fibroblasts do not require cilia for migration. It is possible that in a ciliated fibroblast, cilia-associated factors such as required obligate transducer SMO are preferentially localized to the cilium, thus sequestering non-ciliary ARL13B from necessary factors. Laura's data further shows that SMO localization to cilia is normal in MEFs expressing cilia-excluded ARL13B^{V358A}.

I aimed to examine whether ARL13B function is independent of the cilium by testing ARL13B^{V358A} for sufficiency in fibroblast migration, as well as test whether ARL13B function occurs outside of the cilium by using ARL13B^{V358A} in conjunction with other ciliary factors also excluded from the cilium. Fibroblasts display stronger migration towards Shh in the absence of cilia or with a non-ciliary *Smo* mutation, *Smo* Δ CLD, in which the cilia localization domain (CLD) has been deleted (Bijlsma, Damhofer, and Roelink 2012). Thus, I set out to test whether ARL13B function in fibroblast migration occurs outside of the cilium using ARL13B^{V358A} with non-ciliary SMO Δ CLD. Our collaborator Maarten Bijlsma, PhD trained me to test the ability of experimental MEFs generated by Laura to migrate towards Shh using the modified Boyden chamber assay (**Figure 3.1**). This procedure involves seeding MEFs in typical media in an upper chamber which is separated by a microporous membrane from a lower chamber containing Shh-infused media. Chemotaxis of MEFs towards Shh media is measured by the amount of GFP fluorescence on the lower side of the membrane every 3 minutes for 3 hours. With this assay, I attempted to test how the localization of ARL13B and SMO in fibroblasts affects fibroblast migration, a readout for transcription-independent Shh signaling.

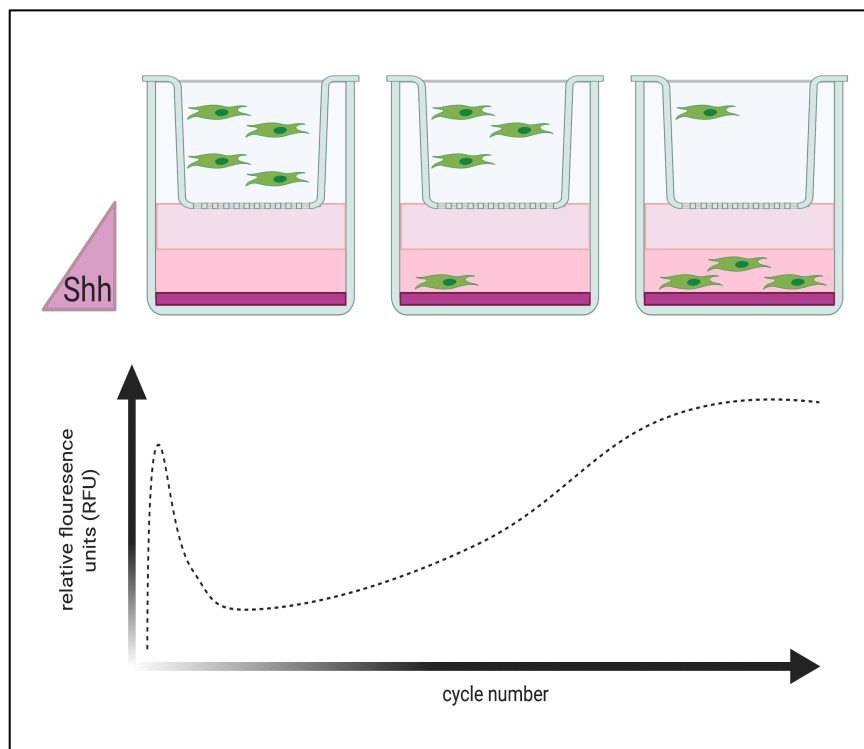


Figure 3.1 Illustration of fibroblast migration assay. Along the X-axis is cycle number, or points in which the data is acquired. Along the Y-axis is the relative fluorescence units, or the amount of GFP in the lower Shh-containing chamber. Above in the representative chambers, fibroblasts will migrate towards Shh over the cycles and thus more GFP will be measured. This involves some noise at the beginning of the assay which requires subjective normalization.

3.3 Results

3.3.1 Lentiviral infection in MEFs drives expression of *Arl13b* constructs

To test the effects of *Arl13b* mutations in the absence of wild-type ARL13B, Laura infected MEFs lacking endogenous ARL13B with lentivirus driving the expression of wild-type or mutant ARL13B-GFP fusion protein, or a GFP-only negative control. (Casparly, Larkins, and Anderson 2007). She then used FACS to purify GFP-positive cells and performed all assays on these heterogeneous cell populations, which are

composed of cells with different insertion sites for the lentiviral expression vector and variable ARL13B-GFP expression levels. I performed western blots on lysates from these cell lines in order to determine the ARL13B-GFP variants protein expression level.

During these efforts I attempted several normalization processes to avoid stripping and re-staining the blots for a housekeeping protein for normalization purposes. To accomplish this, I used the Biolab Chemidoc Gel Imager along with specialized stain-free gels to run the westerns. The benefit of this method is the gel itself can be imaged, prior to blotting. This image shows all protein present in the experiment. From this image, I selected a particular band to use as a normalization factor (**Figure 3.2**). I found that normalization to a chosen band was more consistent than normalization to the total protein in a lane. Normalization involves the imaging software giving intensity to the band selected from each lane at the same molecular weight for comparison. The program will arbitrarily give the first band a value of 1.0, and assess the other bands in comparison to the first band. For example, if band two is more intense and therefore has more protein than band one, band two will be given a normalization factor less than 1.0 such that the band of protein of interest can be normalized by that factor and compared to other lanes. Similarly, if band three is less intense and has less protein than band one, it will be given a normalization factor greater than 1.0 to bring the ARL13B level of that lane up to that of band one. From these efforts, I detected expression of the assayed ARL13b-GFP variants (**Figure 3.3**). I further concluded that while transfections were successful, there is a range of variation of expression of these variants.

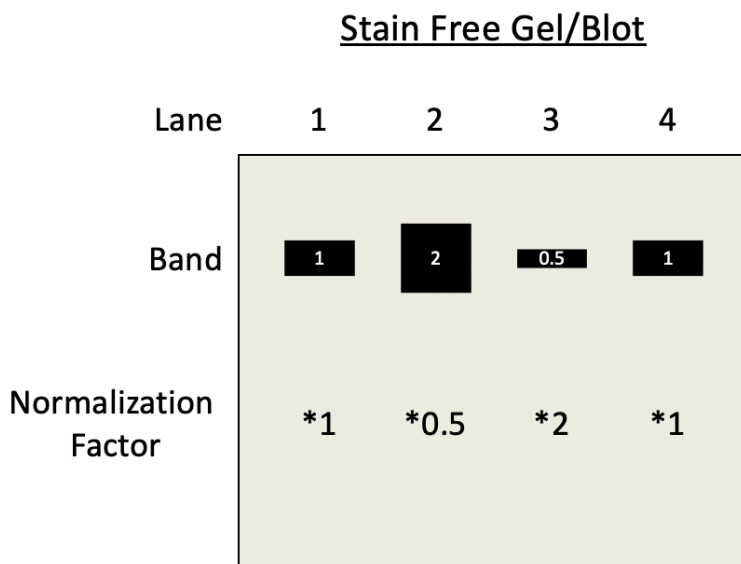


Figure 3.2 Description of integrated density-based normalization factors for total protein amount in western blots. Depicted is a stain free gel blot that shows total lane protein. One consistent size band across the lanes is chosen for the program to measure. Lane 1 band intensity is arbitrarily set to 1. Subsequent band integrated density is compared to that of band 1 and normalization factors correct for difference in total protein amount. These normalization factors will then be applied to the chemiluminescent blot to correct for gel loading inconsistency without the need for stripping and re-staining the blot for a housekeeping protein.

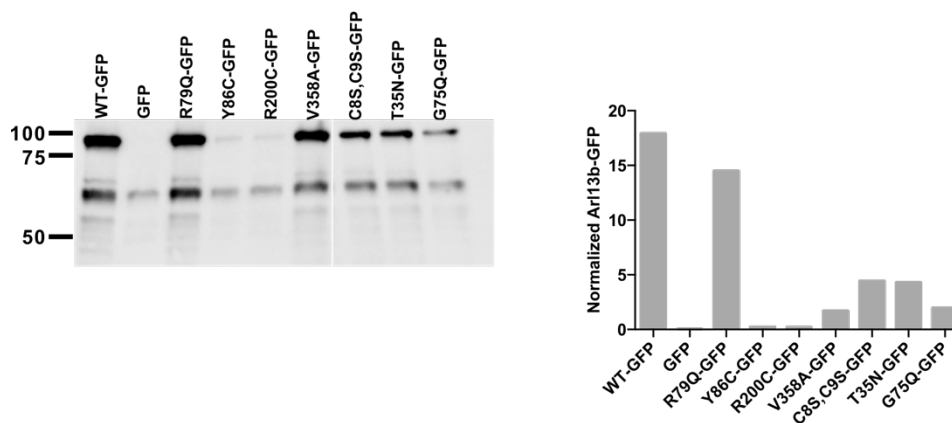


Figure 3.3 Quantification of ARL13B constructs in transfection *Ar113b^{hnn}* MEFs (blot) Representative western blot for ARL13B from *Ar113b^{cond}* MEFs. ARL13B-GFP runs at 100 kDa; endogenous ARL13B runs at 60 kDa. (This blot was cut to rearrange the order of samples.) (graph) Quantification of blot in E. ARL13B-GFP levels were normalized to endogenous ARL13B (60 kDa band in the GFP negative control cells).

3.3.2 Fibroblast migration assays are inconsistent

Laura's data showed that cilia-excluded ARL13B^{V358A} is insufficient for fibroblast migration, potentially due to separation from cilia-localized SMO. To follow-up on this result, I planned several experiments with our collaborator Maarten Bijlsma, who trained me to perform fibroblast migration assays. I would test ARL13B^{V358A} in conjunction with SMO Δ CLD in ciliated MEFs to see if excluding both factors from the cilium would be sufficient for migration. Additionally, I would test the ARL13B^{V358A} construct with endogenous SMO in non-ciliated MEFs to be sure insufficiency of cilia-excluded ARL13B was not due to an artifact of the CiLS mutation.

I learned the fibroblast migration procedure from Maarten and began by introducing *Arll3b^{hnn}* fibroblasts to attractive cues fetal calf serum (FCS/ FBS) and Purmorphomine, a Hh agonist that activates SMO (**Figure 3.1**) (Wu et al. 2004). I assayed *Arll3b^{hnn}* fibroblast migration towards 1% FCS. *Arll3b^{hnn}* show similar migration between the two runs of cells transfected with GFP alone, however there was significant inconsistency of ARL13B-GFP transfected migration with one run showing more migration towards FCS compared to GFP only controls and another showing much less (**Figure 3.4**). Furthermore, *Arll3b^{hnn}* fibroblast migration towards 1:2000 Purmorphomine showed approximately the same migration amount whether transfected with GFP alone or transfected with ARL13B-GFP, but one well of ARL13B-GFP migration was much lower than the other, displaying the lack of consistency within this assay (**Figure 3.5**). Part of these inconsistencies reside in the normalization method, in which I subjectively determine the point in which early assay noise transitions to actual migration. I did this by analyzing "peaks" within the first few cycles of GFP measurement, however, all attempts

at normalization remained inconsistent. Thus, inconsistencies in both data acquisition and normalization resulted in significant differences between runs.

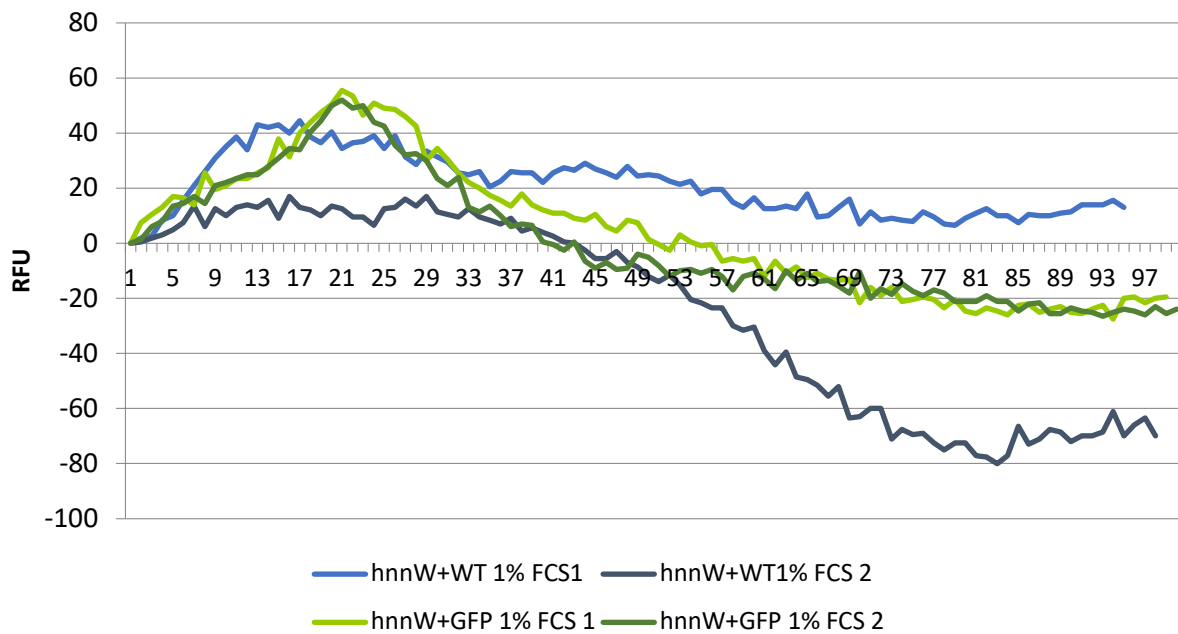


Figure 3.4 *Arl13b*^{hnn} Migration to 1% FCS (performed in Amsterdam). X-axis is the cycle number, Y-axis is relative fluorescence units (RFU). Green lines represent fibroblasts +GFP only, blue lines represent fibroblasts +WT ARL13B-GFP.

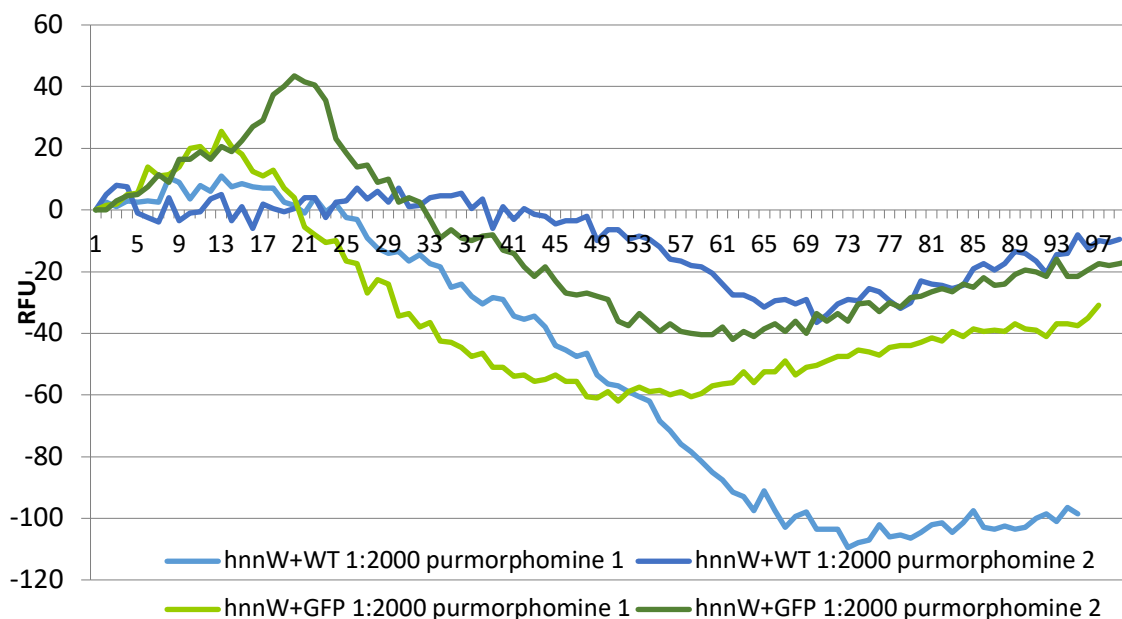


Figure 3.5 *Arl13b^{hnn}* Migration to 1:2000 Purmorphomine (performed in Amsterdam). X-axis is the cycle number, Y-axis is relative fluorescence units (RFU). Green lines represent fibroblasts +GFP only, blue lines represent fibroblasts +WT ARL13B-GFP.

Upon returning to Emory, I ran several assays or “rounds” to measure migration towards 1:500 Shh in either *Arl13b^{hnn}* fibroblasts +GFP alone or +WT ARL13B-GFP with several technical replicates (plated at the same time, harvested the same, and seeded into Boyden chamber wells the same). I found that *Arl13b^{hnn}* fibroblasts +GFP alone were less variable in early rounds, but despite using biological replicates between rounds, the runs were inconsistent (**Figure 3.6**). Further in round 3, I saw a large discrepancy in how the fibroblast migration was reported by the assay, both between the former rounds’ biological replicates and within the technical replicants of round 3. Similarly, I ran 3 rounds of biological replicates of *Arl13b^{hnn}* fibroblasts +WT ARL13B-GFP with several technical replicates in each round and found large discrepancies (**Figure 3.7**). One well from round 1, along with one well from round 3 displayed

extremely low migration towards 1:500 Shh in comparison to others, even within their own round of the assay. When the replicates within a run are averaged, and then averaged across the 3 assays, I saw that *Arl13b^{hnn}* fibroblasts +GFP alone migrated towards 1:500 Shh less than the *Arl13b^{hnn}* fibroblasts +WT ARL13B-GFP (**Figure 3.8**). However, the issues of inconsistencies between replicates and the issue of subjective normalization halted further examination.

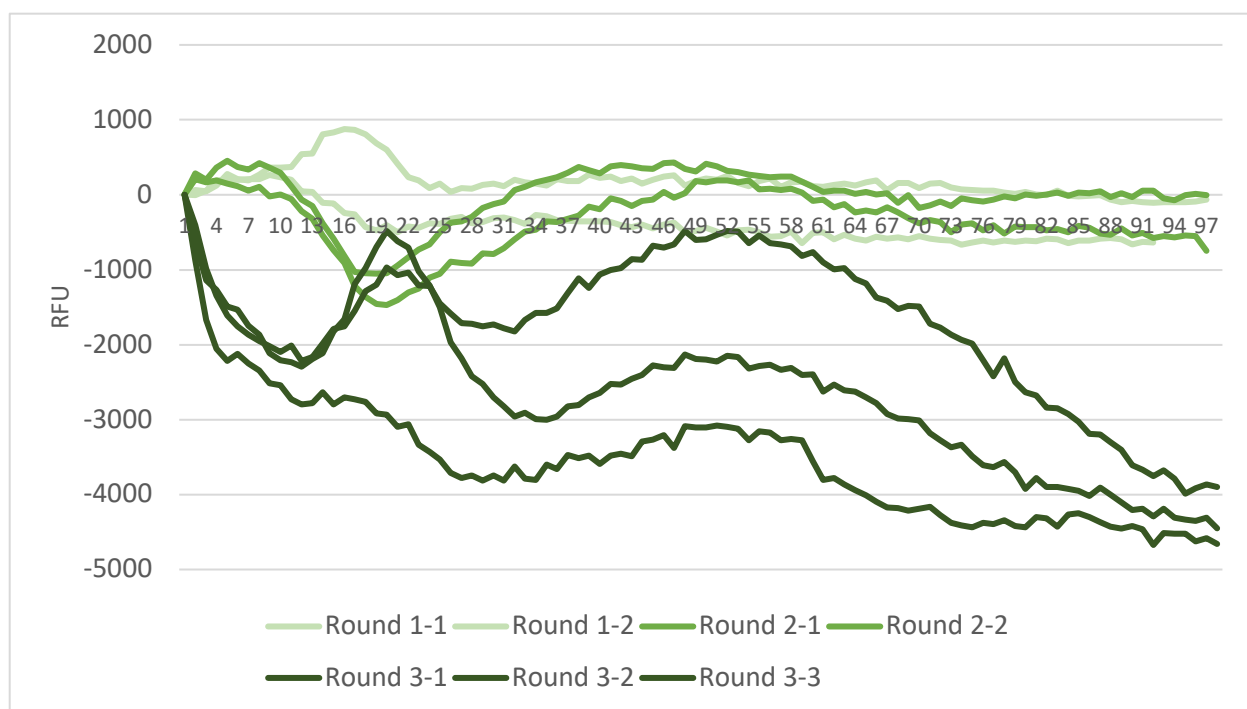


Figure 3.6 *Arl13b^{hnn}* +GFP Only Individual Runs (performed at Emory). X-axis is the cycle number, Y-axis is relative fluorescence units (RFU). Green lines represent fibroblasts +GFP only, different shades of green represent technical replicates run within the same round.

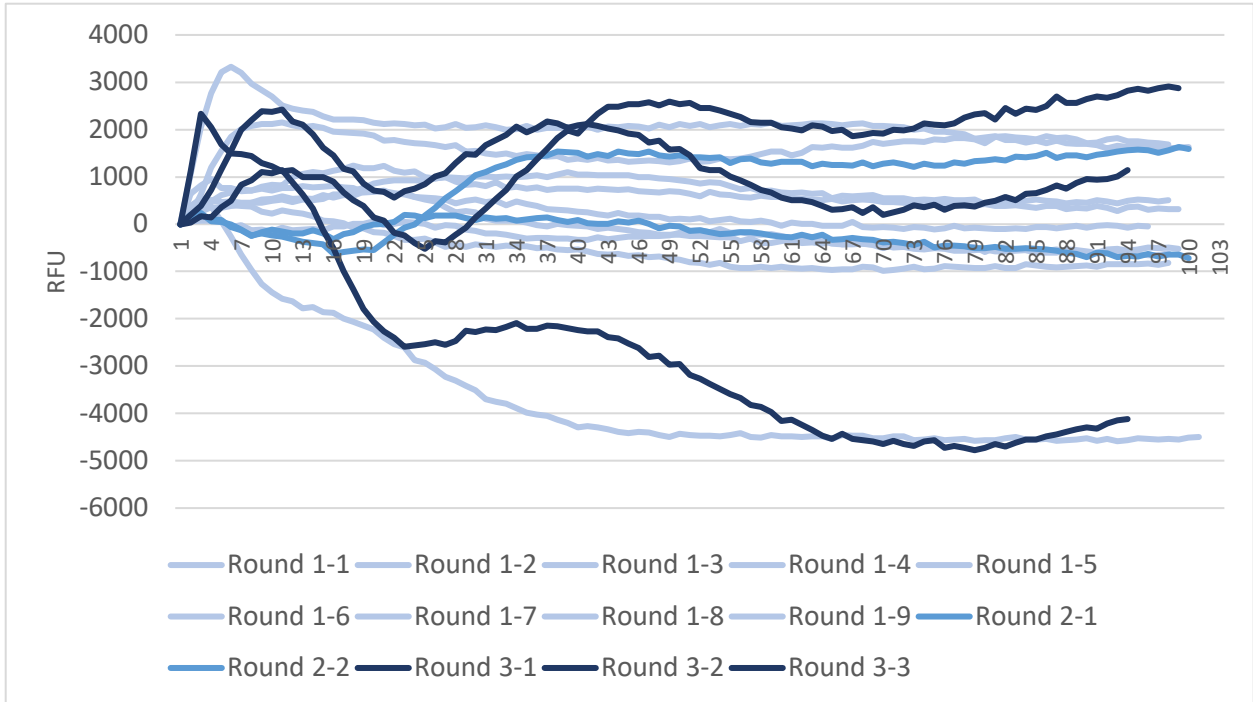


Figure 3.7 *Arl13b^{hnm}* +WT ARL13B-GFP Individual Runs (performed at Emory). X-axis is the cycle number, Y-axis is relative fluorescence units (RFU). Blue lines represent fibroblasts +WT ARL13B-GFP, different shades of blue represent technical replicates run within the same round.

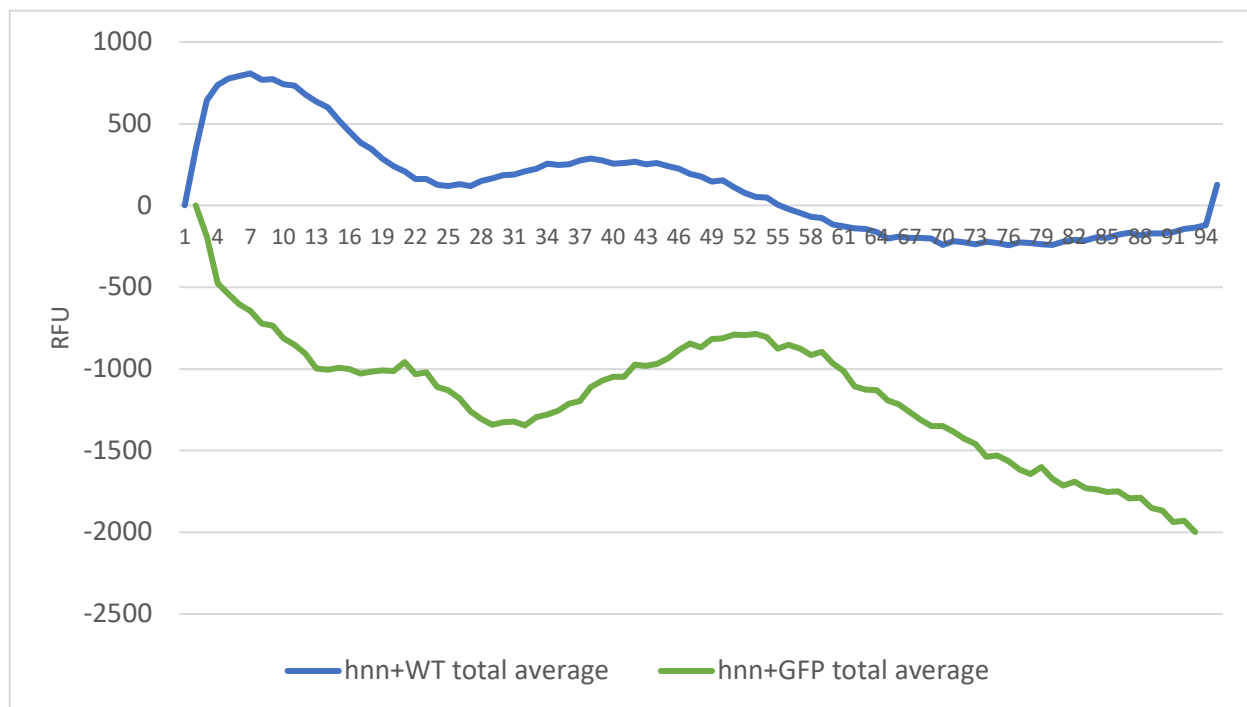


Figure 3.8 Migration averages of *Arl13b^{hnn}* +GFP Only versus *Arl13b^{hnn}* +WT ARL13B-GFP. X-axis is the cycle number, Y-axis is relative fluorescence units (RFU). The green represent the average of all runs of fibroblasts +GFP only, the blue line represents the average of all runs of fibroblasts +WT ARL13B-GFP.

3.3.3 Commissural axon dissection and culture

Following up on the fibroblast migration assays, I worked with a talented undergraduate summer student Sarah Cubells to find a more consistent alternative. Like fibroblast migration, commissural axon guidance relies on transcription-independent Shh signaling (Yam et al. 2009). We were inspired by these growth cone response assays; however, we would want to utilize the mutant mice in the lab to test alleles such as *Arl13b^{V358A}* and *Arl13b^{R79Q}* without the need for transfection. This is particularly important, as transfection of neurons in culture is notably difficult. Thus, Sarah Cubells and I worked from the JoVE rat commissural neuron culture method to culture embryonic mouse commissural neurons (Au - Langlois et al. 2010). If

successful, this method could take over for the fibroblast migration assays, as JS is a disease of axon guidance and commissural axon guidance is a readout of transcription-independent Shh signaling in axon guidance. Through diligent troubleshooting and significant effort, Sarah Cubells was able to create a successful method of mouse commissural neuron culture, confirmed via positive staining of commissural neuron markers. Moving forward, the lab could potentially utilize this method along with the Dunn chamber assay used by Charron *et al.* to assay impact of Arl13b mutation on Shh-dependent commissural axon turning response (Charron et al. 2003).

3.4 Discussion

ARL13B acts at multiple steps in the transcriptional Shh pathway: it regulates the ligand-dependent ciliary enrichment of SMO, and also acts downstream of SMO to regulate Gli activator (Casparly, Larkins, and Anderson 2007; Larkins et al. 2011). Laura found that the cilia-excluded ARL13B^{V358A} disrupts Shh-dependent chemotaxis but has no effect on Shh-dependent ciliary enrichment of SMO, suggesting that ARL13B's role in non-transcriptional Shh signaling lies downstream of SMO. Little is known about the downstream mechanisms of Shh signaling in chemotaxis, but the common role of ARL13B in both the transcriptional and non-transcriptional pathways suggest that other components may be shared between the two.

One of the most surprising results of Laura's study was the fact that the ARL13B^{V358A} variant that does not localize to cilia retains some functions. ARL13B is considered to be a cilia protein, and Joubert Syndrome, like other diseases resulting from cilia-related genetic mutations, is considered a ciliopathy. Transcriptional Shh signaling is tightly linked to cilia. And yet, non-ciliary ARL13B^{V358A} exhibits normal induction of Shh target genes upon ligand stimulation in null *Arl13b*^{hnn} MEFs. Meanwhile, in assays of non-transcriptional Shh signaling, ARL13B^{V358A}

transfected MEFs show significant impairment in their Shh migration response, despite the fact that the cilium itself is not necessary for Shh-dependent cell migration. This suggests distinct roles for ARL13B in transcriptional versus non-transcriptional Shh signaling, one of which requires its CiLS motif and one of which does not. Future studies to determine whether the failing of ARL13B^{V358A} in fibroblast migration is due to loss of interaction with Smo could aid in interpreting possible different roles of ARL13B. Furthermore, adoption of commissural neuron assays using *Arll3b*^{V358A} and *Arll3b*^{R79Q} animals may lead to new connections between ARL13B, transcription-independent Shh signaling, axon guidance, and Joubert Syndrome.

In sum, ARL13B plays multiple roles in regulating Shh signaling both within and outside of cilia and separated these functions using point mutations in *Arll3b*. *Arll3b* mutations have effects on cilia morphology and Shh signaling and Joubert-causing *Arll3b* variants disrupt ARL13B function through multiple mechanisms yet give rise to the same disease phenotypes. This work emphasizes the importance of investigating the diverse functions of ciliary gene products as the field continues to elucidate the molecular etiology of JS and other ciliopathies. As evidenced, the very name “ciliopathy” may be misleading, as at least one ciliopathy gene product need not localize to cilia in order to serve essential regulatory functions and acts on processes that can occur in the absence of a cilium.

CHAPTER 4

MEASURING CELL RESPONSE TO SHH AS AN ATTRACTIVE CUE

4.1 Abstract

Axon guidance is the process by which neurons project the axon away from the cell body towards synaptic targets. This process takes place at the growth cone, the tip of the axon furthest from the cell body. Shh can act as a guidance cue for commissural neurons in the neural tube, where Shh stabilizes the growth cone such that it turns towards Shh signal in a SMO-dependent but transcription-independent mechanism. Axon guidance issues are found in the ciliopathy Joubert Syndrome, which is caused by mutations in over 35 different cilia-associated genes including *ARL13B*. *ARL13B* is characterized as a protein that localizes to cilia, however, the distance of the cilium from the growth cone makes the regulatory mechanism of *ARL13B* and the cilium in axon guidance unclear. Here I demonstrate that Shh is a guidance cue for the superior cerebellar peduncles (SCPs), the white matter tract affected in Joubert's diagnostic hindbrain malformation. Furthermore, I show *ARL13B* is required for SCP guidance, but excluding *ARL13B* from the cilium has no impact on the SCPs. My data indicates that *ARL13B* functions outside of the cilium to regulate Shh-dependent axon guidance.

4.2 Introduction

Joubert Syndrome and Related Disorders (JSRD) are autosomal recessive congenital disorders with a variety of symptoms including developmental delay, intellectual disability, abnormal respiratory rhythms, ataxia, oculomotor apraxia, polydactyly, craniofacial defects, retinal dystrophy, nephronophthisis, and hepatic fibrosis (Parisi et al. 2007). While the exact prevalence of JSRD is not known, published statistics range from 1:80,000 to 1:100,000, but these may be underestimates (Brancati, Dallapiccola, and Valente 2010). The characteristic neuroanatomical feature of JSRD is

diagnosed by Magnetic Resonance Imaging (MRI) and denoted the molar tooth sign (MTS), which is caused by hypoplasia of the cerebellar vermis and thickened, elongated superior cerebellar peduncles (SCPs) that fail to decussate (Poretti et al. 2007; Yachnis and Rorke 1999; Poretti et al. 2011a). However, little is known about the etiology of this hindbrain malformation. This is especially significant in light of the fact that many severe symptoms of JSRD arise from defects in the hindbrain: cerebellar dysfunction commonly causes ataxia, while life-threatening breathing problems are linked to hindbrain nuclei such as the parafacial respiratory group and pre-Bötzinger complex (Onimaru, Kumagawa, and Homma 2006).

To date, mutations in any of 35 genes cause JSRD, and their associated proteins almost always localize to the primary cilium or the centrosome (Parisi 2019). Thus, JSRD is classified as a ciliopathy, a category of human disease stemming from ciliary dysfunction. One of the genes implicated in JSRD is *ARL13B*, which encodes a regulatory GTPase highly enriched in cilia (Cantagrel, Silhavy, Bielas, Swistun, Marsh, Bertrand, Audollent, Attie-Bitach, Holden, Dobyms, Traver, Al-Gazali, Ali, Lindner, Caspary, Otto, Hildebrandt, Glass, Logan, Johnson, Bennett, Brancati, Valente, et al. 2008; Thomas et al. 2015; Shaheen et al. 2016; Bachmann-Gagescu et al. 2015; Rafiullah et al. 2017). As a GTPase, *ARL13B* is expected to have multiple effector proteins which interact with specific *ARL13B* residues. *ARL13B* can function as guanine exchange factor (GEF) for *ARL3*, mutations in which also lead to JSRD (Gotthardt et al. 2015; Ivanova et al. 2017). JSRD-causing mutations in either *ARL3* or *ARL13B* can disrupt their interaction or *ARL13B*'s GEF activity consistent with the notion that specific *ARL13B* function is affected by JS-causing point mutations (Gotthardt et al. 2015; Ivanova et al. 2017; Alkanderi et al. 2018). Most JSRD-causing *ARL13B* mutations cluster within the protein's GTPase domain although two are in the coiled coil domains in the C terminal half of the protein (Cantagrel,

Silhavy, Bielas, Swistun, Marsh, Bertrand, Audollent, Attie-Bitach, Holden, Dobyns, Traver, Al-Gazali, Ali, Lindner, Caspary, Otto, Hildebrandt, Glass, Logan, Johnson, Bennett, Brancati, Valente, et al. 2008; Thomas et al. 2015; Shaheen et al. 2016; Bachmann-Gagescu et al. 2015; Rafiullah et al. 2017). ARL13B complexes with the inositol phosphatase INPP5E, which is also implicated in causing JSRD (Bielas et al. 2009). ARL13B is critical for targeting INPP5E to cilia and JSRD-causing ARL13B mutations disrupt INPP5E ciliary targeting (Humbert et al. 2012). INPP5E controls ciliary lipid composition through its phosphatase activity and most JSRD-causing mutations are within its phosphatase domain (Chavez et al. 2015; Garcia-Gonzalo et al. 2015; Bielas et al. 2009). Other proteins implicated in JS also affect ciliary targeting with many functioning at the transition zone supporting the notion that abnormal ciliary traffic leading to defective signaling underlies JSRD (Srour et al. 2012; Arts et al. 2007; Hopp et al. 2011; Garcia-Gonzalo et al. 2011; Roberson et al. 2015; Delous et al. 2007).

The mechanistic connection between the cilia-related proteins implicated in JSRD and the MTS are elusive. The hypoplastic cerebellar vermis and the abnormal SCP tracts disrupt the distinct biological processes of proliferation and axonal targeting. One signaling pathway potentially linked to both processes is vertebrate Hedgehog (Hh) which relies on cilia (Huangfu et al. 2003). Sonic hedgehog (Shh) is a mitogenic cue that controls proliferation in the developing cerebellum so its misregulation could underlie the cerebellar hypoplasia (Kenney and Rowitch 2000; Dahmane and Ruiz i Altaba 1999; Wechsler-Reya and Scott 1999). While the SCP tracts that normally project from the deep cerebellar nuclei to the contralateral thalamus are guided by unknown signals, Shh is a known axon guidance cue (Charron et al. 2003). JSRD patients also display axon

guidance defects in decussation of pyramidal tracts and in crossing of the tracts in the optic chiasm, the latter of which is a Shh-dependent process (Sanchez-Arrones et al. 2013; Fabre, Shimogori, and Charron 2010).

The JSRD-causing genes *Arl13b* and *Inpp5e* are known to regulate vertebrate Hh signaling. In mouse models, *Arl13b* loss disrupts cell fate specification in the neural tube, proliferation of the cerebellar granule precursor cells in the cerebellum and Shh-directed guidance of commissural axons in the spinal cord (Caspary, Larkins, and Anderson 2007; Ferent et al. 2019; Bay, Long, and Caspary 2018). These data support a model whereby disruption of Shh signaling by *ARL13B* mutation could provide a single mechanism underlying the MTS. This model is bolstered by the fact that additional phenotypes exhibited by JSRD patients, such as craniofacial defects or polydactyly, can arise from aberrant Hh signaling (Lan and Jiang 2009; Lipinski et al. 2010; Valente, Brancati, and Dallapiccola 2008).

As attractive as a Hh-based model for JSRD may be, not all the data support that JSRD phenotypes result from misregulation of Hh signaling. Some features of JSRD, such as the renal and liver anomalies, are not clearly due to misregulation of Hh signaling (Doherty 2009; Breslow et al. 2018). Additionally, of the 35 genes implicated in JSRD, 27 have experimental evidence supporting that they regulate Hh signaling. Others, such as *ARL3*, lack such evidence. *Arl3* mouse mutants do not exhibit any of the phenotypes exhibited by mutants in the Hh pathway suggesting that it may regulate Hh-independent pathways (Schrack et al. 2006). Indeed, additional signaling pathways are linked to cilia including others known to be important in cell proliferation and axon guidance. Loss of the JSRD-linked genes *Ahil* or *Cep290* in mouse leads to a small cerebellar vermis due to aberrant Wnt signaling (Lancaster et al. 2011; Ramsbottom et

al. 2020). Conditional *Arl13b* or *Inpp5e* deletion in the SCPs results in their mistargeting to the thalamus through misregulation of ciliary PI3 kinase and Akt (Guo et al. 2019).

Through multiple methods of SCP tract visualization, I am able to address a wide range of questions regarding the functions of Shh obligate transducer SMO, as well as my protein of interest ARL13B. To that end, various mouse alleles were examined. These include floxed *Smo* and *Arl13b* alleles deleted via a *Nex-Cre* recombinase which initiates CRE recombinase expression at E11.5 in projection neurons (Goebbels et al. 2006). I denote these alleles here as *Smo*^{*Nex-Cre*} and *Arl13b*^{*Nex-Cre*}. Additionally, via CRISPR, we generated mice expressing cilia-excluded *Arl13b*^{*V358A*} and JS GTPase mutation *Arl13b*^{*R79Q*}. To analyze the SCPs in these mutants I used a form of MRI called Diffusion Tensor Imaging (DTI), previously used to characterize the guidance defects in the MTS of patients, in addition to tract tracing injections into the mouse brain. DTI measure directionality in a tract and is useful to examine tract decussation, both for directionality and organization. DTI results are reported in fractional anisotropy (FA), a measure of water diffusion in a primary direction (Alexander et al. 2007). As water diffuses through the brain, it encounters little resistance traveling along an axon tract, but due to the myelin coating of the axons, is less able to diffuse perpendicular or oblique to the tract which results in a high FA value (FA ~1). A lower FA value (FA ~0) implies that water diffusion is more diffuse (illustrated in **Figure 4.1**). Therefore, if the SCPs are correctly guided to project across the midline, a high FA value occurs in the left-right direction along midline crossing fibers. Misguided SCPs would have fewer or more disorganized fibers, resulting in lower FA values at the midline. In addition to DTI, tract tracing injections are key as injections anterograde (into the cell body) will diffuse and stain cell

projections while injections retrograde (into the projections) will stain the originating cell bodies. In this system, by targeting either SCP projections or cell bodies I can determine success or failure of the SCPs to project from the cerebellum to their targets in the dorsal and ventral thalamus. Tract tracing injections can be further visualized by manipulating the sectioning thickness and plane of brain tissue, as well as tissue clearing protocols such as CLARITY. A limitation of tract tracing imaging via sectioning is that the sectioning plane will preclude visualization in another plane (horizontal sectioning cuts off dorsal/ ventral projections, coronal sectioning cuts off rostral/ caudal projections, and sagittal sectioning cuts off medial/ lateral projections). However, 3D imaging of all projection directions can be achieved via CLARITY, which involves taking an *ex vivo* brain and slowly replacing all of the fatty tissue with acrylamide hydrogel monomers (Bohne et al. 2019; Treweek et al. 2015). Lipids are opaque, and so replacing them structurally with the clear hydrogel monomers allows the tissue to become transparent while retaining the structure of the tissue. This allows for deep tissue imaging in 3D whole brain, or in sections much thicker than a normal scope can resolve. Here I will describe my results that SMO is a guidance cue of the SCPs, and that ARL13B is also required for SCP guidance. However, Arl13b excluded from the cilium is sufficient for SCP guidance, as is the JS GTPase *Arl13b* mutation. Thus, my results will demonstrate that ARL13B regulates SCP guidance in a Shh-dependent mechanism, but that this regulation requires neither ARL13B to localize to cilia nor even GTPase function.

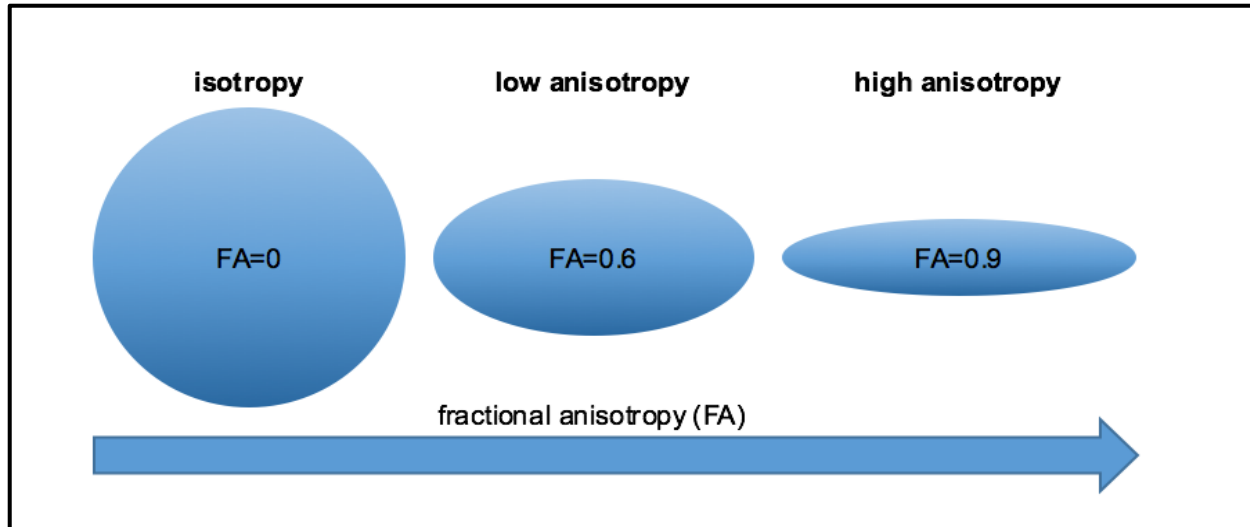


Figure 4.1 Visual description of fractional anisotropy reported in DTI. Lower FA values indicate lack of primary direction in movement through a white matter tract. Higher FA values indicate a strong primary direction of flow.

4.3 Results

4.3.1 Deletion of *Arl13b* or *Smo* results in a larger Corpus callosum tract

Several measurements can be done via DTI analysis in addition to assessing the directionality of a tract through FA. The following data sections will describe multiple methods of DTI analysis. For one, the size of the region of interest (ROI) mask required to capture and analyze a tract is a measure of size and diffusivity of a tract. Guo et al describes an expansion of the corpus callosum (CC) when *Arl13b* is deleted, with the tracts less organized and more diffuse (Guo et al. 2019). In order to test if the CC is expanded in mutants lacking *Arl13b* or *Smo*, I used DTI to measure the mask size needed to cover the CC in *Arl13b* or *Smo*-deleted animals. As *Arl13b* and *Smo* null embryos die during embryogenesis, we deleted specifically in the projection neurons by generating

Nex-Cre;Arl13b^{fl/fl} and *Nex-Cre;Smo^{fl/fl}* mice, which I refer to as *Arl13b^{Nex-Cre}* and *Smo^{Nex-Cre}* respectively (Zhang, Ramalho-Santos, and McMahon 2001; Caspary et al. 2002; Caspary, Larkins, and Anderson 2007). *Nex-Cre* initiates CRE recombinase expression at E11.5, as the precursor cells of the deep cerebellar nuclei (DCN) begin to migrate and become specified (Goebbels et al. 2006; Fink 2006). Compared to controls where the CC is captured in the mask within approximately 70 voxels (3D pixels), the CC mask of brains with *Arl13b* deleted in projection neurons, *Arl13b^{Nex-Cre}*, is slightly increased to about 80 voxels (**Figure 4.2**). Mutants that had *Smo* deleted in projection neurons, *Smo^{Nex-Cre}*, were further diffuse, needing over 100 voxels to capture in the mask. Thus, ARL13B and SMO are required for SCP organization. Double mutants lacking both *Arl13b* and *Smo* in projection neurons resembled the *Arl13b* deleted brains, with the CC with a requirement of 80 voxels to cover in the ROI mask.

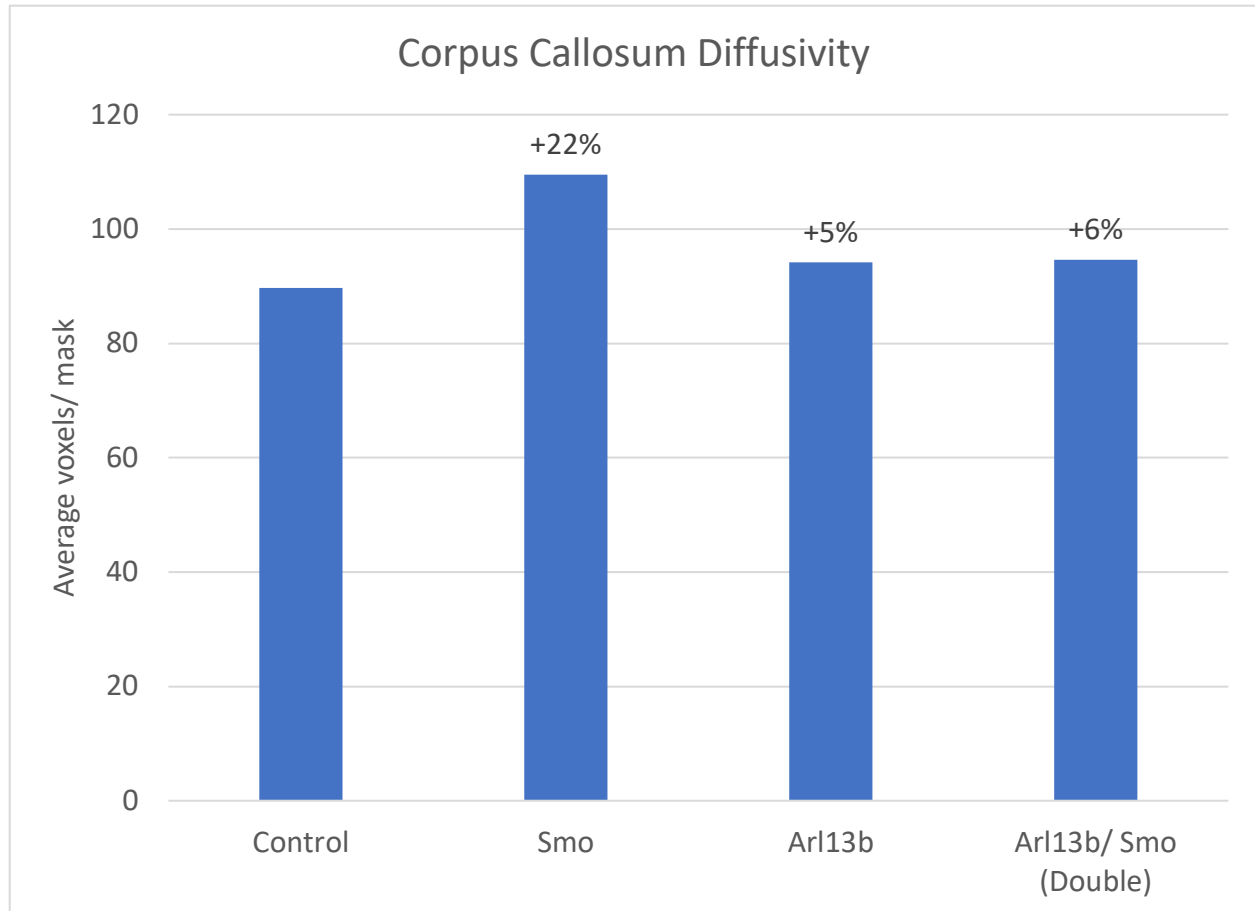


Figure 4.2 Voxel size of Corpus Callosum (CC) masks via DTI. T1 scans were used to capture the CC in voxel masks. SCPs lacking SMO require more voxels to capture the tract, indicating the CC in these mutants is larger and more diffuse. SCPs lacking ARL13B additionally showed a larger CC compared to controls.

4.3.2 Deletion of *Arl13b* or *Smo* results in lessened SCP FA at decussation

In order to determine whether loss of ARL13B or SMO affected SCP directionality at the point of tract decussation in the cortex, I generated SCP ROI masks at the point of midline decussation. This means I only captured voxels that were in the SCPs and at the midline of the cortex in the ROI mask. From these midline voxels, the FA was measured. As previously described, an FA closer to 0 would indicate a lack of primary direction, or disorganization, while an FA closer to 1 would indicate most

movement was in the primary direction. In control SCP voxels at the midline, initially I found an FA of 0.8 (**Figure 4.3**). In midline SCP voxels lacking SMO, the FA was lower compared to controls at about 0.7, indicating a decrease in directionality. This could be interpreted as less movement in the primary direction, as well as decrease of the organization of the tract at that point. Furthermore, there was a greater decrease in the FA value of SCP midline voxels in the *Arll3b* deleted brains compared to controls, with an FA of about 0.6. Thus, from the initial results it appeared that loss of ARL13B or SMO in projection neurons would result in a decreased FA or organization of the SCP at the midline point of decussation. Furthermore, to test the effects of a double mutation, the FA of SCPs lacking both *Arll3b* and *Smo* was measured at the midline point of decussation. These double mutants display an FA that falls somewhere between those of SCPs with *Arll3b* deleted and those with *Smo* deleted (data shown in **Figure 4.5**). Finally, I binned the FA values found within the genotypic groups and plotted them to identify possible FA trends (**Figure 4.4**).

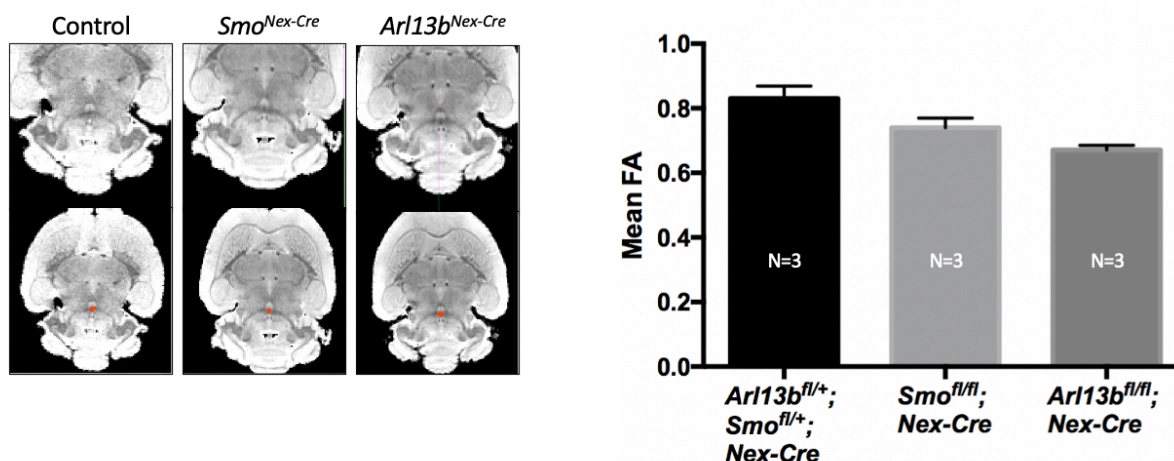


Figure 4.3 Initial results of fractional anisotropy (FA) of SCPs at the midline via DTI. SCPs were analyzed at the point of midline decussation (red dots within T1 scans, left). The FA of SCPs lacking SMO was lower than those of the controls, indicating a decrease of the influence of the primary direction in flow at the SCP decussation. The FA of SCPs lacking ARL13B was further lowered than those of the controls and SMO, indicating a more severe decrease of the influence of the primary direction in flow at the SCP decussation. Thus, SCPs lacking ARL13B or SMO show less organization and directionality at the point of midline decussation.

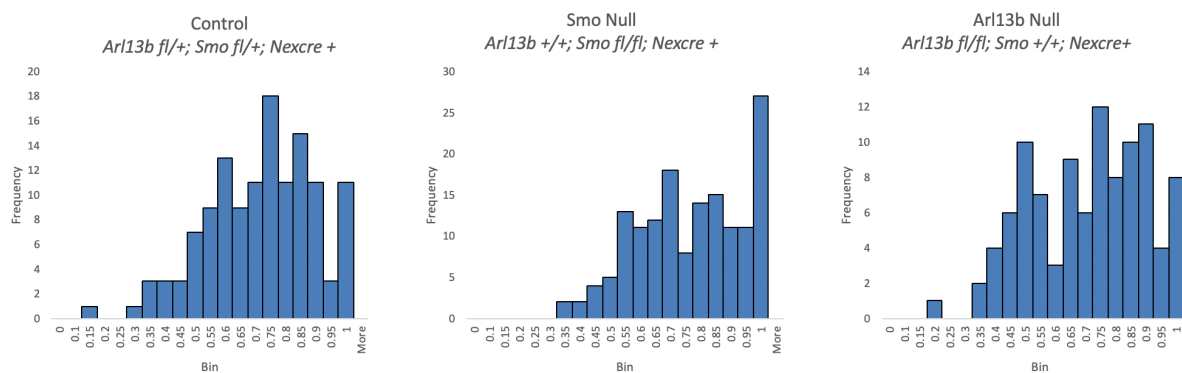


Figure 4.4 Bins of fractional anisotropy of SCPs at the midline via DTI. Further exploration of the FA values averaged in Figure 3 show the distribution of FA values within the voxels of the region of interest mask. Control SCPs peak with an FA of 0.75, while SCPs lacking SMO show a peak at 0.7 as well as at 1. SCPs lacking ARL13B showed a peak FA of 0.75. From the distributions of FA we can see greater detail of the diffusion at the point of SCP midline decussation.

However, variability and lack of consistency in DTI scans resulted in a discrepancy, where the first set of three heterozygous control animals looked drastically different from a second set of three heterozygous controls, of which scans were taken much later. This discrepancy appeared to be linked to when the scans were captured, rather than when the scans were analyzed. The original set of three controls when measured averaged an FA of SCP midline voxels of around 0.83 (**Figure 4.5**). However, the second group of three control brains had an averaged FA of 0.71. Repeated measures of already existing *Arll3b^{Nex-Cre}* and *Smo^{Nex-Cre}* SCPs showed no such discrepancy, leading to my conclusion that the scans must all be done together in order to avoid such changes in acquired measurements.

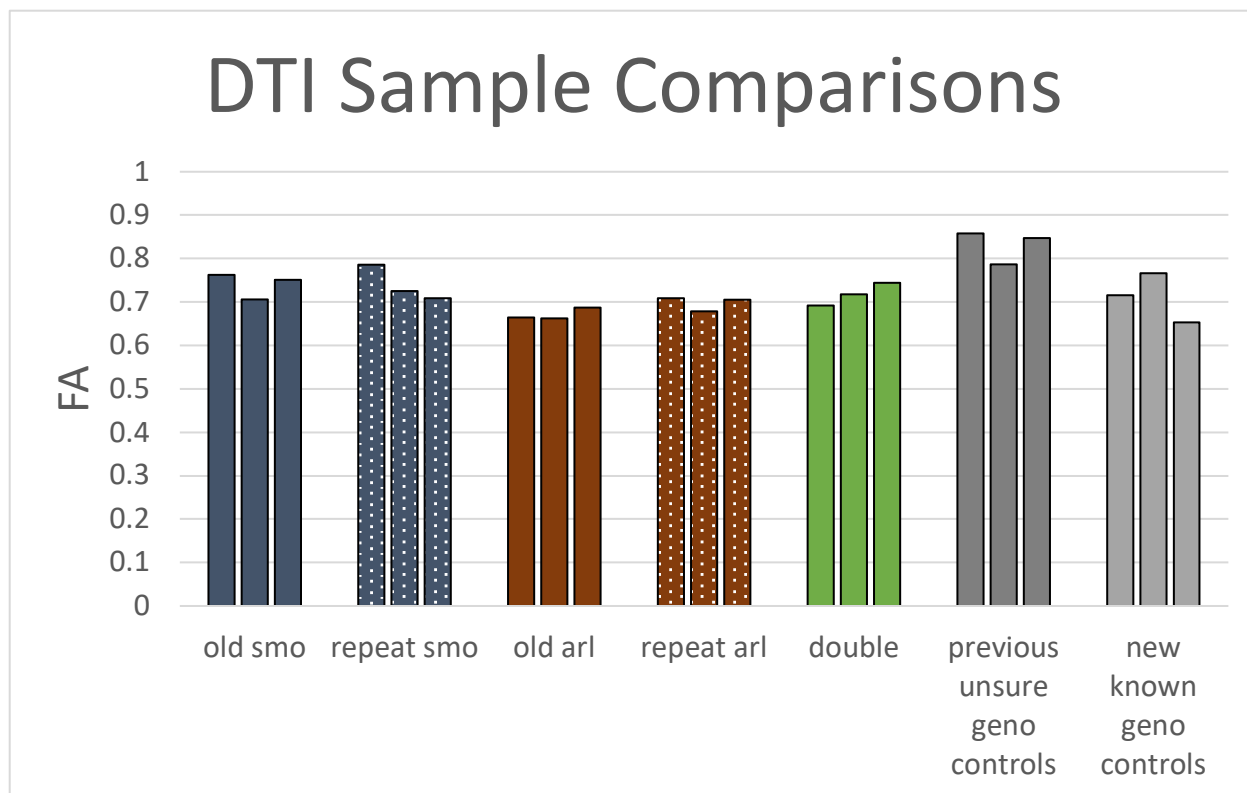


Figure 4.5 Fractional anisotropy of control SCPs at the midline changed when DTI re-analyzed. The dark gray bars represent the FA of initial control animals at the SCP point of decussation. The light gray bars are the FA of secondary control animals scanned at a later date. Green bars represent the FA of double mutant animals (lacking both ARL13B and SMO) in which the FA falls between that of SCPs lacking ARL13B or SMO. While re-analysis of existing brain scans changed little (blue bars compared to spotted blue bars and red bars compared to spotted red bars) the control animals were drastically different. Thus, difference in control groups was due to timing of scan acquisition, rather than timing of scan analysis.

4.3.3 Deletion of *Arl13b* or *Smo* results in a larger SCP tract

While FA is useful to determine directionality, I used ROI masking to determine whether deletion of *Arl13b* or *Smo* would result in a larger, disorganized SCP tract. As in the CC experiment described above, I used DTI to examine organization of mutant SCPs by analyzing the size of the ROI mask required for capture. However, rather than focusing on SCP voxels at the midline, I captured every SCP voxel I could identify

within the mask. From these masks I averaged the number of voxels needed to capture the SCP in the different genotypes. Control SCPs could be captured in about 160 voxels, while SCPs lacking ARL13B required fewer, about 145 voxels to capture (**Figure 4.6**). *Arl13b*^{Nex-Cre} SCPs require fewer voxels to capture, and thus this could be interpreted as a smaller, more organized tract. However, it is difficult to reconcile this result with the midline FA of SCPs lacking ARL13B, which shows more disorganization. It could be that while the SCPs are tightly organized, they are still directionally promiscuous, particularly at the midline which is the only place FA was measured. In contrast, SCPs lacking SMO required more voxels to capture, approximately 200. While the FA of SCPs lacking SMO at the midline is not as reduced as those lacking ARL13B, the tract is clearly bigger within the cortex, which implies disorganization, though the FA at the midline implies this disorganization is most found outside the point of decussation. Finally, to test effects of a double mutation, I repeated this measure for double mutants in which both *Arl13b* and *Smo* were deleted. As in the FA measurements at the midline, the double mutant seems to fall in between the phenotypes of SCPs lacking ARL13B and SMO. This indicates that dual deletion of *Arl13b* and *Smo* has a mitigating effect on the more severe *Smo*^{Nex-Cre} phenotype. This section concludes the use of DTI analysis.

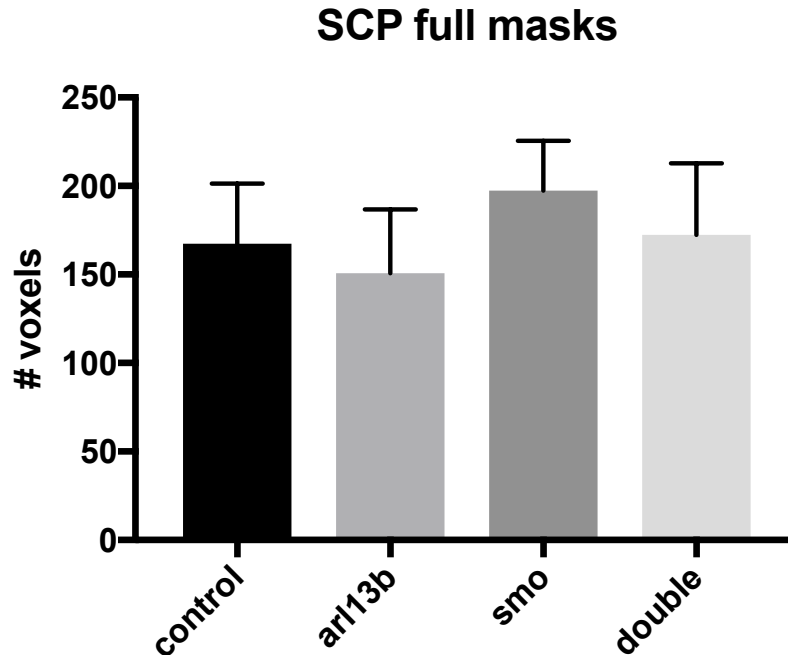


Figure 4.6 SCPs lacking SMO are larger and more diffuse via voxel size in DTI. More voxels are required to capture the entirety of the SCP in *Smo* mutants compared to controls. SCPs lacking ARL13B require fewer voxels to capture the SCPs compared to control. Double mutants displayed mask size in between those lacking SMO or ARL13B.

4.3.4 Anterograde injections indicate SCPs lacking *Smo* or *Arl13b* failed to project dorsally

In order to determine the projection sites of the SCPs in the mouse models, I began tract tracing experiments with anterograde tract tracing. The following data sections will include anterograde injection analyses. Here the Deep Cerebellar Nuclei (DCN) were injected at coordinates Bregma(AP:-6.24, ML:+1.50, DV:-2.6, angle: 0°) with dye diffusing out towards the SCP projection sites in the cortex. When imaged in the horizontal plane, I visualized SCPs from control anterograde injections from the point of midline decussation to a just slightly rostral point. In contrast, when I imaged SCPs lacking ARL13B or SMO at the same thickness in the horizontal plane, I visualized SCPs past the point of decussation and further out rostrally towards the thalamus. This

indicated that in no point in the projection to the thalamus had mutant SCPs projected dorsal/ventrally, as this cannot be visualized in the horizontal sectioning plane. I concluded that while control SCPs project dorsally, *Arl13b*^{Nex-Cre} and *Smo*^{Nex-Cre} SCPs failed to project dorsally, and instead I posited that they project to the ventral thalamus. Furthermore, this result set the scene for future ventral thalamus injections in control SCPs, where they do project to the ventral thalamus but not to the same degree of the mutants. The mutant SCPs are visualized easily in the horizontal plane of the ventral thalamus because there is no dorsal projection (confirmed by retrograde injections). However, control SCPs in retrograde injections project both to the dorsal and ventral thalamus, dividing the tract and leaving fewer control SCP fibers to visualize in the horizontal plane at the ventral thalamus.

4.3.5 Decussation in SCPs lacking Smo or Arl13b is disorganized

While examining anterograde dye tracing to find potential projection sites, I analyzed the tracing of SCP fibers at the point of decussation to look for a possible midline crossing phenotype. Of my anterograde injections that allowed for SCP visualization in the horizontal plane, I had N=2 heterozygous Cre⁺ controls, N=2 *Arl13b*^{Nex-Cre} and N=1 *Smo*^{Nex-Cre} brains to image. From these brains, I found that I could see more SCP fibers decussating at the midline in the mutants compared to the control. Furthermore, I noted the SCPs decussating over a greater span of horizontal sections in the mutants compared to the control. In control horizontal sections, I saw decussating SCPs at the midline in sections spanning 480 microns (**Figure 4.7**). In SCPs lacking ARL13B I saw decussating SCPs in 780 microns (62.5% increase) and in mutants lacking SMO I could see SCPs decussating across sections spanning 1020 microns (112.5% increase). To test if the increased decussation was due to more fibers of decussating SCPs in

mutants, I followed up by measuring and summing the lengths of visible decussating SCPs. In control sections, the total axon length was measured as ~19000 pixels (**Figure 4.8**). In mutant SCPs lacking ARL13B the sum total axon was 100% greater than that of the control group at ~38000 pixels. Finally, in mutants with SCPs lacking SMO the total axon length was 321% greater than controls at ~80000 pixels. Thus, deletion of *Arll3b* or *Smo* results in wider, more diffuse and disorganized SCPs at midline decussation. Once again, deletion of *Smo* in projection neurons had the greatest impact on SCP thickness through the dorsal/ ventral plane, with deletion of *Arll3b* resulting in a similar, but more modest phenotype. This result is intriguing, as through imaging and measuring of decussating SCPs more small, thin, “wispy” sections are seen in the mutants compared to the controls which are straighter with less branching. This phenotype will be discussed further in the retrograde SCP decussation characterization section.

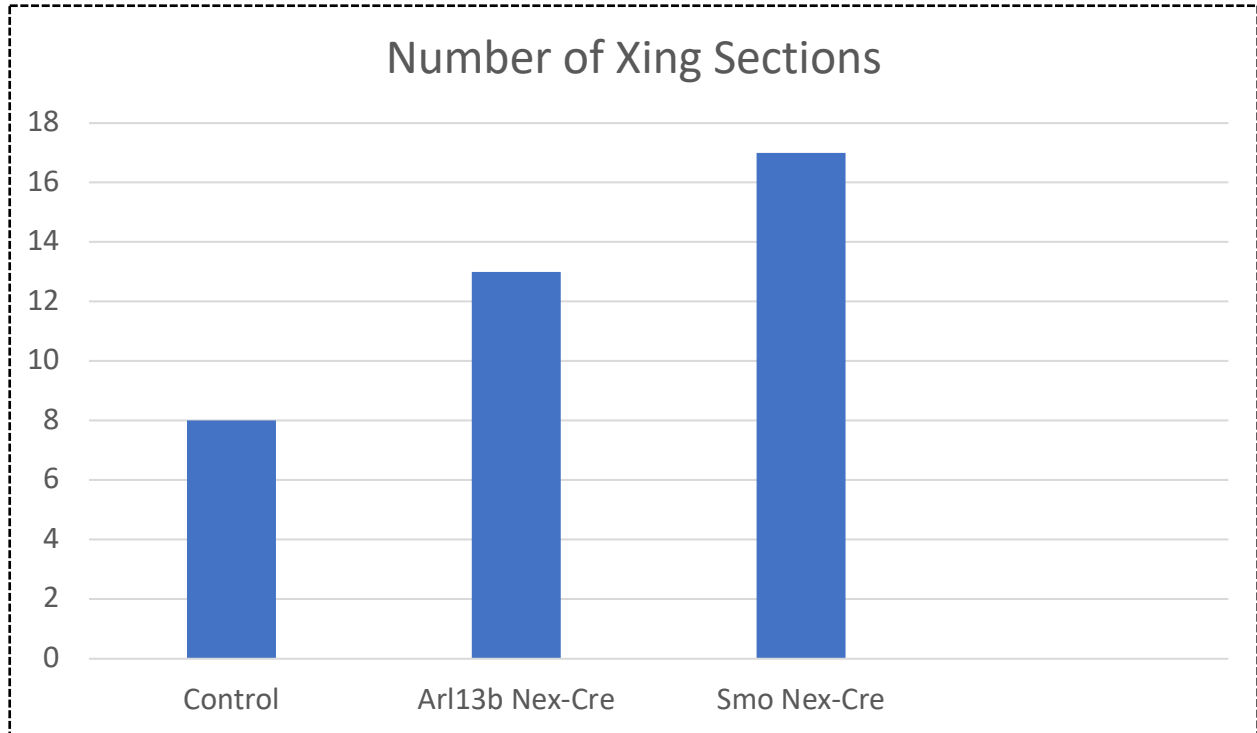


Figure 4.7 Anterograde SCP trace analysis of sections containing decussating SCPs. SCPs lacking ARL13B show increased sections in which decussation could be identified compared to controls with SCPs lacking SMO displaying a further increase. This indicates that SCP decussation in mutant animals results in larger, more diffuse SCP tracts at decussation.

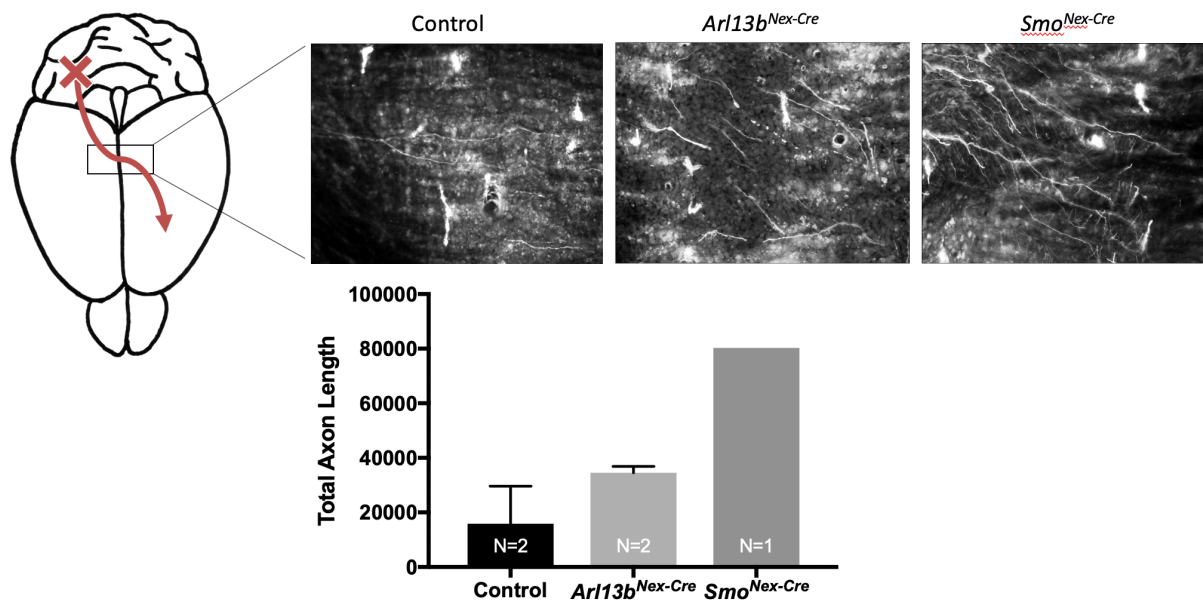


Figure 4.8 Anterograde SCP trace analysis of total axon length. SCPs lacking ARL13B show increased axon length compared to controls with SCPs lacking SMO displaying a further increase. This is likely a combination of thickness of SCP decussation at the midline with additional branching and thin wispy fibers present in mutants.

4.3.6 Clarity imaging is a promising method to image SCPs in whole brain with appropriate injected tracer

To test whether CLARITY can be used to visualize my tract tracing experiments in 3D and in all visual planes, I attempted the CLARITY on anterograde injected brains. Using these CLARITY-cleared whole brains, I saw once again that SCPs lacking ARL13B or SMO were visualized in one horizontal plane as they project rostrally in the brain, while control SCPs could not be visualized, as they project dorsally (**Figure 4.9**). Moving forward, research into CLARITY in whole brain imaging showed that certain tracers are bound to lipids (as in the case of the fluorodextran tracer I used) while others will bind to proteins within the axon, presumably able to survive the loss of lipids in

brain tissue, and so changes to injected materials can be further explored. This section concludes anterograde injection experiments.

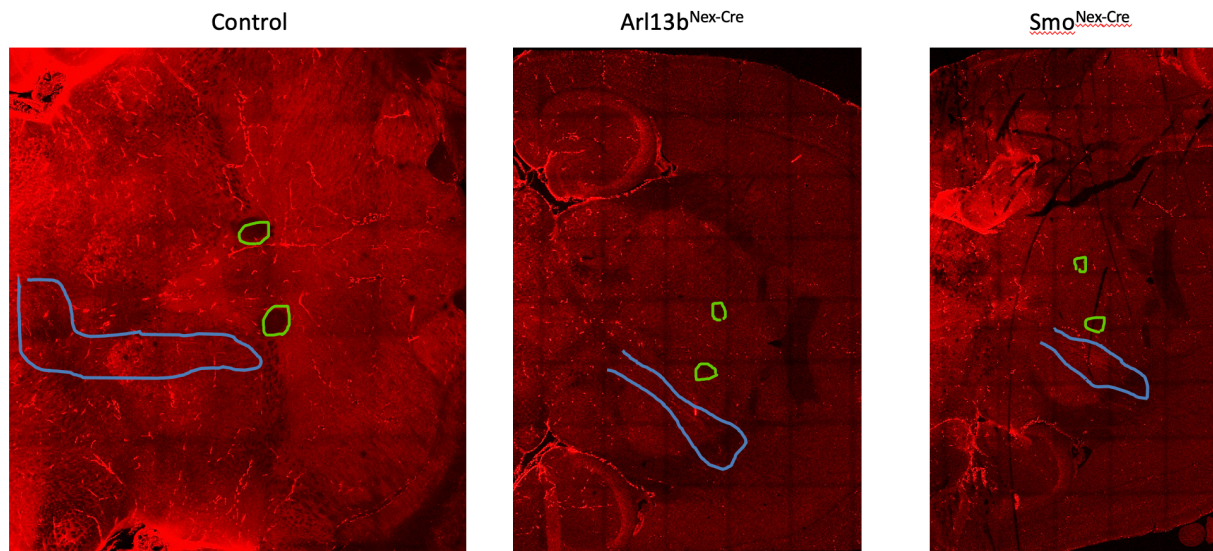


Figure 4.9 Following SCPs in the horizontal plane via CLARITY imaging. Control SCPs were traceable up to the middle of the cortex (green circles). Control SCPs were not visualized beyond this point as they project dorsally and cannot be visualized in the horizontal plane. SCPs lacking ARL13B or SMO were traceable beyond the middle of the cortex and up towards the thalamus, indicating that these SCPs fail to project dorsally, and instead project to the ventral thalamus.

4.3.7 SCP retrograde decussation characterization

The following data sections will describe my retrograde injection analyses. To test whether the *Arl13b^{Nex-Cre}* and *Smo^{Nex-Cre}* mouse mutants displayed a midline crossing defect in the SCPs at the point of decussation, I analyzed images of SCPs at decussation from dorsal and ventral thalamus retrograde injections. I found that SCPs at decussation fell into four qualitative categories (**Figure 4.10**). At decussation, SCPs crossing the midline would either project straight across the midline or would project across the midline at an angle and thus appear wavy. In addition, SCP fibers crossing the midline either projected in a tight, defined pattern or would splinter and branch off of themselves resulting in a wispy appearance. Thus, I categorized SCP

decussation as either straight or wavy, as well as either defined or wispy. Finally, the height of SCP fibers crossing the midline was recorded to examine tract organization at decussation.

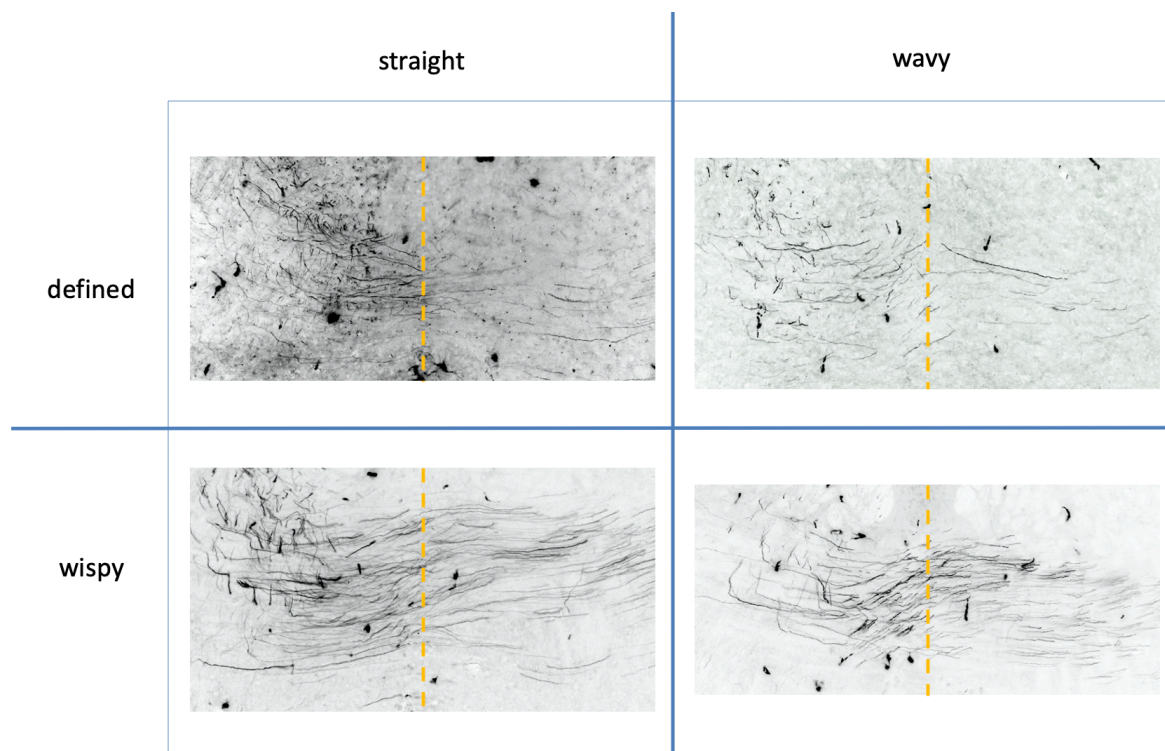


Figure 4.10 SCP decussation characteristics. SCPs crossing the midline were categorized as either defined (distinct fibers) or wispy (layers of fibers), as well as straight (no angle at crossing the midline) or wavy (crossing the midline at an angle).

In control animals that had heterozygous floxed *Arl13b* and *Smo* alleles I categorized the SCPs at the midline as defined (78.3%) and straight (69.6%) with an average crossing height of 385.7 pixels at decussation (**Figures 4.11 and 4.14**). I categorized mutant SCPs lacking ARL13B as defined (62.5%) as well as equally straight and wavy (50.0%) at midline decussation with an average crossing height of 328.6 pixels.

I categorized mutant SCPs lacking SMO as wispy (62.5%) and straight (75.0%) at decussation with an average crossing height of 412.8 pixels. As in DTI analysis of SCP tract size, SCPs lacking ARL13B appear smaller than control SCPs while SCPs lacking SMO are larger than controls.

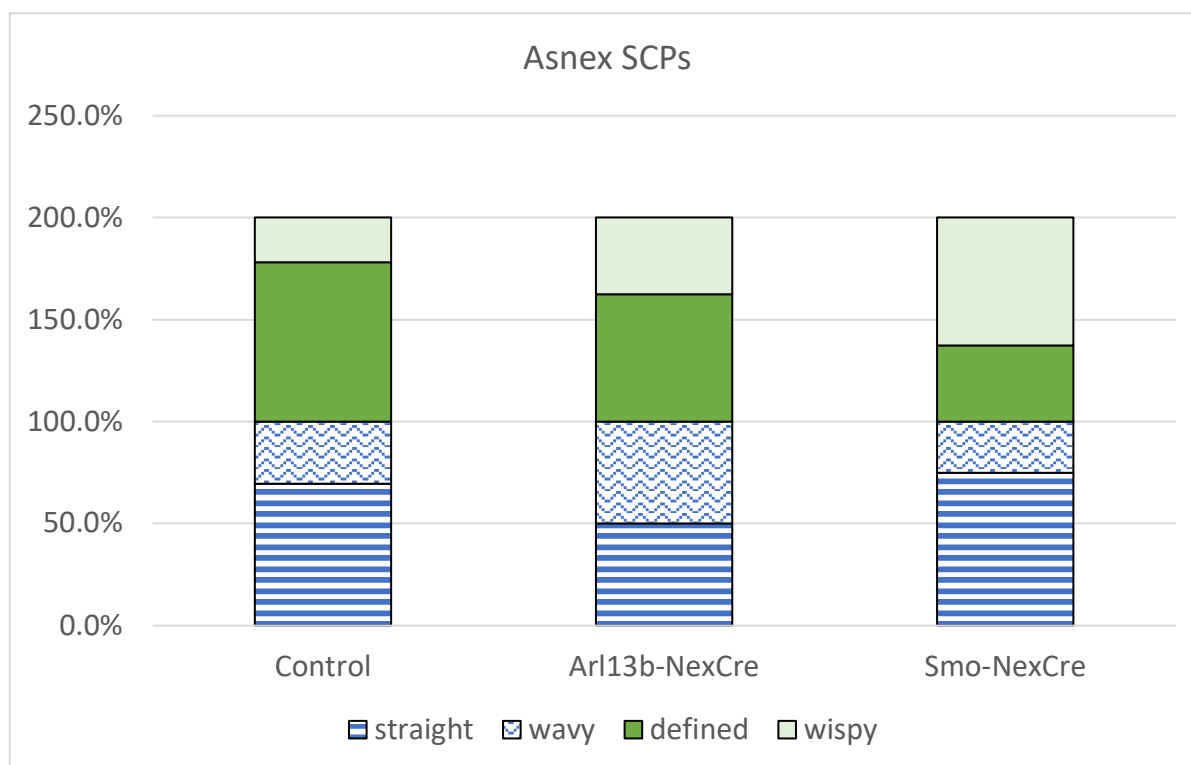


Figure 4.11 SCP decussation characterization of ARL13B or SMO conditional deletion. SCPs lacking ARL13B were wispier and wavier compared to controls at midline decussation. SCPs lacking SMO were wispier and straighter compared to controls.

In order to understand the relationship between ARL13B and MTS formation in Joubert syndrome, I generated a mouse expressing the JSRD-causing R79Q mutation. I used CRISPR/Cas9 editing to change the conserved residue in the mouse genome. This amino acid

change disrupts ARL13B's GEF activity for ARL3 (Ivanova et al. 2017; Gotthardt et al. 2015). I found *Arl13b*^{R79Q/R79Q} mice were viable and fertile. I bred the *Arl13b*^{R79Q} allele to the null *Arl13b*^A allele to make *Arl13b*^{R79Q/A} animals, which survived to adulthood (Su et al. 2012a). As *Arl13b*^{A/A} are embryonic lethal, this genetically demonstrates that *Arl13b*^{R79Q} is a hypomorphic allele of *Arl13b* (Su et al. 2012a). I categorized decussating SCPs of *Arl13b*^{R79Q/+} heterozygous controls at the midline as defined (60%) and wavy (70%) with an average crossing height of 253.3 pixels at decussation, with *Arl13b*^{R79Q/R79Q} mutant SCPs at decussation also categorized as defined (80%) and wavy (90%) with an average crossing height of 319.4 pixels at decussation (**Figures 4.12 and 4.14**).

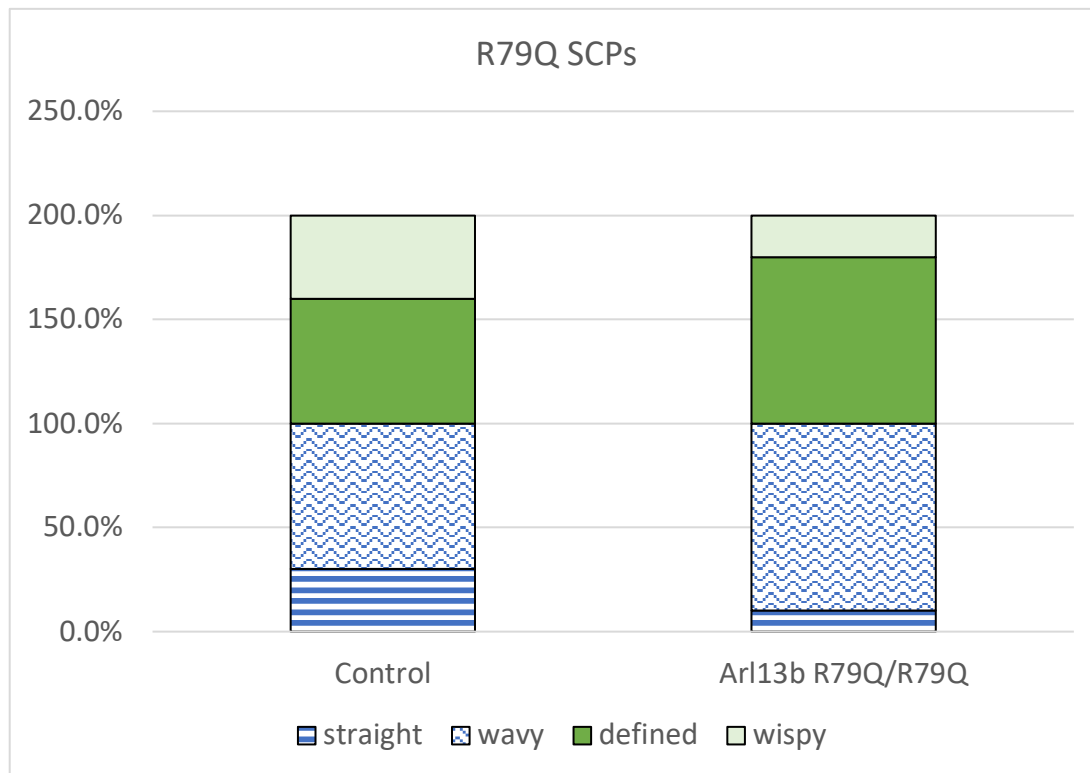


Figure 4.12 SCP decussation characterization of *Arl13b*^{R79Q} GTPase and JS mutant. SCPs expressing *Arl13b*^{R79Q} were more defined and wavy compared to controls.

ARL13B and the other 35 genes implicated in Joubert syndrome associate with the cilium or centrosome leading to the assumption that protein dysfunction from these locales underlies JSRD phenotypes (Parisi 2019). I previously demonstrated that *ARL13B*^{V358A} retains all known *ARL13B* biochemical activity, is undetectable in cilia, yet transduces vertebrate Hh signaling normally (Chapter 3) (Gigante et al. 2020; Mariani et al. 2016). I categorized decussating SCPs of *Arl13b*^{V358A/+} heterozygous controls at the midline as defined (63.2%) and straight (68.4%) with an average crossing height of 294.4 pixels at decussation, with *Arl13b*^{V358A/V358A} mutant SCPs at decussation also categorized as defined (57.1%) and straight (71.4%) with an average crossing height of 307.2 pixels at decussation (**Figures 4.13 and 4.14**).

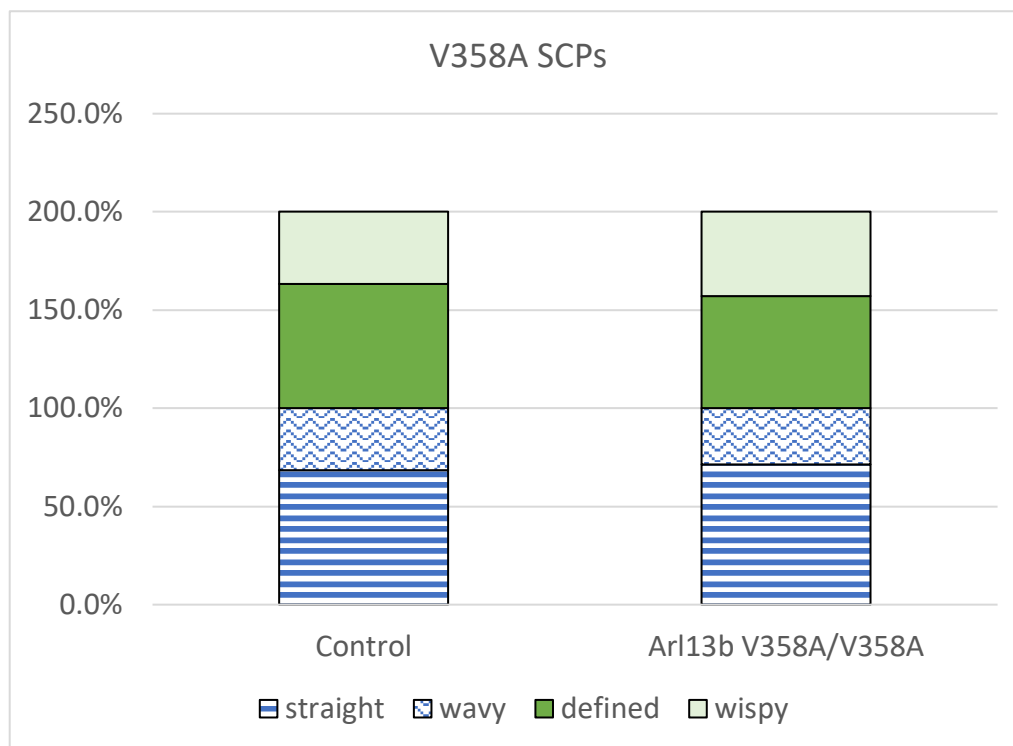


Figure 4.13 SCP decussation characterization of *Arl13b*^{V358A} cilia-excluded mutant. SCPs expressing *Arl13b*^{V358A} were very similar to controls at the point of midline decussation.

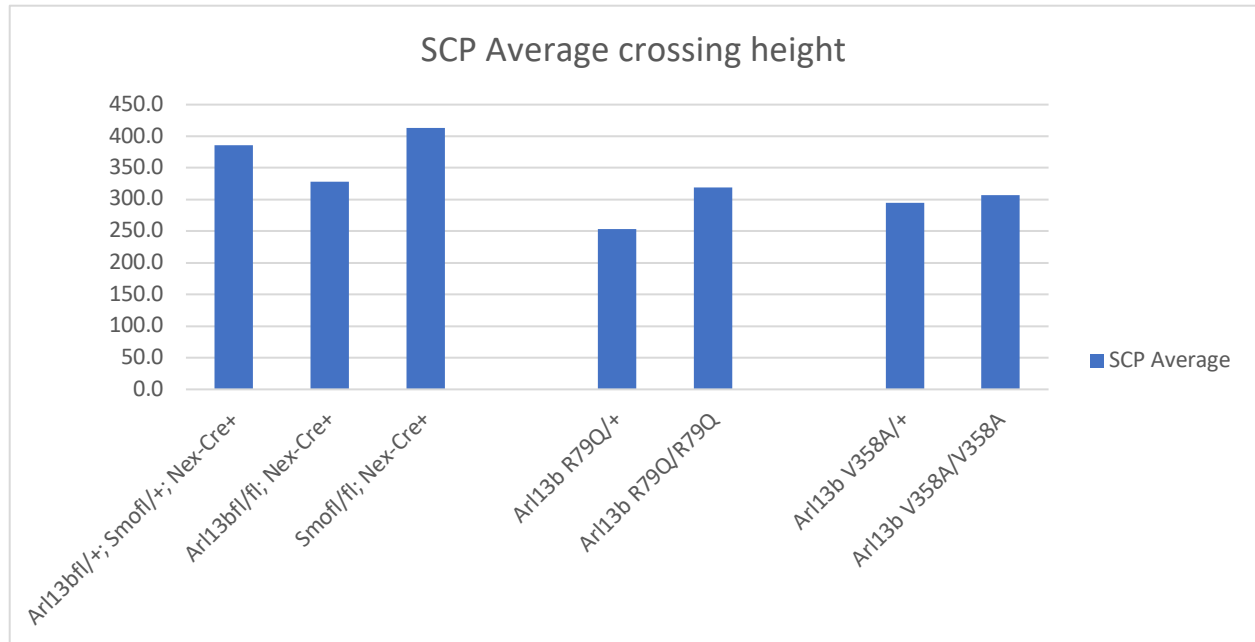


Figure 4.14 Height of SCP decussation fibers crossing the midline. Lines were drawn and measured to assess the thickness of fibers decussating. SCPs lacking SMO (N=4) showed greater height of decussation fibers compared to controls (N=8) while SCPs lacking ARL13B (N=4) showed less. Deletion of *Ift88* via *Nex-Cre* at E11.5 (7) showed no phenotype compared to controls (7). SCPs expressing JS and GTPase mutant *Ar113b^{R79Q}* (5) were thicker compared to controls (4) at decussation. SCPs expressing cilia-excluded mutant *Ar113b^{V358A}* (4) were thicker compared to controls (7) at decussation.

4.3.8 SMO is required for normal SCP projection to the dorsal thalamus

In order to test whether proper projection of SCPs requires Hedgehog (Hh) signaling, I compared the SCP tracts in mice in which I deleted the gene encoding the obligate Hh transducer *Smo* to controls. In the mature cerebellum, the SCPs project rostrally from the DCN (illustrated in **Figure 4.15A**). After entering the midbrain, the SCPs cross the midline and again turn rostrally to project to two positions in the thalamus: one tract takes a slight dorsal path and the other tract remains in the same plane; for simplicity here, I term these projection sites the dorsal and ventral thalamus,

respectively (Bohne et al. 2019). To examine the SCP tracts, I used retrograde tract tracing in which I performed stereotaxic injections of a lipophilic fluorodextran dye into either the dorsal thalamus at coordinates Bregma(AP: -0.70, ML: +1.13, DV: -3.28, angle: 0°) or the anterograde-identified site of the ventral thalamus at coordinates Bregma(AP: -0.70, ML: -2.68, DV: -4.52, angle: 20°) and allowed the dye to diffuse through the axons to the associated neuron's cell body (~7 days); I then sacrificed the animal and examined the cerebellum for evidence of the lipophilic dye indicating tracing.

I found that both dorsal and ventral thalamus injections resulted in visible clusters of dye-stained cells in the contralateral DCN, and not the ipsilateral DCN, in control animals indicating the retrograde tract tracing reliably labelled the SCPs in my hands (**Figure 4.15D-E**, dorsal: 6/8; ventral: 8/11). In the *Smo^{Nex-Cre}* mice, the results differed depending on whether I injected in the dorsal or ventral thalamus (**Figure 4.15F-G**). In the ventral thalamus injections, I detected dye-stained clusters of cells in the contralateral DCN but not the ipsilateral DCN, indicating normal SCP projection to the ventral thalamus (**Figure 4.15G**, 4/4 injections). This indicates that at least some SCPs cross the midline. In the dorsal thalamus injections, I could not detect dye-stained clusters of cells in either the contralateral or ipsilateral DCN (**Figure 4.15F**, 0/6 injections) suggesting that SCPs lacking SMO do not project to the dorsal thalamus. These data implicate SMO as critical for proper projection of the SCPs to the dorsal thalamus (all injections displayed in **Figure 4.16** and **Figure 4.17**).

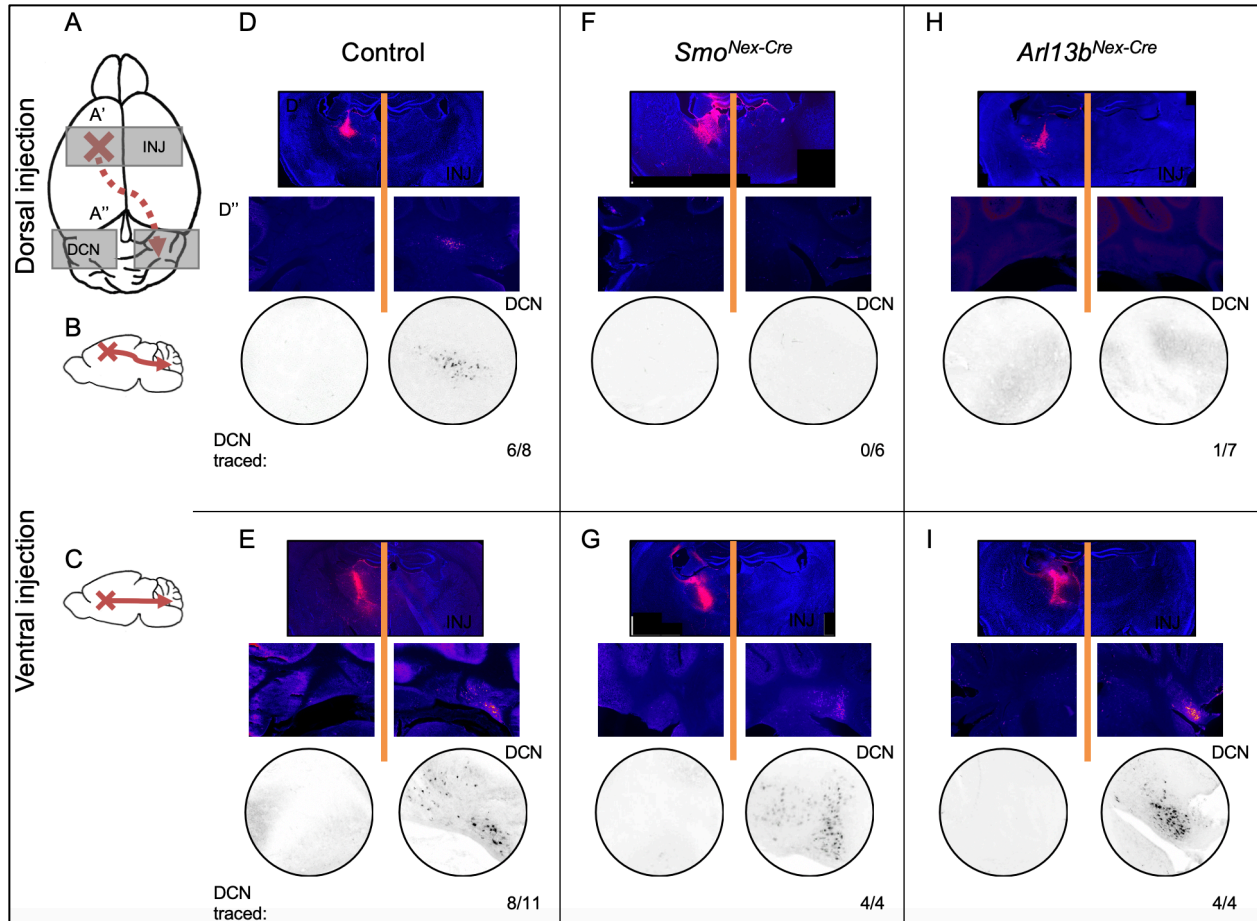


Figure 4.15 SCPs lacking ARL13B or SMO fail to project to the dorsal thalamus. (A-C) Schematics of injections and fluorescent tracer diffusion shown horizontally (A) or sagittally (B-C). (A) Red dashed arrow depicts dye path in a successful injection from injection site (red X) caudal through the brain and across the midline and into the contralateral cerebellar DCN (red arrowhead). Grey background boxes indicate area of subsequent images: the injection site (INJ) and cerebellum (DCN) (D-I) Representative images of dorsal (D, F, H) or ventral (E, G, I) thalamus injection site (top panel) and cerebellum (middle panel) with the DCN in hatched grey circle and magnified (bottom panel) with recoloring to black and white to aid visualization. The retrograde fluorescent tracer is pink-red and sections are stained with DAPI. Red numbers indicate the number of positively stained DCN clusters (DCN traced) out of the total number of injected animals. Note that no tracing was observed on ipsilateral side to injection. (D, E) Fluorescent tracer injection in *Smo^{fl/+}; Arl13b^{fl/+}; Nex-Cre* control animals resulted in contralateral DCN staining in (D) 6/8 dorsal thalamus injections and (E) 8/11 ventral thalamus injections. (F, G) Fluorescent tracer injection in *Smo^{Nex-Cre}* animals resulted in contralateral DCN staining in (F) 0/6 dorsal thalamus injections (Fisher's exact test, two-tailed, significant difference, $P=0.0097$) and (G) 4/4 ventral thalamus injections (not significant (ns), $P=0.5165$). (H, I) Fluorescent tracer injection in *Arl13b^{Nex-Cre}* animals resulted in contralateral DCN staining in (H) 1/7 dorsal thalamus injections (significant difference, $P=0.0406$) and (I) 4/4 ventral thalamus injections (ns, $P=0.5165$).

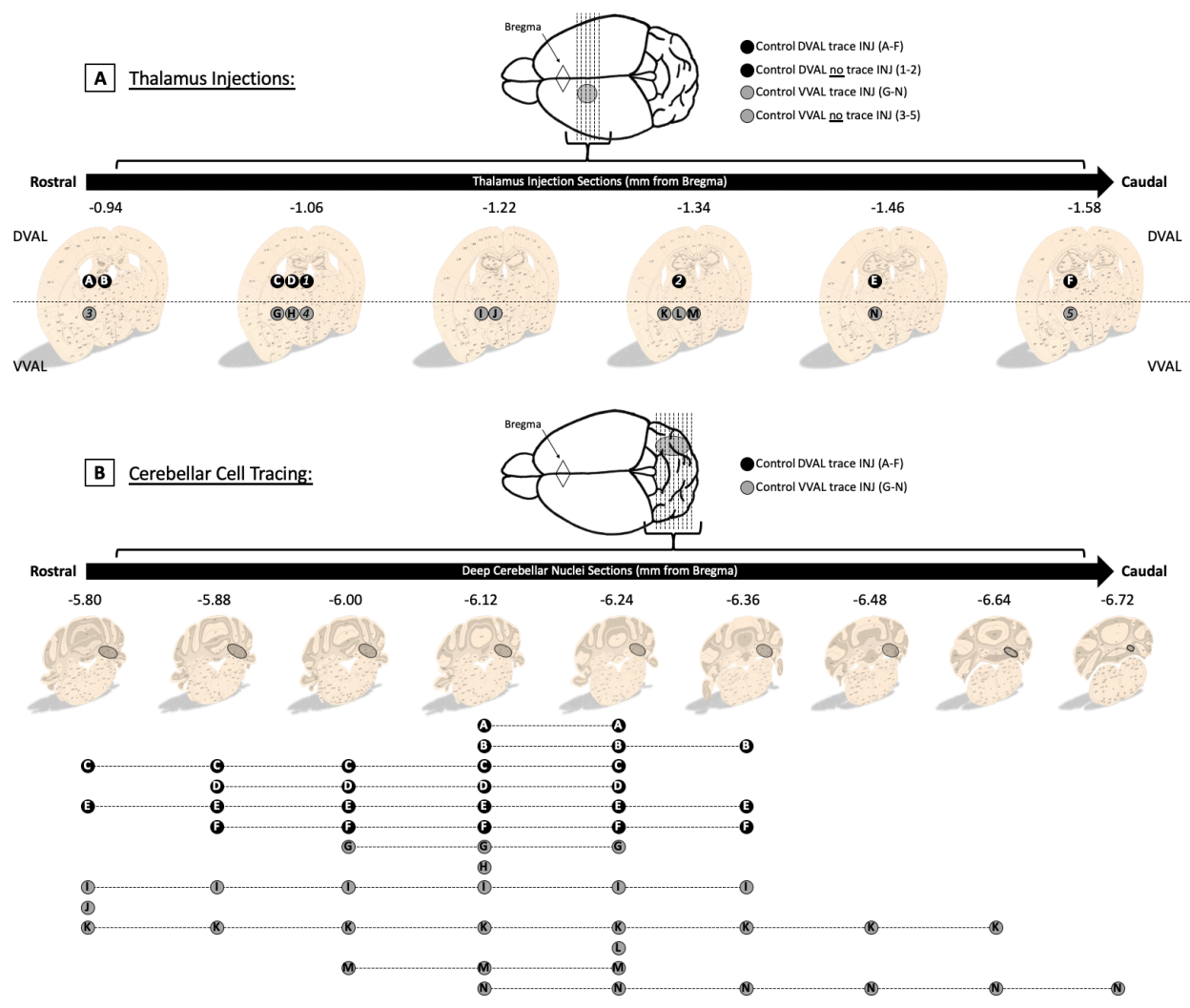


Figure 4.16 Total injection results of *Arl13b*^{fl/+}; *Smo*^{fl/+} heterozygous controls. (A) Range of injection sites. Shown at top are coronal sections of the cortex at the location of the thalamus labeled with distance from Bregma (diamond) in mm. Circles represent injection sites as identified by needle mark, presence of dye, and tissue landmarks. Injections that resulted in fluorescent deep cerebellar nuclei (DCN) are labeled by letter, injections that did not result in fluorescent DCN are labeled by number. Injections into the dorsal thalamus (DVAL) are dark color labeled in white, injections into the ventral thalamus (VVAL) are lighter color labeled in black. (B) Range of DCN sites. Shown at top are sections of the cerebellum where DCN cell clusters can be identified labeled with distance from Bregma in mm. Lines correspond to lettered injection circles that resulted in fluorescent traced DCN. The lines stretch to cover and mark the cerebellar sections in which fluorescent DCN could be identified.

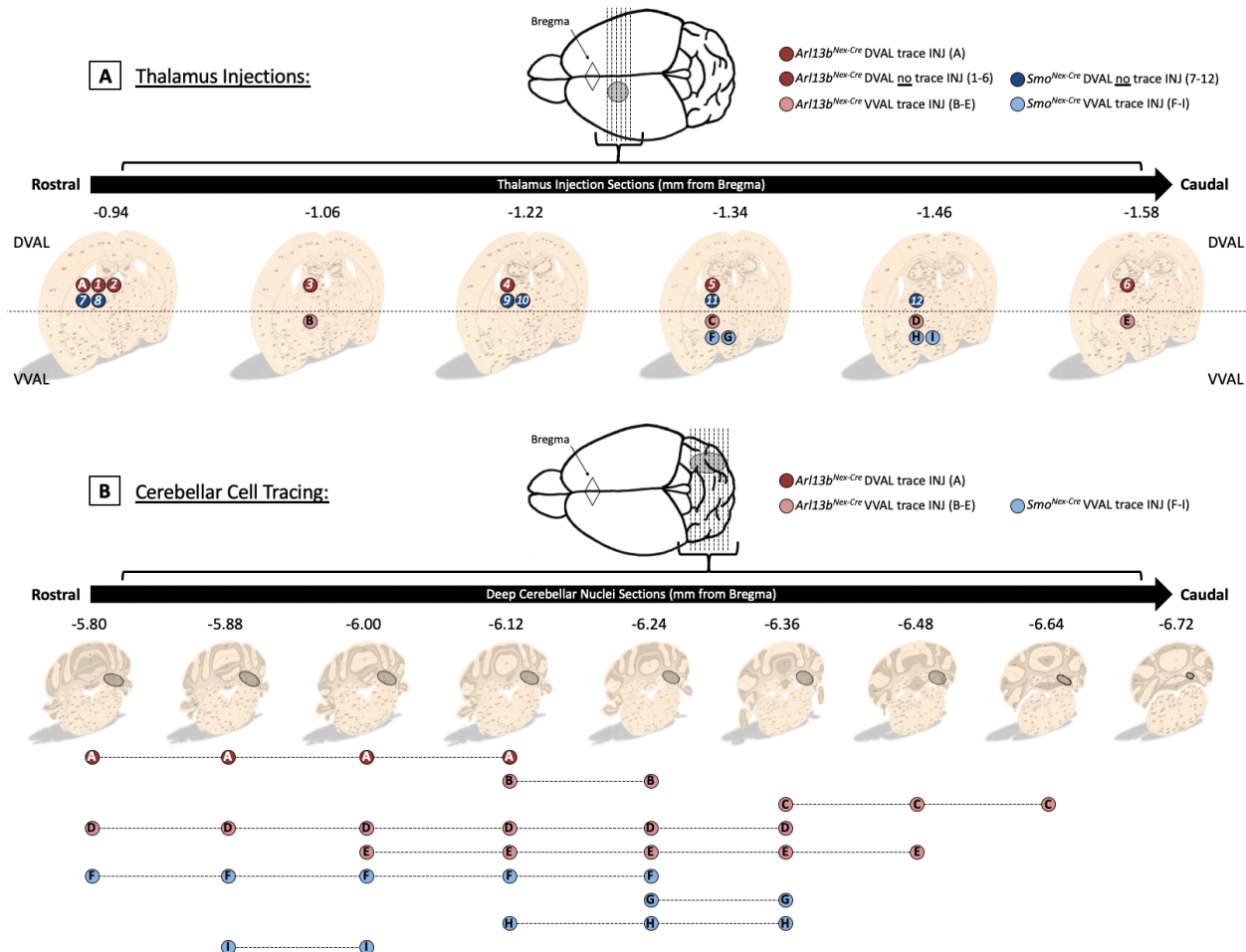


Figure 4.17 Total injection results of *Arl13b^{Nex-Cre}* and *Smo^{Nex-Cre}* mutants. (A) Range of injection sites. Shown at top are coronal sections of the cortex at the location of the thalamus labeled with distance from Bregma (diamond) in mm. Circles represent injection sites as identified by needle mark, presence of dye, and tissue landmarks. Injections that resulted in fluorescent deep cerebellar nuclei (DCN) are labeled by letter, injections that did not result in fluorescent DCN are labeled by number. Injections into the dorsal thalamus (DVAL) are dark color labeled in white, injections into the ventral thalamus (VVAL) are lighter color labeled in black. (B) Range of DCN sites. Shown at top are sections of the cerebellum where DCN cell clusters can be identified labeled with distance from Bregma in mm. Lines correspond to lettered injection circles that resulted in fluorescent traced DCN. The lines stretch to cover and mark the cerebellar sections in which fluorescent DCN could be identified.

4.3.9 *ARL13B* is required for normal SCP projection to the dorsal thalamus

Given that ARL13B regulates vertebrate Hh signaling in a variety of contexts, I next assessed ARL13B's role in proper SCP projection using *Ar13b^{Nex-Cre}* mice. I performed dorsal and ventral thalamus injections for retrograde tract tracing to examine the SCPs (**Figure 4.15H-I**). In the ventral thalamus injections of *Ar13b^{Nex-Cre}* mice, I found dye-stained clusters of cells in the contralateral DCN consistent with normal SCP projections crossing the midline and projecting to the ventral thalamus (**Figure 4.15I**, 4/4 injections). In contrast, in the dorsal thalamus injections of *Ar13b^{Nex-Cre}* mice, I generally did not detect dye-stained clusters of cells in either the contralateral or ipsilateral DCN suggesting that the SCPs lacking ARL13B do not project to the dorsal thalamus (**Figure 4.15H**, 1/7 injections). These data link ARL13B function to normal SCP projection. Furthermore, they reveal the same phenotype in *Smo^{Nex-Cre}* and *Ar13b^{Nex-Cre}* mice (all injections displayed in **Figure 16** and **Figure 17**).

4.3.10 *ARL13B* does not function from within cilia to mediate SCP guidance

To directly ask whether ARL13B mediates SCP guidance to the dorsal thalamus from within cilia, I examined mice expressing the cilia-excluded variant of ARL13B, ARL13B^{V358A} (**Figure 4.18**)(Gigante et al. 2020). I found that either dorsal or ventral thalamus injections resulted in visible clusters of dye-stained cells in the contralateral DCN in control (**Figure 4.18A-B**, dorsal: 3/3; ventral: 5/5) and *Ar13b^{V358A/V358A}* (**Figure 4.18C-D**, dorsal: 3/3; ventral: 3/3) animals. In the context of the previous result showing that *Ar13b^{Nex-Cre}* mice display abnormal SCP projections to the dorsal thalamus, these data demonstrate that ARL13B does not function from within cilia to regulate SCP projections (all injections displayed in **Figure 19**).

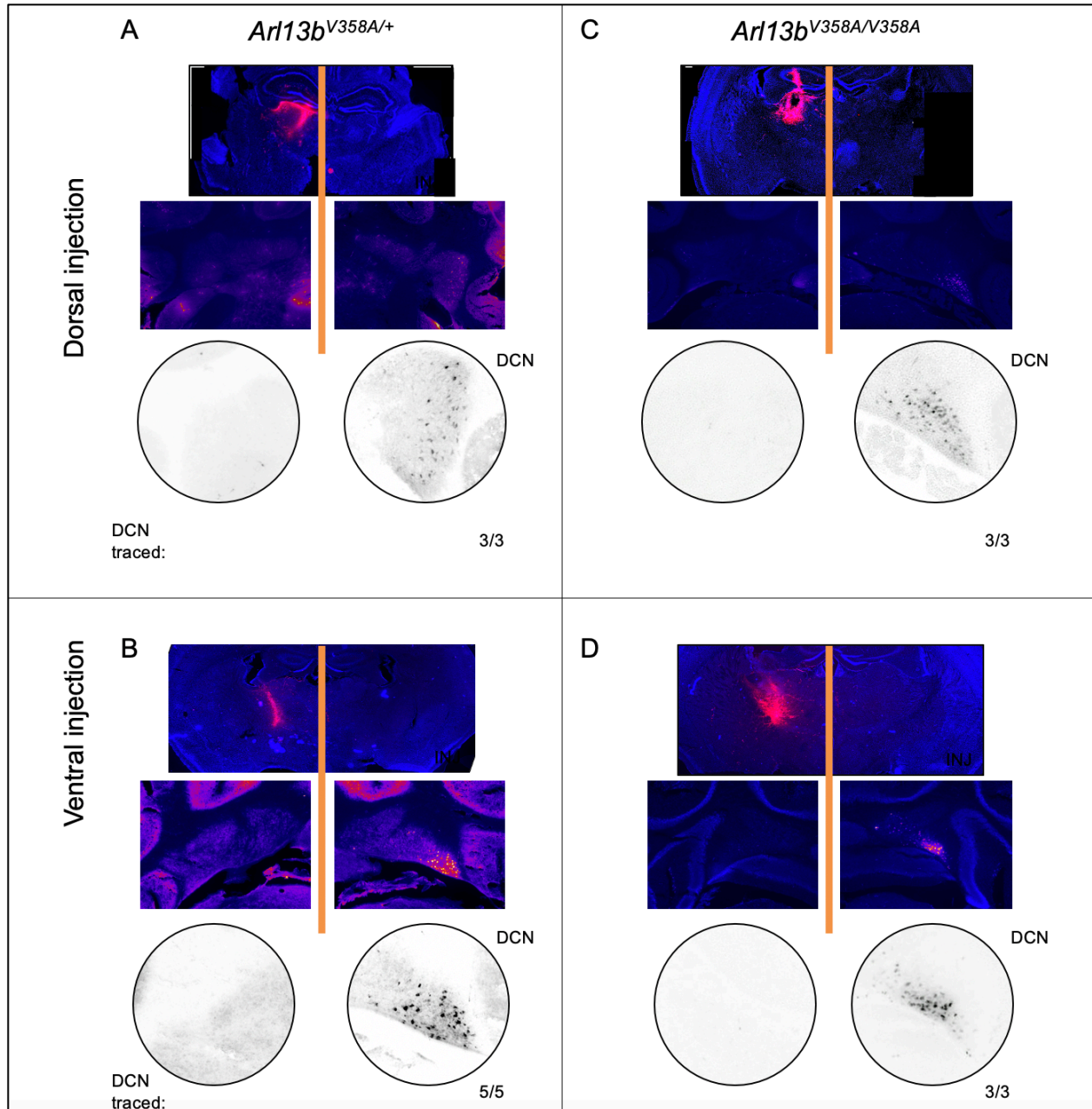


Figure 4.18 SCPs expressing cilia-excluded *ARL13B*^{V358A} project normally to both the dorsal and ventral thalamus. (A-D) Representative images of dorsal (A, C) or ventral (B, D) thalamus injection site (top panel) and cerebellum (middle panel) with the DCN in hatched grey circle and magnified (bottom panel) with recoloring to black and white to aid visualization. Red numbers indicate the number of positively stained DCN clusters out of the total number of injected animals. Note that no tracing was observed on the injection's ipsilateral side. (A, B) Fluorescent tracer injection in *Arl13b*^{V358A/+} control animals resulted in contralateral DCN staining in (A) 3/3 dorsal thalamus injections and (B) 5/5 ventral thalamus injections. (C-D) Fluorescent tracer injection in *Arl13b*^{V358A/V358A} animals resulted in contralateral DCN staining in (C) 3/3 dorsal thalamus injections (Fisher's exact test, two-tailed, ns, $P > 0.9999$) and (D) 5/5 ventral thalamus injections (ns, $P > 0.9999$).

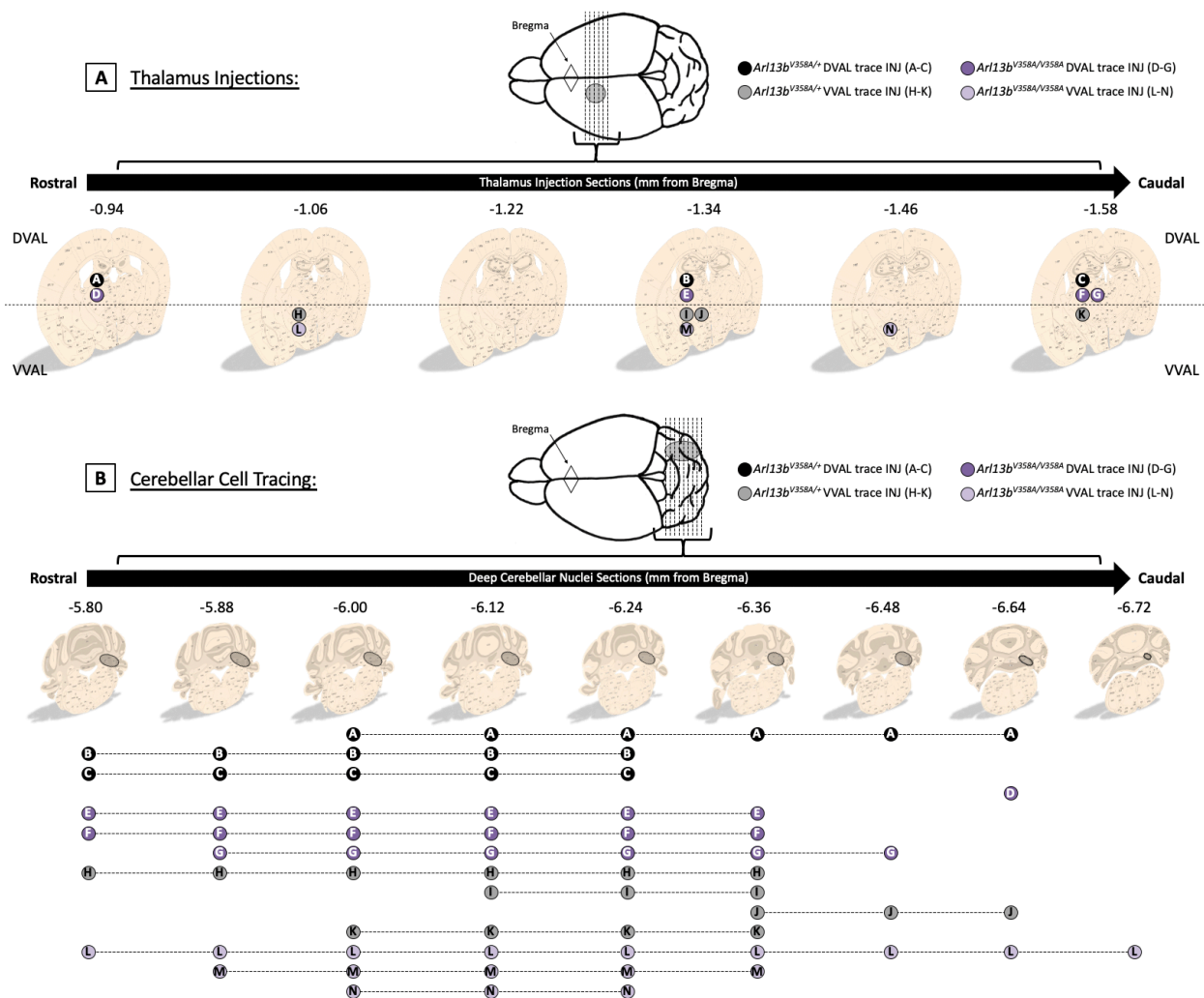


Figure 4.19 Total *Arl13b*^{V358A} injection results. (A) Range of injection sites. Shown at top are coronal sections of the cortex at the location of the thalamus labeled with distance from Bregma (diamond) in mm. Circles represent injection sites as identified by needle mark, presence of dye, and tissue landmarks. Injections that resulted in fluorescent deep cerebellar nuclei (DCN) are labeled by letter, injections that did not result in fluorescent DCN are labeled by number. Injections into the dorsal thalamus (DVAL) are dark color labeled in white, injections into the ventral thalamus (VVAL) are lighter color labeled in black. (B) Range of DCN sites. Shown at top are sections of the cerebellum where DCN cell clusters can be identified labeled with distance from Bregma in mm. Lines correspond to lettered injection circles that resulted in fluorescent traced DCN. The lines stretch to cover and mark the cerebellar sections in which fluorescent DCN could be identified.

4.3.11 SCP projection in mice expressing a Joubert-causing allele, *Arl13b*^{R79Q}

In order to assess the role of ARL13B^{R79Q} in SCP guidance, I performed dorsal and ventral thalamus dye injections in control and *Arll3b*^{R79Q/R79Q} mice (**Figure 4.20**). I identified visible clusters of dye-stained cells in the contralateral DCN in control (**Figure 4.20A-B**, dorsal: 4/4; ventral: 3/3) and *Arll3b*^{R79Q/R79Q} (**Figure 4.20C-D**, dorsal: 3/3; ventral: 3/4) animals. Thus, despite the constitutive expression of the JSRD-causing allele throughout development, I did not detect a SCP projection defect in the *Arll3b*^{R79Q/R79Q} mouse model (all injections displayed in **Figure 4.21**). In the context of the abnormal SCP projections to the dorsal thalamus that I identified in the *Smo*^{Nex-Cre} and *Arll3b*^{Nex-Cre} mice, this result suggests that the *Arll3b*^{R79Q} allele does not disrupt SMO function or any ARL13B function that regulates SMO.

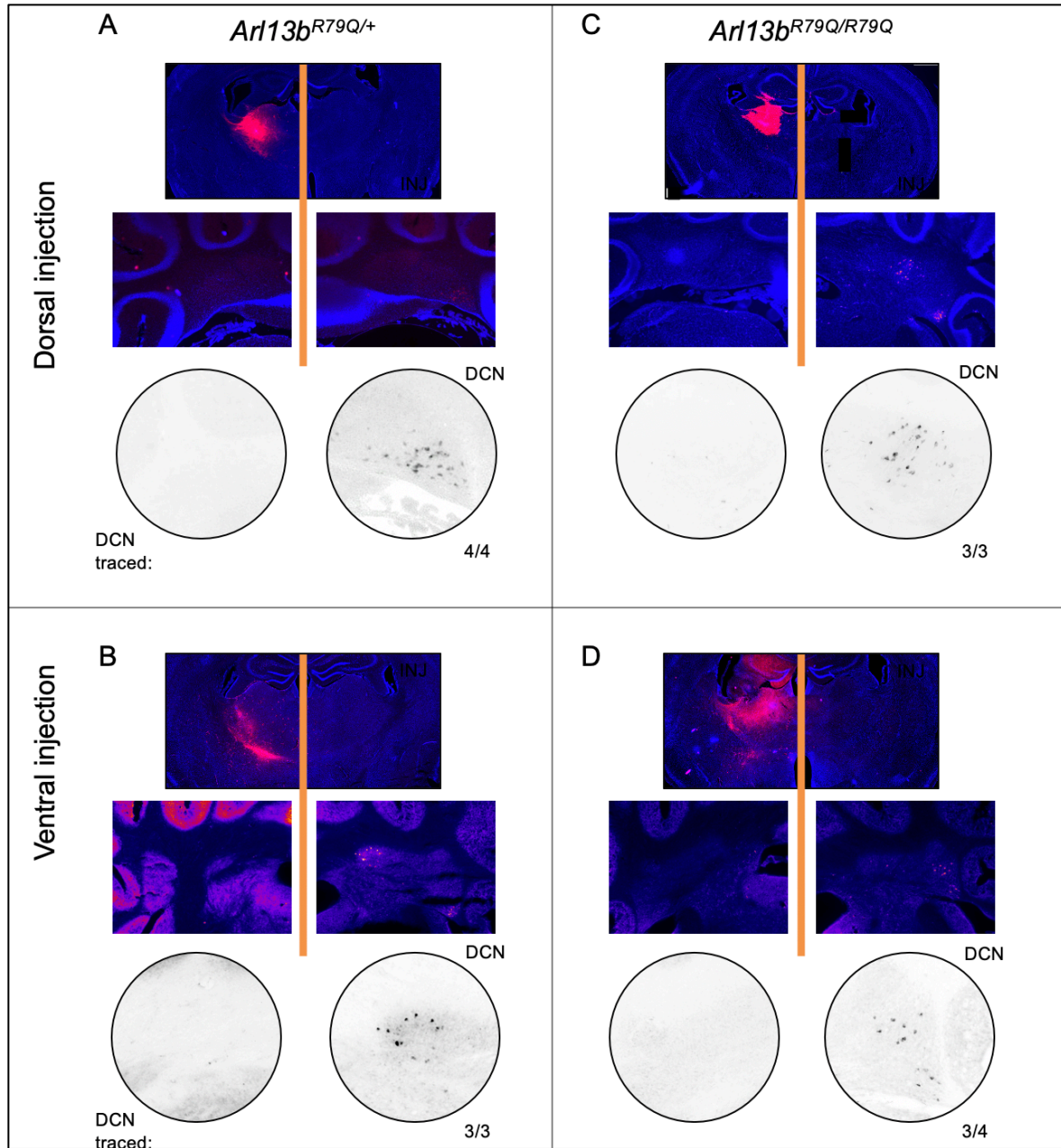


Figure 4.20 SCPs expressing JS allele *Arl13b^{R79Q}* project normally to both the dorsal and ventral thalamus (A-D) Representative images of dorsal (A, C) or ventral (B, D) thalamus injection site (top panel) and cerebellum (middle panel) with the DCN in hatched grey circle and magnified (bottom panel) with recoloring to black and white to aid visualization. Red numbers indicate the number of positively stained DCN clusters out of the total number of injected animals. Note that no tracing was observed on the injection's ipsilateral side. (A, B) Fluorescent tracer injection in *Arl13b^{R79Q/+}* control animals resulted in contralateral DCN staining in (A) 4/4 dorsal thalamus injections and (B) 3/3 ventral thalamus injections. (C-D) Fluorescent tracer injection in *Arl13b^{R79Q/R79Q}* animals resulted in contralateral DCN staining in (C) 3/3 dorsal thalamus injections (Fisher's exact test, two-tailed, ns, $P > 0.9999$) and (D) 3/4 ventral thalamus (ns, $P > 0.9999$).

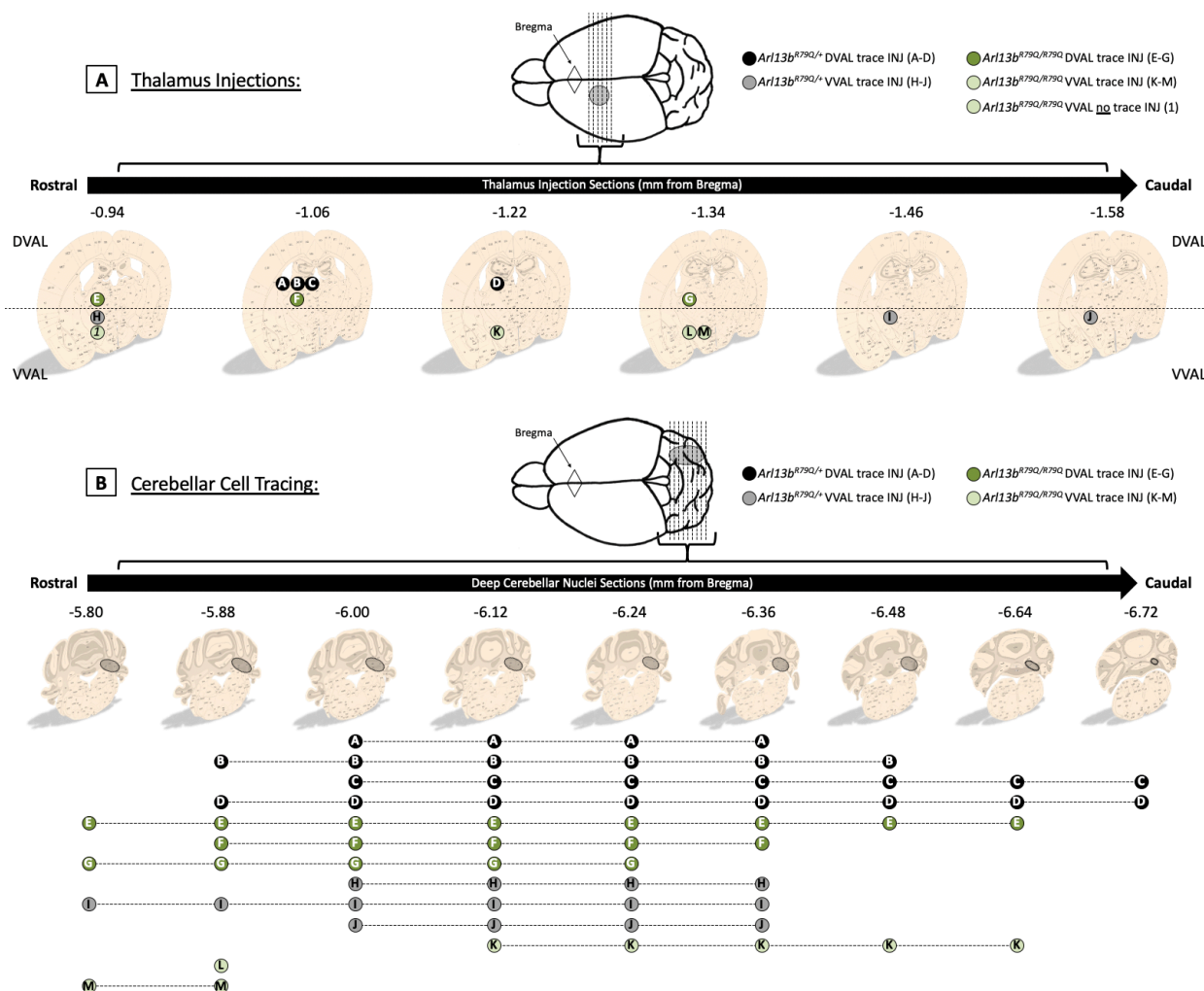


Figure 4.21 Total *Arl13b*^{R79Q} injection results. (A) Range of injection sites. Shown at top are coronal sections of the cortex at the location of the thalamus labeled with distance from Bregma (diamond) in mm. Circles represent injection sites as identified by needle mark, presence of dye, and tissue landmarks. Injections that resulted in fluorescent deep cerebellar nuclei (DCN) are labeled by letter, injections that did not result in fluorescent DCN are labeled by number. Injections into the dorsal thalamus (DVAL) are dark color labeled in white, injections into the ventral thalamus (VVAL) are lighter color labeled in black. (B) Range of DCN sites. Shown at top are sections of the cerebellum where DCN cell clusters can be identified labeled with distance from Bregma in mm. Lines correspond to lettered injection circles that resulted in fluorescent traced DCN. The lines stretch to cover and mark the cerebellar sections in which fluorescent DCN could be identified.

4.4 Discussion

Here I demonstrate that complete loss of *Arll3b* function in mouse can recapitulate a JS dysmorphology that leads to the MTS: aberrant SCP thalamic targeting. I expand the role of Hh signaling as a critical guidance cue by showing it is required for proper SCP projection to the dorsal thalamus. My finding that the SCP phenotype is identical in *Smo^{Nex-Cre}* and *Arll3b^{Nex-Cre}* mice is consistent with a model whereby ARL13B regulates SCP projections to the dorsal thalamus via a SMO-dependent mechanism. In line with previous work showing that ARL13B does not function from within cilia to regulate of Shh-guided axon guidance, I found normal SCP thalamic targeting in mice expressing only a cilia-excluded ARL13B variant (Feret et al. 2019). By mutating a conserved arginine to glutamine, I generated a mouse expressing a JSRD-causative mutation and in which we observed no change in vertebrate Hh signaling (Ivanova et al. 2017; Mariani et al. 2016). I further identified no defects in JS mutation *Arll3b^{R79Q/R79Q}* SCP projections.

Through DTI, anterograde injections, and retrograde injections it is clear that SCPs lacking SMO are more diffuse, disorganized, and thus larger than controls indicating SMO is required for SCP organization. *Arll3b^{Nex-Cre}* also displayed a lower FA at the midline through DTI, consistent with wider SCPs decussating in anterograde injections, however, *Arll3b^{Nex-Cre}* displayed a smaller decussation height in retrograde injections. These two examples show that the SCPs are complicated in how they are regulated, or perhaps that visualizing them in different methods yields different insights. Further, while SCPs lacking ARL13B display increased decussation height in anterograde injections, in retrograde injections they do not demonstrate a phenotype. SCPs lacking ARL13B do consistently display increased wispieness of axon fibers compared to control. A possible explanation resides in what the different methods of injection

show, where injection of the thalamus will result in DCN staining of cells that project to that site and anterograde show what all injected DCN do. Thus, it is possible that as some SCPs project to the dorsal and some to the ventral thalamus, so too could I be picking up a wider decussation of SCPs in anterograde injections as these are not restricted by which thalamic site the mutant SCPs project to. Thus, it remains possible that deep characterization of SCPs will be best explored via anterograde injections going forward. This would indicate that areas most in need of exploration moving forward are how to ensure all DCN take up dye, as well as how to properly image such injections, potentially via CLARITY. Furthermore, I attempted a similar but much less intensive type of clearing using TDE (Aoyagi et al. 2015). In this method, I sectioned the brain horizontally at 300 microns thick. This increase in thickness, compared to the 60-micron thickness of previous horizontal sections, would allow for greater visualization of the SCP tract as it would be less divided among horizontal sections. Upon introduction of sections to TDE, tissue became less opaque (**Figure 2.2**). This clearer tissue via TDE could be a good alternative to CLARITY in future efforts to image whole SCP tracts.

Overall my data indicate ARL13B function is critical for SCP targeting. At one level, my data implicate Hh signaling in the etiology of the MTS since I show that SCP targeting requires SMO. However, at another level, my data indicate that Hh-independent pathways are at play as I don't observe Hh defects in the presence of the JSRD-causing *Arl13b^{R79Q}* allele. The MTS could be due to disruption of different pathways in the SCPs, and this would imply that the 35 JSRD implicated genes all affect the distinct pathways in a similar manner (Parisi 2019). Alternatively, the MTS may form due to alterations in any of a few pathways- and it is even possible that alterations in one pathway could

impact other pathways- or the ability of cells to respond to those other pathways. Such a model is hinted at by previous work showing interplay between the Hh and Wnt pathways underlying the severity of hindbrain phenotypes (Bashford and Subramanian 2019; Hagemann and Scholpp 2012). Parallel reasoning would thus suggest that while *Arll3b*^{R79Q/R79Q} mice clearly transduce Hh reasonably well, there may be subtle changes in Shh signaling or even changes that influence Wnt signaling.

In patients, the SCP targeting deficit is more severe than what I observed in the mice. The SCPs in patients do not cross the midline, appearing thickened on the ipsilateral side relative to their DCN (Poretti et al. 2007; Yachnis and Rorke 1999). However, in the mouse I infer midline crossing of the SCPs. In the case of the *Smo*^{Nex-Cre} conditional mice, it is formally possible that the SCPs do not rely on SMO for midline crossing but only for subsequent targeting to the dorsal thalamus. The fact that the *Arll3b*^{Nex-Cre} conditional mice phenocopied the *Smo*^{Nex-Cre} phenotype makes this less likely, since ARL13B is directly implicated in JSRD and regulates SMO-dependent axon guidance in other contexts (Cantagrel, Silhavy, Bielas, Swistun, Marsh, Bertrand, Audollent, Attie-Bitach, Holden, Dobyns, Traver, Al-Gazali, Ali, Lindner, Caspary, Otto, Hildebrandt, Glass, Logan, Johnson, Bennett, Brancati, Valente, et al. 2008; Ferent et al. 2019). It is also plausible that the protein turnover driven by *Nex-Cre* completed after midline crossing occurred. *Nex-Cre* expression initiates at E11.5 in the cells on the rhombic lip of the cerebellar anlage as they start to migrate and be specified before occupying the deep cerebellar nuclei (Fink 2006; Goebbels et al. 2006). I expect deletion would occur in the precursors and therefore the neurons of the DCN would not express protein. Finally, it is possible that mouse is not a valid system in which to model the SCP midline crossing defect. This might explain why I saw no defects in the SCP targeting of the *Arll3b*^{R79Q/R79Q} mice, as this is a constitutive mutation

that requires no protein turnover, yet ARL13B^{R79Q} prevents SCP midline crossing in patients (Miertzschke et al. 2014). Indeed, other mouse mutants such as *Cep290* and *Ahi1* which recapitulate the MTS cerebellar vermis hypoplasia, also do not display midline crossing defects in the SCPs (Bourgeois and Ferland 2019; Romano et al. 2006; Lancaster et al. 2011). Whether this is due to anatomical distinctions between the cerebellum in mouse and human or the genetic background on which these models were examined are open questions.

Examining SCP projections is labor intensive and it has not been done systematically among the JSRD mouse models (Bourgeois and Ferland 2019; Romano et al. 2006; Lancaster et al. 2011; Bashford and Subramanian 2019). While previous work showed that *Ar113b*^{Nex-Cre} and *Inpp5e*^{Nex-Cre} mice exhibit SCP targeting deficits, here I pinpoint the *Ar113b*^{Nex-Cre} defect as specific to the projection to the dorsal thalamus (Guo et al. 2019). The projection to the ventral thalamus remains intact, suggesting there is not a generalized deficit in axon outgrowth within the tract. Work on the *Ar113b*^{Nex-Cre} and *Inpp5e*^{Nex-Cre} SCP targeting deficits argue that PI3K/Akt signaling from within cilia led to the tract defects (Guo et al. 2019). However, I found that cilia-excluded ARL13B^{V358A} mediated SCP targeting normally. These conflicting results could be explained by differences in the experimental details as the data supporting ciliary ARL13B function used viral rescue whereas I used genetic mutations engineered at the endogenous locus in this study. Alternatively, these data could indicate that ARL13B plays an important cellular role in the ciliary trafficking of key components needed for the PI3K/Akt pathways.

JSRD-causing mutations in ARL13B are generally restricted to the GTPase domain of the protein, although 2 residues in the C-terminus are implicated in disease (Cantagrel, Silhavy, Bielas, Swistun, Marsh, Bertrand, Audollent, Attie-Bitach, Holden, Dobyns, Traver, Al-Gazali, Ali, Lindner, Caspary, Otto, Hildebrandt, Glass, Logan, Johnson, Bennett, Brancati, Valente, et al. 2008; Thomas et al. 2015; Shaheen et al. 2016; Bachmann-Gagescu et al. 2015; Rafiullah et al. 2017). Based on other ARL proteins, ARL13B likely assumes distinct conformations upon the binding either GDP or GTP, permitting different binding partners or altering affinities for binding partners (Miertzschke et al. 2014; Pasqualato, Renault, and Cherfils 2002). None of the tested JSRD-causing mutations (R79Q, Y86C or R200C) disrupt GTP binding or hydrolysis, however, all three mutations disrupt ARL13B function as an ARL3 GEF (Ivanova et al. 2017). Given that complete deletion of ARL13B is embryonic lethal and thus impacts broader biological processes development compared to the R79Q mutation and that the null mutant misregulates Hh signaling whereas R79Q does not, I conclude that a subset of ARL13B function is disrupted in JSRD.

CHAPTER 5
PERSPECTIVE

Parts of this chapter published in:

Suciu, S.K., and Caspary, T. (2020) Cilia, neural development and disease. *Seminars in Cell & Developmental Biology*

5.1 Introduction

My dissertation explores the cilia-associated GTPase ARL13B and its role in transcription-independent Shh signaling, both in fibroblast migration and in axon guidance in the mouse hindbrain. The human ciliopathy Joubert Syndrome inspired much of my work, as it displays clear misguidance of axons, a process connected to Shh but not the cilium. Uncovering mechanistic functions of Arl13b in axon guidance revealed a fascinating result where ARL13B, a protein well-known to localize to the cilium, regulates Shh from outside of the cilium to regulate transcription-independent Shh signaling; and furthermore that its function as a GTPase is not consistent between these processes. In my dissertation I investigated the role of ARL13B in relation to Shh signaling in one of the two major features of the MTS: the targeting of the SCPs to the thalamus (with the other being hypoplasia of the cerebellar vermis). I explored SCP guidance using a series of mouse alleles through which I first defined the role of ARL13B and subsequently untangled the role of ARL13B from within the cilium from its cellular role and investigated a JS-causing patient allele. Taken together, my data illuminate the roles of ARL13B in MTS etiology and the complexity in modeling aspects of the MTS in mouse. In fact, my data are consistent with the complexity exhibited by other JSRD mouse models examined to date (Delous et al. 2007; Garcia-Gonzalo et al. 2011; Roberson et al. 2015; Bashford and Subramanian 2019). In this final chapter I will show preliminary data on ARL13B function in cerebellar proliferation, further implicating ARL13B in the regulatory processes gone awry in the diagnostic Joubert MTS. With these results, I offer my perspective on the role of ARL13B in development and in JS as well as highlight the processes in which it does and does not function as a cilia-associated GTPase. Finally, I will conclude with a discussion of the microtubule code and Future Directions to posit that the common theme of ARL13B regulation of both cilia-

dependent and -independent Shh may be found in the shared microtubule-based structures of the cilium and axon.

5.2 Preliminary results indicate *Arl13b* plays a critical role in cerebellar development

5.2.1 *Arl13b* may function as a GTPase to regulate cerebellar vermis size

As described in Chapter 4, I examined SCP projection in mice expressing the JS allele *Arl13b*^{R79Q/R79Q}. The SCPs showed no projection phenotype, where SCPs target both the dorsal and ventral thalamus appropriately. The lack of a SCP projection phenotype in the *Arl13b*^{R79Q/R79Q} mice surprised us, since JS patients expressing this allele display the MTS. However, in addition to defects in the SCPs, the MTS is due to an underdeveloped cerebellar vermis, so I examined the size of the cerebellar vermis and hemisphere in control and *Arl13b*^{R79Q/R79Q} mice (**Figure 5.1**) (Aguilar et al. 2012; Yachnis and Rorke 1999). Furthermore, ARL13B is shown to have a role in the development of the cerebellum in zebrafish, supporting the likelihood of discovering a phenotype when ARL13B is not present or aberrant in mouse cerebellar development (Zhu et al. 2020). To quantify cerebellar size, I obtained sagittal cerebellar sections through either the left or right hemisphere along with the entire vermis of animals at weaning. I measured the cerebellar area of each section and calculated the mean area for sections from the hemisphere as well as from those of the vermis. I detected no difference in the cerebellar hemisphere size between control and *Arl13b*^{R79Q/R79Q} mice (**Figure 5.1D**). In contrast, I found in preliminary analysis that the mean area of the cerebellar vermis of *Arl13b*^{R79Q/R79Q} mice was 11.6% smaller than that of control animals (**Figure 5.1G**). Thus, *Arl13b*^{R79Q/R79Q} mice may display a small cerebellar vermis consistent with

the JS patient phenotype, though results require a higher sample size to potentially reach statistical significance.

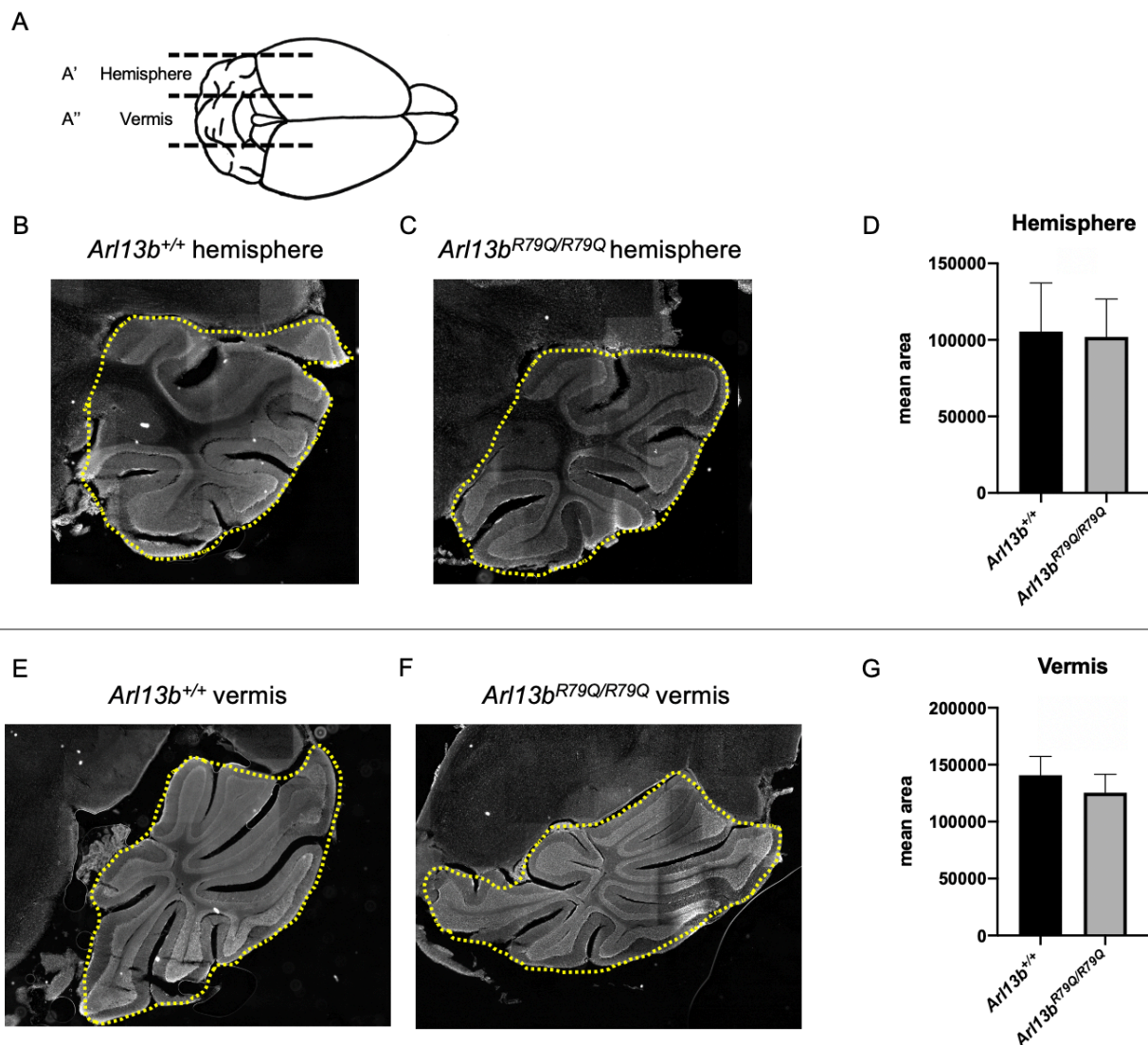


Figure 5.1 Expression of JSRD-causing allele *Arl13b*^{R79Q} results in small cerebellar vermis. (A) Schematic of analyzed cerebellar areas: (A') one hemisphere and (A'') the entire vermis for each sample brain. (B, C, E, F) Representative images of cerebellar sections with analyzed area outlined by dashed yellow line. (B-D) Representative cerebellar hemispheres in (B) *Arl13b*^{+/+} control (n=3 brains, 126 total sections) and (C) *Arl13b*^{R79Q/R79Q} mutant (n=3 brains, 126 total sections). (D) No difference in mean pixel area quantification of cerebellar hemisphere size between *Arl13b*^{+/+} and *Arl13b*^{R79Q/R79Q} animals. (E-G) Representative cerebellar vermes in (E) *Arl13b*^{+/+} control mice (n=3 brains, 126 total sections) and (F) *Arl13b*^{R79Q/R79Q} mice (n=3 brains, 117 total sections). (G) *Arl13b*^{R79Q/R79Q} mutant vermes displayed a mean pixel area 11.6% smaller than that in *Arl13b*^{+/+} controls (ns).

5.2.2 Global cerebellar hypoplasia in mice lacking *Ar13b* in all neurons

Given that *Ar13b*^{R79Q} is a hypomorphic mutation, I wanted to investigate how ARL13B regulates cerebellar size globally. To do so, I crossed the *Brn4-Cre* allele into the conditional null *Ar13b*^{fl/fl} background, called *Ar13b*^{Brn4-Cre} (**Figure 5.2**). *Brn4-Cre* initiates expression at E8.5 throughout the neurectoderm so the cerebellum develops in the absence of ARL13B (Hazen et al. 2012; Heydemann, Nguyen, and Crenshaw Iii 2001). *Ar13b*^{Brn4-Cre} mice develop hydrocephaly just after weaning which often leads to death. Thus, I measured the cerebellar area of sagittal cerebellar sections from animals at weaning. I found the cerebellar hemispheres of *Ar13b*^{Brn4-Cre} mice were 23.4% smaller than those of the controls (**Figure 5.2C**). Similarly, I observed the cerebellar vermes were 24.7% smaller than those in the control animals (**Figure 5.2F**). From these data, I conclude that loss of ARL13B leads to a global cerebellar size deficit.

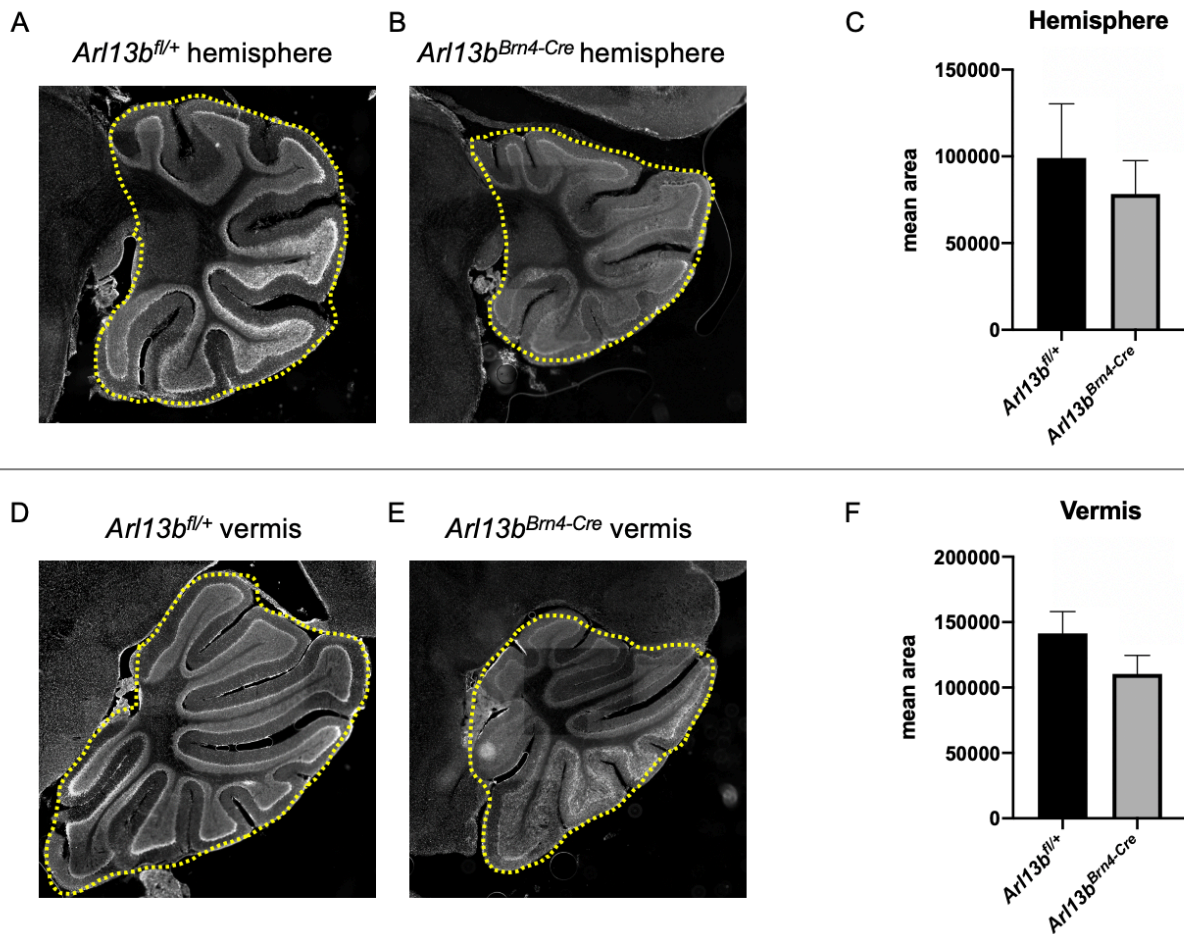


Figure 5.2 Pan-neuronal deletion of ARL13B result in small cerebellum. (A, B, D, E) Representative images of cerebellar sections with analyzed area outlined by dashed yellow line. (A-C) Representative cerebellar hemispheres in (A) *Arl13b^{fl/+}* control (n=3 brains, 118 total sections) and (B) *Arl13b^{Brn4-Cre}* mutant (n=3 brains, 110 total sections). (C) The hemispheres of the *Arl13b^{Brn4-Cre}* mutant animals exhibited a 23.4% reduction in mean pixel area compared to *Arl13b^{fl/+}* control animals. (D-F) Representative cerebellar vermes in (D) *Arl13b^{fl/+}* control (n=3 brains, 139 total sections) and (E) *Arl13b^{Brn4-Cre}* mutant (n=3 brains, 147 total sections). (F) *Arl13b^{Brn4-Cre}* mutant vermes exhibited a mean pixel area 24.7% smaller than that in *Arl13b^{fl/+}* controls.

5.2.3 *Arll3b* functions from within cilia to regulate cerebellar vermis size

Cerebellar size is well established to be regulated, in part, via cilia-dependent Shh signaling which controls proliferation of the cerebellar granule precursor cells (Kenney and Rowitch 2000; Chizhikov et al. 2007). In order to better understand the cerebellar size phenotype in relation to ARL13B and cilia, I examined cerebellar size in the mice expressing the cilia-excluded variant ARL13B^{V358A} (**Figure 5.3**) (Gigante et al. 2020). I detected no difference in the cerebellar hemisphere size between control and *Arll3b*^{V358A/V358A} mice (**Figure 5.3C**). In contrast, I found in preliminary analysis that the mean area of the cerebellar vermes of *Arll3b*^{V358A/V358A} mice were 6.6% smaller than those in control animals (**Figure 5.3F**). Thus, if preliminary data holds true with a higher sample size and statistical analysis, *Arll3b*^{V358A/V358A} mice display a small cerebellar vermis. This result, if consistent in future analyses, argues that the pathways regulated by ARL13B are specific to the vermis. Further, this also appears disrupted in the preliminary *Arll3b*^{R79Q/R79Q} result, and indicates that vermis regulation depends on ARL13B function from within cilia. Taken together, my preliminary data indicate that ARL13B regulates cerebellar size through multiple pathways.

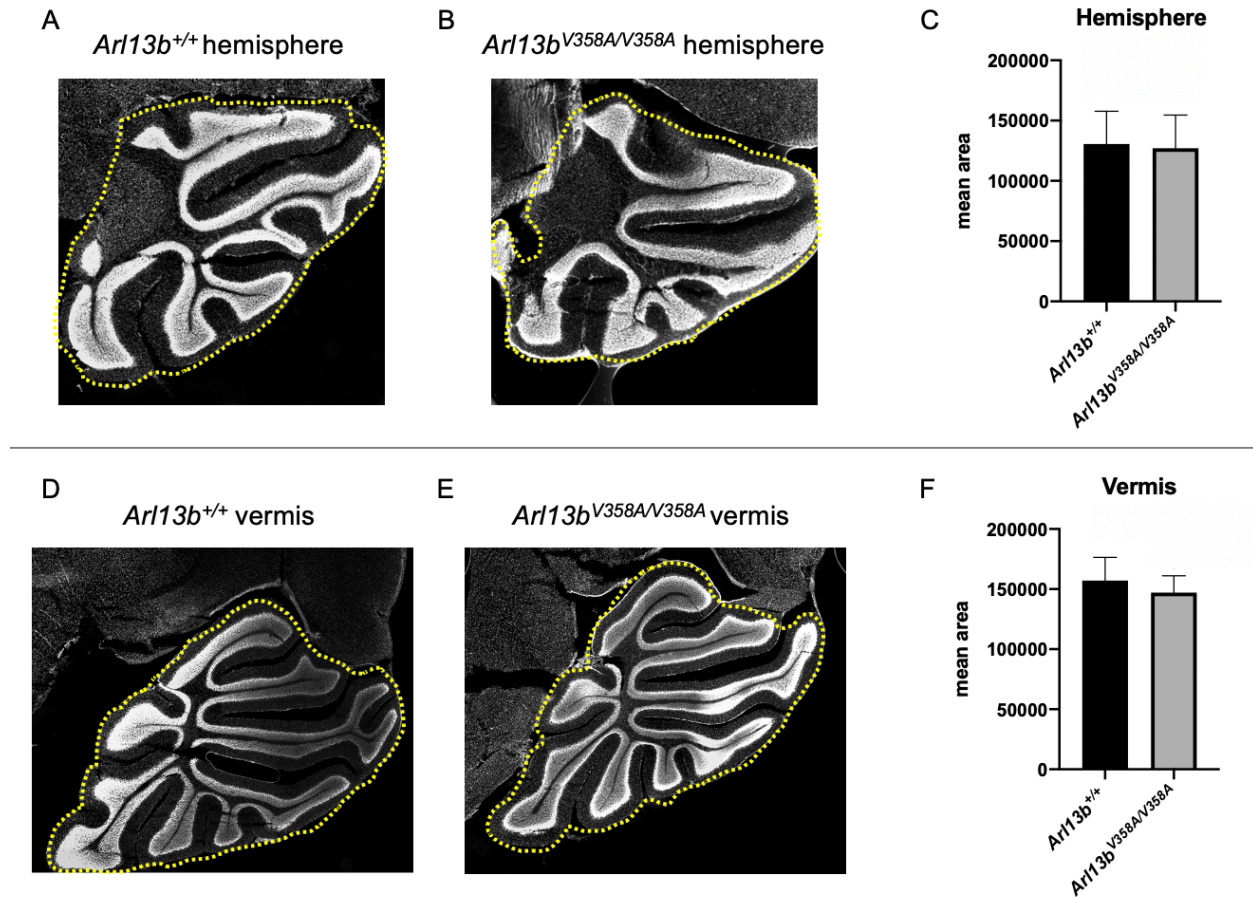


Figure 5.3 Expression of cilia-excluded *Arl13b*^{V358A} results in small cerebellar vermis. (A, B, D, E) Representative images of cerebellar sections with analyzed area outlined by dashed yellow line. (A-C) Representative cerebellar hemisphere in (A) *Arl13b*^{+/+} control (n=3 brains, 102 total sections) and (B) *Arl13b*^{V358A/V358A} mutant (n=3 brains, 110 total sections). (C) No difference in mean pixel area quantification of cerebellar hemisphere size between *Arl13b*^{+/+} and *Arl13b*^{V358A/V358A} animals. (D-F) Representative cerebellar vermes in (D) *Arl13b*^{+/+} control (n=3 brains, 138 total sections) and (E) *Arl13b*^{V358A/V358A} mutant (n=3 brains, 132 total sections). (F) *Arl13b*^{V358A/V358A} mutants displayed a mean pixel area 6.6% smaller than that in *Arl13b*^{+/+} controls (ns).

5.2.4 Cilia are required to regulate cerebellar development

Because cilia-excluded *Ar13b*^{V358A} is sufficient cerebellar hemisphere development, I questioned whether the presence of a cilium is required for cerebellar development. In order to answer that question, I employed an *Ift88* floxed allele which affects ciliary anterograde intraflagellar transport machinery and results in cells that do not build a cilium. I examined the role of cilia in cerebellar development by deleting *Ift88* throughout the neuroectoderm in E8.5 embryos via *Brn4-Cre* (Heydemann, Nguyen, and Crenshaw Iii 2001). By examining 24 animals at P21 (weaning age) the 8 that were *Ift88*^{Brn4-Cre} had severe hydrocephaly and visibly smaller cerebella compared to control littermates (data not shown). This global and severe hydrocephaly phenotype was similar to that of *Ar13b*^{Brn4-Cre}. This indicates that cilia or ciliary signaling is required for cerebellar development, though preliminary data implies ARL13B is not required to localize to the cilium in hemisphere development.

5.2.5 Summary

Whereas complete ARL13B or IFT88 deletion (*Ar13b*^{Brn4-Cre}, *Ift88*^{Brn4-Cre}) in the cerebellum led to global cerebellar hypoplasia and hydrocephaly, my preliminary data implies the hypoplasia in *Ar13b*^{R79Q/R79Q} mice is specific to the cerebellar vermis. These data suggest that Arl13b regulates global cerebellar size via multiple effectors, and *Ar13b*^{R79Q} disrupts a subset (or single) effector that regulates vermis size exclusively. Other mouse models of JSRD where the hypoplasia is specific to the cerebellar vermis affect Wnt signaling. My finding that mice expressing a cilia-excluded ARL13B variant (*Ar13b*^{V358A/V358A}) also display a small cerebellar vermis is consistent with misregulation of such a non-Shh pathway and argue

ARL13B functions from within cilia to control vermis size. Thus, further exploration of cerebellar development in the mouse models is likely to be a fruitful area of follow-up research.

5.3 Perspective

Thus, I conclude the results presented in this dissertation (summarized in **Table 5.1**). My data can be used to form some key takeaways: ARL13B is required for transcription-dependent and -independent Shh signaling, ARL13B function differs between these processes even within a mechanistic arm of the pathway, and despite ARL13B being a cilia-associated GTPase neither cilia localization nor GTPase function are required in some ARL13B regulation of these processes (**Figure 5.4**). Furthermore, as ARL13B is required for Shh signaling and Shh signaling is a key regulator of cerebellar proliferation and SCP guidance, *Arl13b* mutations resulting in disrupted Shh signaling is a unifying mechanism for the hindbrain malformation MTS in JS patients. These results point to further areas of potential exploration. For one, if Shh signaling is a unifying mechanism for the MTS during development, does that indicate that all 35 JS-associated genes also function both at the growth cone and from within the cilium? Or could the explanation lie in *Arl13b* functions as a protein trafficking component, as in INPP5E? Thus, further exploration of the JS proteins localization and trafficking is likely to yield interesting results. To that end, my data points to ARL13B being a surprisingly complicated cilia-associated GTPase, where regulatory function does not require either of those aspects. Thus, the final question my data brings to light revolves around ARL13B function. If ARL13B regulates SCP guidance and cerebellar hemisphere development as neither a cilia protein nor a GTPase, what further functions and regulatory mechanisms of

ARL13B remain to be explored? I posit that the common theme of ARL13B function in development resides in the microtubule code, a beautifully complicated system that regulates both cilia and axons where ARL13B has an established role. I anticipate exciting results and revelations in the field regarding ARL13B function in development. I will conclude my dissertation with a description of the microtubule code, where ARL13B has a role in tethering glutamylases to the base of the cilium and a Future Directions section to highlight next steps (He et al. 2018).

		<i>Transcription-independent Shh</i>			<i>Transcription-dependent Shh</i>	
Allele	Description	Fibroblast Migration	SCP Projection		Cerebellar Development	
		<u>Response to Shh</u>	<u>Dorsal thalamus</u>	<u>Ventral thalamus</u>	<u>Hemisphere</u>	<u>Vermis</u>
WT	Control	✓	✓	✓	✓	✓
<i>Smo</i> ^Δ	Delete Shh pathway response <i>Smo is Shh obligate transducer</i>	X	X	✓		
<i>Arl13b</i> ^Δ	Arl13b deleted	X	X	✓	X	X
<i>Arl13b</i> ^{R79Q}	Joubert Syndrome ARL13B allele <i>GTPase domain mutation</i>	✓	✓	✓	✓	X
<i>Arl13b</i> ^{V358A}	Arl13b excluded from cilia	X	✓	✓	✓	X

Table 5.1 Summary of dissertation results. Check marks indicate the mutant phenotype resembled control results. X marks indicate the mutant displayed an aberrant phenotype. Dark gray box indicates phenotype was not explored. Light gray box indicates preliminary ns data.

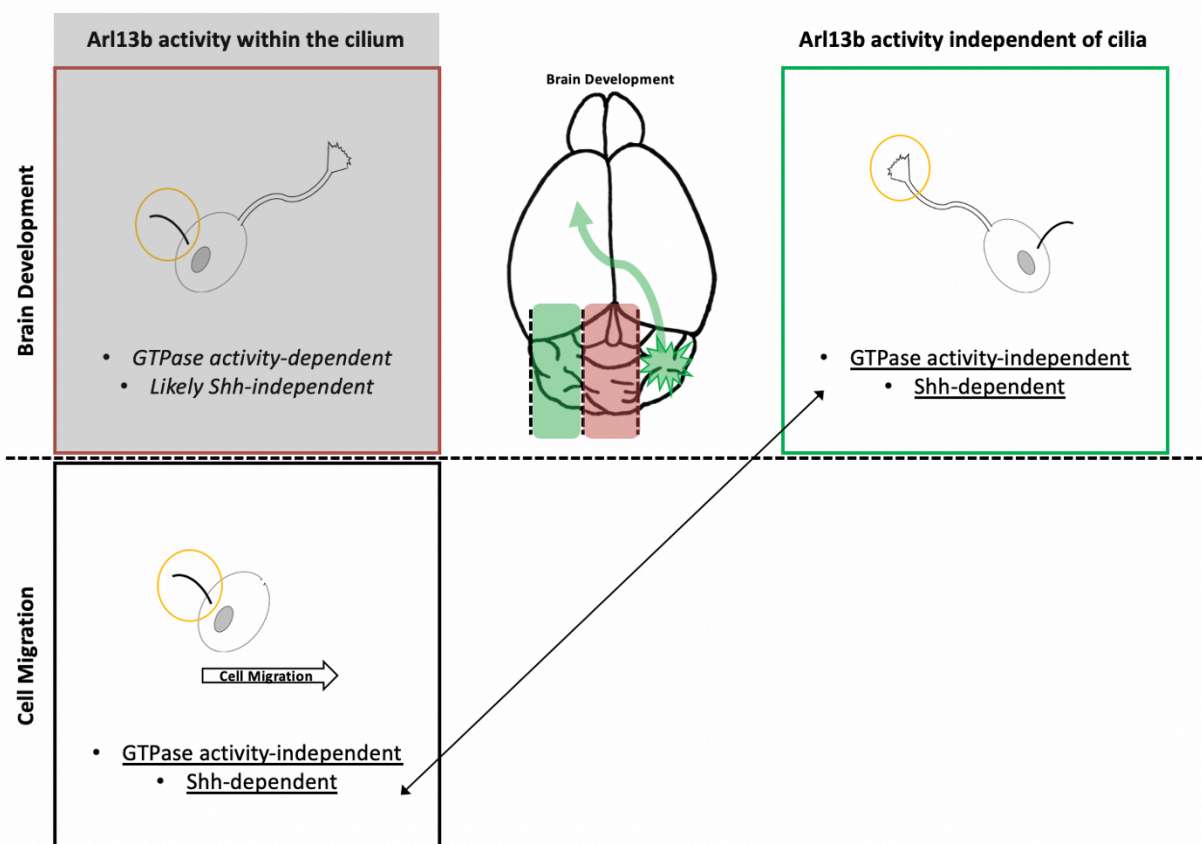


Figure 5.4 The mechanism of ARL13B regulation in development differs depending on both cilia localization and cellular context. In brain development, ARL13B functions outside of the cilium via a Shh-dependent but GTPase-independent mechanism. Preliminary data indicates that ARL13B may function from within the cilium in a GTPase-dependent mechanism that does not seem to depend on Shh (gray box to indicate experiments need repeating with higher sample size). In Shh-dependent cell migration, ARL13B functions from within the cilium, although in a GTPase-independent mechanism. Thus, both cilia localization and cellular context impact whether ARL13B must function within the cilium, as well as whether it functions as a GTPase.

5.4 Connecting cilia to axons via shared microtubule-based structures and modifications

Microtubules comprise both the ciliary axoneme and the axon shaft and share similar regulation. Entry and exit of proteins into cilia and axons are regulated at the transition zone and pre-axonal exclusion zone respectively (Farías et al. 2015; Jiang et al. 2009). Microtubules are composed of α and β tubulin monomers that heterodimerize to form chains of protofilaments. Within cilia, the microtubule doublets are composed of 13 protofilaments in the A tubule and 11 in the B tubule (Mandelkow and Mandelkow 1994). Within the primary cilium, the 9 microtubule doublets are arranged around the circumference and compose the axoneme whereas along the length of the axon, the microtubules appear to randomly overlap. Microtubules grow, or nucleate, at the plus end such that the plus end extends out away from the cell body towards the distal ends of the cilium or axon (Mitchison 1993; Nogales et al. 1999). Microtubules of the cilium and growth cone are both dynamic, with concurrent structure growth and disassembly resulting in tubulin turnover. In order to achieve this turnover, tubulin must be constantly trafficked in and out of the structures. In the cilium, this is achieved through intraflagellar transport (IFT) machinery (Ishikawa and Marshall 2017). Microtubule turnover in the growth cone is also regulated by anterograde kinesin motors and retrograde dynein motors that move along the microtubules of the axon shaft and are similarly required for axon assembly and trafficking (Theiss, Napirei, and Meller 2005).

The regulatory power of microtubules comes from the microtubule code: a collection of tubulin isoforms and removable post-translational modifications (PTMs) that regulate the structures' stability, polarity, trafficking, and signaling. These microtubule PTMs include glycylation, tyrosination, acetylation, and glutamylation (**Figure 5.5**). The tubulin code is also important for recruiting microtubule associated proteins (MAPs) that function through binding to

tubulin dimers (Janke and Kneussel 2010). Thus tubulin post-translation modifications are critical for the microtubule track's organization. PTMs attract selective binding of MAPs and molecular motors to specific microtubule tracks. The tubulin molecules on such tracks contain multiple PTMs and different motors possess distinct preferences for the amount and/or combination of PTMs (Sirajuddin, Rice, and Vale 2014). Furthermore, axon transport cargoes pause at polymer termini, allowing for motors to interpret PTM combinations to release cargo or switch microtubule tracks. The greater the density of microtubules along the axonal length, the shorter the pause between switching tracks (Yogev et al. 2016). Thus, modifications affect the rate of cargo transport as well as where cargo can be dropped at specific pause sites. This further allows efficient transport of cargo while also preventing MAPs and motors from all binding to singular microtubule tracks and thus preventing traffic jams in small neurite spaces (Janke and Kneussel 2010).

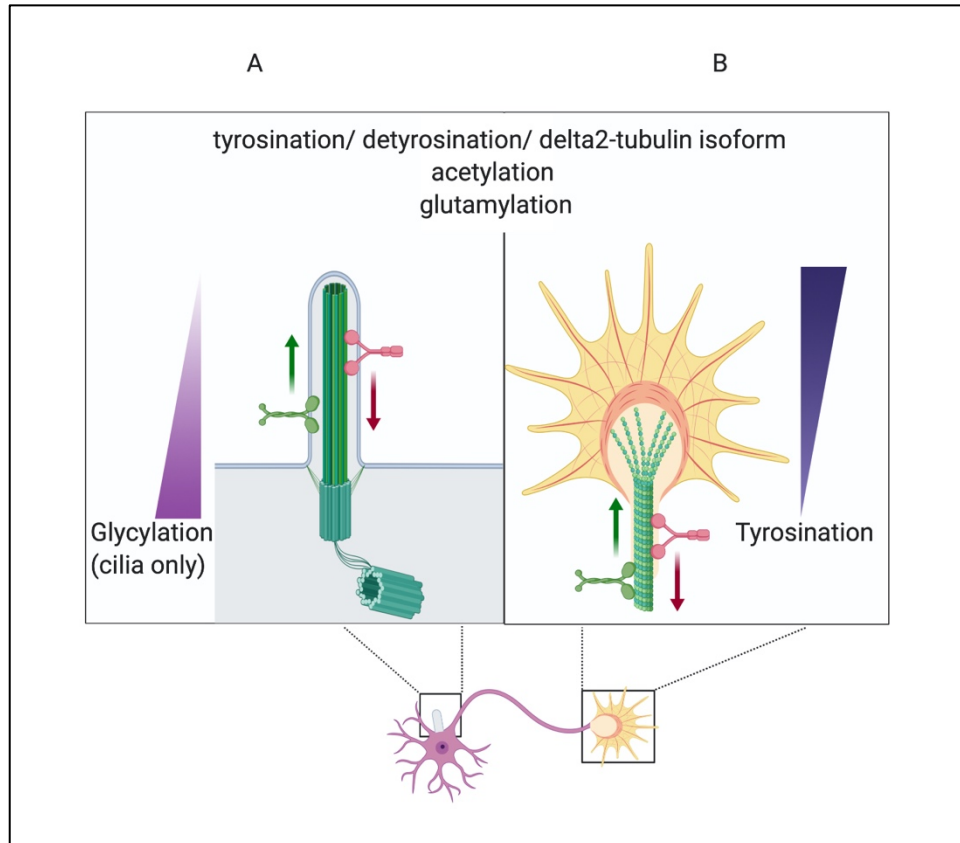


Figure 5.5 The ciliary axoneme and the axon are microtubule projections that share regulation via post-translational modifications of tubulin. In a neuron (bottom), microtubules project as a cilium (left) and an axon (right). These structures share many characteristics. The tubulin composing these microtubules can be post-translationally modified in several ways including being tyrosinated, detyrosinated, converted to the isoform delta2-tubulin, acetylated and deacetylated, and glutamylated/ deglutamylated. Kinesin motors are used for anterograde trafficking and dynein motors for retrograde trafficking in both structures. (A) Glycylation is the only microtubule post-translational modification exclusive to cilia. Glycylation is important for regulating axoneme stability and length and is found in a gradient along the axoneme with most at the cilia base. (B) The microtubule-based shaft of the axon ends at the growth cone which is composed of a microtubule and actin network. Newly formed microtubules are tyrosinated, which leads to enriched tyrosination near the growth cone. Tyrosinated microtubules can be detyrosinated and converted to a stable delta2-tubulin isoform which is very stable and found at the proximal axon base. Thus, tyrosination is critical for axon polarity and outgrowth.

Glycylation is unique as to-date it is the microtubule modification observed solely in cilia (Magiera, Singh, et al. 2018). As the cell begins to build its cilium, tubulin tyrosine ligase-like (TTLL) proteins in the cytoplasm monoglycylate tubulin molecules (Wloga et al. 2009). As tubulin molecules are incorporated in the ciliary axoneme, ciliary glycylation increases in a length-dependent manner (Gadadhar et al. 2017). If glycylation is depleted, the cell interprets it as a signal to stop building the ciliary axoneme, resulting in short cilia (Rocha et al. 2014). Therefore, glycylation of ciliary microtubules is critical to influence the constant tug-of-war between cilia breakdown and buildup to tell the cell when to build, maintain, or eventually break down the cilium to re-enter the cell cycle. Glycylation is needed to stabilize the cilium for signal transduction; glycylation loss results in aberrant ciliary breakdown and premature loss of ciliary signal transduction for the cell (Gadadhar et al. 2017).

Newly polymerized microtubules in both cilia and axons are tyrosinated (Webster et al. 1987; Gundersen, Khawaja, and Bulinski 1987). Tyrosinated microtubules can be detyrosinated and further retyrosinated by tubulin carboxypeptidase and tubulin tyrosine ligase (TTL), respectively (Barra, Arce, and Argaraña 1988). If detyrosinated, tubulin can be irreversibly converted to delta2-tubulin, an isoform reserved for stable microtubules and therefore often found at the less dynamic base of structures (Baas et al. 2016). Detyrosinated tubulin is less depolymerized and slower to turnover compared to tyrosinated tubulin making it an excellent substrate for the attachment and movement of kinesin and dynein motor proteins (Konishi and Setou 2009). In young neurons, newly polymerized microtubules are tyrosinated and extend beyond the stable delta2-tubulin in the axon shaft thereby conferring axon polarity (Arregui et al. 1991). In mouse lack of

TTL proteins, results in failure of neural projections and postnatal lethality (Erck et al. 2005). Tyrosination is therefore required for proper neurite outgrowth and structure polarity.

Acetylation is found on stable microtubules and allows kinesin and dynein motors to recognize appropriate binding sites. Loss of acetylation results in lack of KINESIN-1 binding to the axon shaft or reduced ciliary axoneme dynein motility and thus loss of trafficking of structural components and signaling effectors (Reed et al. 2006; Alper et al. 2014). Acetylation is therefore required for trafficking of essential components for processes such as growth cone turning or cell migration and furthermore, inhibition of deacetylases rescues the axonal trafficking defects (Dompierre et al. 2007). Thus, acetylation is important for both ciliary and axonal trafficking.

Tubulin can also be glutamylated with removable glutamylation of tubulin found throughout the cell. Polyglutamylated tubulin is found in neuronal microtubules resulting in much polyglutamylase activity in the brain (Ikegami et al. 2006). Polyglutamylated tubulin is performed by TTL proteins, which in cilia localize to vesicles tethered by my protein of interest, ARL13B, at the ciliary base; loss of glutamylation results in ciliary collapse (He et al. 2018; Lee et al. 2012). Microtubule glutamylation is also critical in the axon where it is required for microtubule remodeling allowing for severing and breakdown or for new microtubules to be added on during projection (Valenstein and Roll-Mecak 2016). Furthermore, Tll7 is a polyglutamylase that is required for neurite growth; it is highly transcribed in the nervous system and its loss results in aberrant synaptic transmission (Ikegami et al. 2006). Polyglutamylated tubulin must be tightly regulated as too much is also deleterious. Mice lacking the deglutamylase Ccpp1, exhibit excessive glutamylation in Purkinje neurons resulting in degeneration (O'Hagan et al. 2011; Magiera, Bodakuntla, et al. 2018).

Because cilia and axons draw from the same pools of tubulin in the cell, it is experimentally challenging to distinguish whether alterations in the PTMs and MAPs matter specifically within cilia or in axons. In fact, it is perhaps likely that perturbations in either one also could impact the other. This is akin to mutations in kinesins or dyneins dramatically impacting both structures, with loss of structural integrity or loss of necessary in-trafficked components and effectors. Similarly, mutations in glutamylase TTLLs would alter the markings on both structures and therefore result in ciliary collapse and lack of neurite outgrowth (Ikegami et al. 2006; Pathak et al. 2007). Regardless, the PTMs and MAPs regulating cilia and axon structure and trafficking play critical developmental roles which underlie their impact in disease states.

5.5 Future Directions

Because ARL13B has an established role in tethering glutamylases to the base of the cilium, I posit that microtubule stability and trafficking disruption may be the connection between the primary cilium and axon guidance. While the cilium remains on the cell body and the axon projects out, the ever distal growth cone is the site of axon guidance. Joubert Syndrome illustrates that several cilia-associate proteins are implicated in axon guidance, as all patients display a hindbrain malformation with misguided superior cerebellar peduncles. While my data demonstrates that ARL13B need not function from within the cilium to regulate axon guidance, it would be premature to assume that all 35 Joubert-implicated cilia proteins also function outside the cilium. Rather, because the cilium and the axon are both built from microtubules, I would encourage future scientists interested in this field to look further into some key questions centered around the microtubule code. For one, because ciliary and axonal microtubules arise

from the same cellular pool it is possible that loss of structural integrity in one structure would beget similar issues in the other. I would recommend an experiment to examine the non-incorporated microtubule population of the cell, the ciliary axoneme, and the axon shaft/ growth cone to look for gross changes in glutamylation in the absence of ARL13B. If axons lacking ARL13B show disruption to glutamylation, this would imply that ARL13B function as a glutamylase tether is not exclusive to the cilium and potentially explain the disruption of guidance demonstrated in my dissertation data. Alternatively, if the unincorporated microtubule population PTM signature changes in the absence of ARL13B or another Joubert-implicated protein, this could indicate that proteins are involved in the availability of suitable microtubules for incorporation. Further, if this is true, it could explain the discrepancy between cilia-associated proteins functioning in axon guidance in a cilia-independent (perhaps temporal) mechanism.

References

- Abdelhamed, Z. A., D. I. Abdelmottaleb, M. E. El-Asrag, S. Natarajan, G. Wheway, C. F. Inglehearn, C. Toomes, and C. A. Johnson. 2019. 'The ciliary Frizzled-like receptor Tmem67 regulates canonical Wnt/beta-catenin signalling in the developing cerebellum via Hoxb5', *Sci Rep*, 9: 5446.
- Abdelhamed, Zakia A., Gabrielle Wheway, Katarzyna Szymanska, Subaashini Natarajan, Carmel Toomes, Chris Inglehearn, and Colin A. Johnson. 2013. 'Variable expressivity of ciliopathy neurological phenotypes that encompass Meckel-Gruber syndrome and Joubert syndrome is caused by complex de-regulated ciliogenesis, Shh and Wnt signalling defects', *Human Molecular Genetics*, 22: 1358-72.
- Aguilar, Andrea, Alice Meunier, Laetitia Strehl, Jelena Martinovic, Maryse Bonniere, Tania Attie-Bitach, Féréchté Encha-Razavi, and Nathalie Spassky. 2012. 'Analysis of human samples reveals impaired SHH-dependent cerebellar development in Joubert syndrome/Meckel syndrome', *Proceedings of the National Academy of Sciences*, 109: 16951-56.
- Ahn, K, Y Mishina, M C Hanks, R R Behringer, and E B Crenshaw 3rd. 2001. 'BMPR-IA signaling is required for the formation of the apical ectodermal ridge and dorsal-ventral patterning of the limb', *Development*, 128: 4449-61.
- Alexander, Andrew L, Jee Eun Lee, Mariana Lazar, and Aaron S Field. 2007. 'Diffusion tensor imaging of the brain', *Neurotherapeutics*, 4: 316-29.
- Alkanderi, S., E. Molinari, R. Shaheen, Y. Elmaghloob, L. A. Stephen, V. Sammut, S. A. Ramsbottom, S. Srivastava, G. Cairns, N. Edwards, S. J. Rice, N. Ewida, A. Alhashem, K. White, C. G. Miles, D. H. Steel, F. S. Alkuraya, S. Ismail, and J. A. Sayer. 2018. 'ARL3 Mutations Cause Joubert Syndrome by Disrupting Ciliary Protein Composition', *Am J Hum Genet*, 103: 612-20.
- Alper, Joshua D., Franziska Decker, Bernice Agana, and Jonathon Howard. 2014. 'The motility of axonemal dynein is regulated by the tubulin code', *Biophysical journal*, 107: 2872-80.
- Aoyagi, Y., R. Kawakami, H. Osanai, T. Hibi, and T. Nemoto. 2015. 'A rapid optical clearing protocol using 2,2'-thiodiethanol for microscopic observation of fixed mouse brain', *PLoS One*, 10: e0116280.
- Arregui, C., J. Busciglio, A. Caceres, and H. S. Barra. 1991. 'Tyrosinated and detyrosinated microtubules in axonal processes of cerebellar macroneurons grown in culture', *Journal of Neuroscience Research*, 28: 171-81.
- Arts, Heleen H., Dan Doherty, Sylvia E. C. van Beersum, Melissa A. Parisi, Stef J. F. Letteboer, Nicholas T. Gordon, Theo A. Peters, Tina Märker, Krysta Voesenek, Aileen Kartono, Hamit Ozyurek, Federico M. Farin, Hester Y. Kroes, Uwe Wolfrum, Han G. Brunner, Frans P. M. Cremers, Ian A. Glass, Nine V. A. M. Knoers, and Ronald Roepman. 2007. 'Mutations in the gene encoding the basal body protein RPGRIP1L, a nephrocystin-4 interactor, cause Joubert syndrome', *Nature Genetics*, 39: 882-88.
- Au - Langlois, Sébastien D., Steves Au - Morin, Patricia T. Au - Yam, and Frédéric Au - Charron. 2010. 'Dissection and Culture of Commissural Neurons from Embryonic Spinal Cord', *JoVE*: e1773.
- Avasthi, Prachee, and Wallace F Marshall. 2013. 'Ciliary Regulation: Disassembly Takes the Spotlight', *Current Biology*, 23: R1001-R03.

- Baas, Peter W., Anand N. Rao, Andrew J. Matamoros, and Lanfranco Leo. 2016. 'Stability properties of neuronal microtubules', *Cytoskeleton (Hoboken, N.J.)*, 73: 442-60.
- Bachmann-Gagescu, R., J. C. Dempsey, I. G. Phelps, B. J. O'Roak, D. M. Knutzen, T. C. Rue, G. E. Ishak, C. R. Isabella, N. Gordon, J. Adkins, E. A. Boyle, N. de Lacy, D. O'Day, A. Alswaid, Radha Ramadevi A, L. Lingappa, C. Lourenço, L. Martorell, À Garcia-Cazorla, H. Ozyürek, G. Haliloğlu, B. Tuysuz, M. Topçu, Genomics University of Washington Center for Mendelian, P. Chance, M. A. Parisi, I. A. Glass, J. Shendure, and D. Doherty. 2015. 'Joubert syndrome: a model for untangling recessive disorders with extreme genetic heterogeneity', *Journal of medical genetics*, 52: 514-22.
- Barra, Héctor S., Carlos A. Arce, and Carlos E. Argaraña. 1988. 'Posttranslational tyrosination/detyrosination of tubulin', *Molecular Neurobiology*, 2: 133-53.
- Barral, Duarte C, Salil Garg, Cristina Casalou, Gerald F M Watts, José L Sandoval, José S Ramalho, Victor W Hsu, and Michael B Brenner. 2012. 'Arl13b regulates endocytic recycling traffic.', *Proc Natl Acad Sci U S A*, 109: 21354-9.
- Bashford, A. L., and V. Subramanian. 2019. 'Mice with a conditional deletion of Talpid3 (KIAA0586) - a model for Joubert syndrome', *J Pathol*, 248: 396-408.
- Baudoin, Jean-Pierre, Lucie Viou, Pierre-Serge Launay, Camilla Luccardini, Sergio Espeso Gil, Vera Kiyasova, Théano Irinopoulou, Chantal Alvarez, Jean-Paul Rio, Thomas Boudier, Jean-Pierre Lechaire, Nicoletta Kessarar, Nathalie Spassky, and Christine Métin. 2012. 'Tangentially Migrating Neurons Assemble a Primary Cilium that Promotes Their Reorientation to the Cortical Plate', *Neuron*, 76: 1108-22.
- Bay, S. N., A. B. Long, and T. Caspary. 2018. 'Disruption of the ciliary GTPase Arl13b suppresses Sonic hedgehog overactivation and inhibits medulloblastoma formation', *Proc Natl Acad Sci U S A*, 115: 1570-75.
- Beales, P. L., N. Elcioglu, A. S. Woolf, D. Parker, and F. A. Flintner. 1999. 'New criteria for improved diagnosis of Bardet-Biedl syndrome: results of a population survey', *J Med Genet*, 36: 437-46.
- Bergmann, Carsten, Lisa M. Guay-Woodford, Peter C. Harris, Shigeo Horie, Dorien J. M. Peters, and Vicente E. Torres. 2018. 'Polycystic kidney disease', *Nature Reviews Disease Primers*, 4: 50.
- Besse, Laurianne, Mariame Neti, Isabelle Anselme, Christoph Gerhardt, Ulrich Rütter, Christine Laclef, and Sylvie Schneider-Maunoury. 2011. 'Primary cilia control telencephalic patterning and morphogenesis via Gli3 proteolytic processing', *Development*, 138: 2079-88.
- Bielas, S. L., J. L. Silhavy, F. Brancati, M. V. Kisseleva, L. Al-Gazali, L. Sztriha, R. A. Bayoumi, M. S. Zaki, A. Abdel-Aleem, R. O. Rosti, H. Kayserili, D. Swistun, L. C. Scott, E. Bertini, E. Boltshauser, E. Fazzi, L. Travaglini, S. J. Field, S. Gayral, M. Jacoby, S. Schurmans, B. Dallapiccola, P. W. Majerus, E. M. Valente, and J. G. Gleeson. 2009. 'Mutations in INPP5E, encoding inositol polyphosphate-5-phosphatase E, link phosphatidyl inositol signaling to the ciliopathies', *Nat Genet*, 41: 1032-6.
- Bijlsma, M. F., K. S. Borensztajn, H. Roelink, M. P. Peppelenbosch, and C. A. Spek. 2007. 'Sonic hedgehog induces transcription-independent cytoskeletal rearrangement and migration regulated by arachidonate metabolites', *Cell Signal*, 19: 2596-604.
- Bijlsma, M. F., M. P. Peppelenbosch, C. A. Spek, and H. Roelink. 2008. 'Leukotriene synthesis is required for hedgehog-dependent neurite projection in neuralized embryoid bodies but not for motor neuron differentiation', *Stem Cells*, 26: 1138-45.

- Bijlsma, Maarten F, Helene Damhofer, and Henk Roelink. 2012. 'Hedgehog-Stimulated Chemotaxis Is Mediated by Smoothed Located Outside the Primary Cilium', *Science Signaling*, 5: ra60-ra60.
- Bisgrove, Brent W., and H. Joseph Yost. 2006. 'The roles of cilia in developmental disorders and disease', *Development*, 133: 4131.
- Bohne, Pauline, Martin K. Schwarz, Stefan Herlitze, and Melanie D. Mark. 2019. 'A New Projection From the Deep Cerebellar Nuclei to the Hippocampus via the Ventrolateral and Laterodorsal Thalamus in Mice', *Frontiers in Neural Circuits*, 13.
- Bonaguidi, Michael A., Michael A. Wheeler, Jason S. Shapiro, Ryan P. Stadel, Gerald J. Sun, Guo-li Ming, and Hongjun Song. 2011. 'In vivo clonal analysis reveals self-renewing and multipotent adult neural stem cell characteristics', *Cell*, 145: 1142-55.
- Bond, A. M., G. L. Ming, and H. Song. 2015. 'Adult Mammalian Neural Stem Cells and Neurogenesis: Five Decades Later', *Cell Stem Cell*, 17: 385-95.
- Bourgeois, Justin R., and Russell J. Ferland. 2019. 'Loss of the neurodevelopmental Joubert syndrome causing protein, Ahi1, causes motor and muscle development delays independent of central nervous system involvement', *Dev Biol*, 448: 36-47.
- Brancati, F., B. Dallapiccola, and E. M. Valente. 2010. 'Joubert Syndrome and related disorders', *Orphanet J Rare Dis*, 5: 20.
- Breslow, David K., Sascha Hoogendoorn, Adam R. Kopp, David W. Morgens, Brandon K. Vu, Margaret C. Kennedy, Kyuho Han, Amy Li, Gaelen T. Hess, Michael C. Bassik, James K. Chen, and Maxence V. Nachury. 2018. 'A CRISPR-based screen for Hedgehog signaling provides insights into ciliary function and ciliopathies', *Nature Genetics*, 50: 460-71.
- Briscoe, J., and J. Ericson. 1999. 'The specification of neuronal identity by graded Sonic Hedgehog signalling', *Semin Cell Dev Biol*, 10: 353-62.
- Cantagrel, V., J. L. Silhavy, S. L. Bielas, D. Swistun, S. E. Marsh, J. Y. Bertrand, S. Audollent, T. Attie-Bitach, K. R. Holden, W. B. Dobyns, D. Traver, L. Al-Gazali, B. R. Ali, T. H. Lindner, T. Caspary, E. A. Otto, F. Hildebrandt, I. A. Glass, C. V. Logan, C. A. Johnson, C. Bennett, F. Brancati, Group International Joubert Syndrome Related Disorders Study, E. M. Valente, C. G. Woods, and J. G. Gleeson. 2008. 'Mutations in the cilia gene ARL13B lead to the classical form of Joubert syndrome', *Am J Hum Genet*, 83: 170-9.
- Cantagrel, Vincent, Jennifer L. Silhavy, Stephanie L. Bielas, Dominika Swistun, Sarah E. Marsh, Julien Y. Bertrand, Sophie Audollent, Tania Attie-Bitach, Kenton R. Holden, William B. Dobyns, David Traver, Lihadh Al-Gazali, Bassam R. Ali, Tom H. Lindner, Tamara Caspary, Edgar a. Otto, Friedhelm Hildebrandt, Ian a. Glass, Clare V. Logan, Colin a. Johnson, Christopher Bennett, Francesco Brancati, Enza Maria Valente, C. Geoffrey Woods, and Joseph G. Gleeson. 2008. 'Mutations in the Cilia Gene ARL13B Lead to the Classical Form of Joubert Syndrome', *American Journal of Human Genetics*, 83: 170-79.
- Casalou, C., C. Seixas, A. Portelinha, P. Pintado, M. Barros, J. S. Ramalho, S. S. Lopes, and D. C. Barral. 2014. 'Arl13b and the non-muscle myosin heavy chain IIA are required for circular dorsal ruffle formation and cell migration', *J Cell Sci*, 127: 2709-22.
- Caspary, T., M. J. Garcia-Garcia, D. Huangfu, J. T. Eggenschwiler, M. R. Wyler, A. S. Rakeman, H. L. Alcorn, and K. V. Anderson. 2002. 'Mouse Dispatched homolog1 is required for long-range, but not juxtacrine, Hh signaling.', *Current Biology*, 12: 1628-32.
- Caspary, T., C. E. Larkins, and K. V. Anderson. 2007. 'The graded response to Sonic Hedgehog depends on cilia architecture', *Dev Cell*, 12: 767-78.

- Cevik, S., A. A. Sanders, E. Van Wijk, K. Boldt, L. Clarke, J. van Reeuwijk, Y. Hori, N. Horn, L. Hetterschijt, A. Wdowicz, A. Mullins, K. Kida, O. I. Kaplan, S. E. van Beersum, K. Man Wu, S. J. Letteboer, D. A. Mans, T. Katada, K. Kontani, M. Ueffing, R. Roepman, H. Kremer, and O. E. Blacque. 2013. 'Active transport and diffusion barriers restrict Joubert Syndrome-associated ARL13B/ARL-13 to an Inv-like ciliary membrane subdomain', *PLoS Genet*, 9: e1003977.
- Chang, Bo, Hemant Khanna, Norman Hawes, David Jimeno, Shirley He, Concepcion Lillo, Sunil K. Parapuram, Hong Cheng, Alison Scott, Ron E. Hurd, John A. Sayer, Edgar A. Otto, Massimo Attanasio, John F. O'Toole, Genglin Jin, Chengchao Shou, Friedhelm Hildebrandt, David S. Williams, John R. Heckenlively, and Anand Swaroop. 2006. 'In-frame deletion in a novel centrosomal/ciliary protein CEP290/NPHP6 perturbs its interaction with RPGR and results in early-onset retinal degeneration in the rd16 mouse', *Human Molecular Genetics*, 15: 1847-57.
- Charron, Frédéric, Elke Stein, Juhee Jeong, Andrew P McMahon, and Marc Tessier-Lavigne. 2003. 'The Morphogen Sonic Hedgehog Is an Axonal Chemoattractant that Collaborates with Netrin-1 in Midline Axon Guidance', *Cell*, 113: 11-23.
- Chavez, M., S. Ena, J. Van Sande, A. de Kerchove d'Exaerde, S. Schurmans, and S. N. Schiffmann. 2015. 'Modulation of Ciliary Phosphoinositide Content Regulates Trafficking and Sonic Hedgehog Signaling Output', *Dev Cell*, 34: 338-50.
- Chiang, C., Y. Litingtung, E. Lee, K. E. Young, J. L. Corden, H. Westphal, and P. A. Beachy. 1996. 'Cyclopia and defective axial patterning in mice lacking Sonic hedgehog gene function', *Nature*, 383: 407-13.
- Chizhikov, Victor V., James Davenport, Qihong Zhang, Evelyn Kim Shih, Olga A. Cabello, Jannon L. Fuchs, Bradley K. Yoder, and Kathleen J. Millen. 2007. 'Cilia Proteins Control Cerebellar Morphogenesis by Promoting Expansion of the Granule Progenitor Pool', *The Journal of Neuroscience*, 27: 9780-89.
- Constable, Sandii, Alyssa B Long, Katharine A Floyd, Stéphane Schurmans, and Tamara Caspary. 2019. 'Ciliary phosphatidylinositol phosphatase Inpp5e plays positive and negative regulatory roles in Shh signaling', *bioRxiv*: 721399.
- Consugar, Mark B., Vickie J. Kubly, Donna J. Lager, Cynthia J. Hommerding, Wai Chong Wong, Egbert Bakker, Vincent H. Gattone, Vicente E. Torres, Martijn H. Breuning, and Peter C. Harris. 2007. 'Molecular diagnostics of Meckel–Gruber syndrome highlights phenotypic differences between MKS1 and MKS3', *Human Genetics*, 121: 591-99.
- Corbit, K. C., P. Aanstad, V. Singla, A. R. Norman, D. Y. Stainier, and J. F. Reiter. 2005a. 'Vertebrate Smoothed functions at the primary cilium', *Nature*, 437: 1018-21.
- Corbit, Kevin C, Pia Aanstad, Veena Singla, Andrew R Norman, Didier Y R Stainier, and Jeremy F Reiter. 2005b. 'Vertebrate Smoothed functions at the primary cilium.', *Nature*, 437: 1018-21.
- Cortellino, S., C. Wang, B. Wang, M. R. Bassi, E. Caretti, D. Champeval, A. Calmont, M. Jarnik, J. Burch, K. S. Zaret, L. Larue, and A. Bellacosa. 2009. 'Defective ciliogenesis, embryonic lethality and severe impairment of the Sonic Hedgehog pathway caused by inactivation of the mouse complex A intraflagellar transport gene Ift122/Wdr10, partially overlapping with the DNA repair gene Med1/Mbd4', *Dev Biol*, 325: 225-37.
- Dahmane, N., and A. Ruiz i Altaba. 1999. 'Sonic hedgehog regulates the growth and patterning of the cerebellum', *Development*, 126: 3089-100.

- Davenport, James R., Amanda J. Watts, Venus C. Roper, Mandy J. Croyle, Thomas van Groen, J. Michael Wyss, Tim R. Nagy, Robert A. Kesterson, and Bradley K. Yoder. 2007. 'Disruption of Intraflagellar Transport in Adult Mice Leads to Obesity and Slow-Onset Cystic Kidney Disease', *Current Biology*, 17: 1586-94.
- Daynac, M., L. Tirou, H. Faure, M. A. Mouthon, L. R. Gauthier, H. Hahn, F. D. Boussin, and M. Ruat. 2016. 'Hedgehog Controls Quiescence and Activation of Neural Stem Cells in the Adult Ventricular-Subventricular Zone', *Stem Cell Reports*, 7: 735-48.
- Delous, Marion, Lekbir Baala, Rémi Salomon, Christine Laclef, Jeanette Vierkotten, Kàlmàn Tory, Christelle Golzio, Tiphane Lacoste, Laurianne Besse, Catherine Ozilou, Imane Moutkine, Nathan E. Hellman, Isabelle Anselme, Flora Silbermann, Christine Vesque, Christoph Gerhardt, Eleanor Rattenberry, Matthias T. F. Wolf, Marie Claire Gubler, Jéléna Martinovic, Féréchté Encha-Razavi, Nathalie Boddaert, Marie Gonzales, Marie Alice Macher, Hubert Nivet, Gérard Champion, Jean Pierre Berthéléme, Patrick Niaudet, Fiona McDonald, Friedhelm Hildebrandt, Colin A. Johnson, Michel Vekemans, Corinne Antignac, Ulrich Rüter, Sylvie Schneider-Maunoury, Tania Attié-Bitach, and Sophie Saunier. 2007. 'The ciliary gene RPGRIP1L is mutated in cerebello-oculo-renal syndrome (Joubert syndrome type B) and Meckel syndrome', *Nature Genetics*, 39: 875-81.
- Deretic, D., A. H. Williams, N. Ransom, V. Morel, P. A. Hargrave, and A. Arendt. 2005. 'Rhodopsin C terminus, the site of mutations causing retinal disease, regulates trafficking by binding to ADP-ribosylation factor 4 (ARF4)', *Proc Natl Acad Sci U S A*, 102: 3301-6.
- Doherty, D. 2009. 'Joubert syndrome: insights into brain development, cilium biology, and complex disease', *Semin Pediatr Neurol*, 16: 143-54.
- Domanitskaya, E., A. Wacker, O. Mauti, T. Baeriswyl, P. Esteve, P. Bovolenta, and E. T. Stoeckli. 2010. 'Sonic hedgehog guides post-crossing commissural axons both directly and indirectly by regulating Wnt activity', *J Neurosci*, 30: 11167-76.
- Dompierre, Jim P., Juliette D. Godin, Bénédicte C. Charrin, Fabrice P. Cordelières, Stephen J. King, Sandrine Humbert, and Frédéric Saudou. 2007. 'Histone deacetylase 6 inhibition compensates for the transport deficit in Huntington's disease by increasing tubulin acetylation', *The Journal of neuroscience : the official journal of the Society for Neuroscience*, 27: 3571-83.
- Ellison, D. W., J. Dalton, M. Kocak, S. L. Nicholson, C. Fraga, G. Neale, A. M. Kenney, D. J. Brat, A. Perry, W. H. Yong, R. E. Taylor, S. Bailey, S. C. Clifford, and R. J. Gilbertson. 2011. 'Medulloblastoma: clinicopathological correlates of SHH, WNT, and non-SHH/WNT molecular subgroups', *Acta Neuropathol*, 121: 381-96.
- Engle, E. C. 2010. 'Human genetic disorders of axon guidance', *Cold Spring Harb Perspect Biol*, 2: a001784.
- Erck, Christian, Leticia Peris, Annie Andrieux, Claire Meissirel, Achim D. Gruber, Muriel Vernet, Annie Schweitzer, Yasmina Saoudi, Hervé Pointu, Christophe Bosc, Paul A. Salin, Didier Job, and Juergen Wehland. 2005. 'A vital role of tubulin-tyrosine-ligase for neuronal organization', *Proceedings of the National Academy of Sciences*, 102: 7853.
- Fabre, P. J., T. Shimogori, and F. Charron. 2010. 'Segregation of ipsilateral retinal ganglion cell axons at the optic chiasm requires the Shh receptor Boc', *J Neurosci*, 30: 266-75.
- Falkenstein, Kristin N., and Steven A. Vokes. 2014. 'Transcriptional regulation of graded Hedgehog signaling', *Seminars in Cell & Developmental Biology*, 33: 73-80.

- Farías, Ginny G., Carlos M. Guardia, Dylan J. Britt, Xiaoli Guo, and Juan S. Bonifacino. 2015. 'Sorting of Dendritic and Axonal Vesicles at the Pre-axonal Exclusion Zone', *Cell Reports*, 13: 1221-32.
- Farkas, Lilla M., and Wieland B. Huttner. 2008. 'The cell biology of neural stem and progenitor cells and its significance for their proliferation versus differentiation during mammalian brain development', *Current Opinion in Cell Biology*, 20: 707-15.
- Ferent, Julien, Sandii Constable, Eduardo D. Gigante, Patricia T. Yam, Laura E. Mariani, Emilie Legué, Karel F. Liem, Jr., Tamara Caspary, and Frédéric Charron. 2019. 'The Ciliary Protein Arl13b Functions Outside of the Primary Cilium in Shh-Mediated Axon Guidance', *Cell Reports*, 29: 3356-66.e3.
- Fink, A. J. 2006. 'Development of the Deep Cerebellar Nuclei: Transcription Factors and Cell Migration from the Rhombic Lip', *Journal of Neuroscience*, 26: 3066-76.
- Franklin, K.B.J., and G. Paxinos. 1997. *The Mouse Brain in Stereotaxic Coordinates* (Academic Press).
- Gadadhar, S., H. Dadi, S. Bodakuntla, A. Schnitzler, I. Bieche, F. Rusconi, and C. Janke. 2017. 'Tubulin glycylation controls primary cilia length', *J Cell Biol*, 216: 2701-13.
- Garcia-Gonzalo, F. R., K. C. Corbit, M. S. Simerly, G. Ramaswami, E. A. Otto, T. R. Noriega, A. D. Seol, J. F. Robinson, C. L. Bennett, D. J. Josifova, J. M. Garcia-Verdugo, N. Katsanis, F. Hildebrandt, and J. F. Reiter. 2011. 'A transition zone complex regulates mammalian ciliogenesis and ciliary membrane composition', *Nat Genet*, 43: 776-84.
- Garcia-Gonzalo, F. R., S. C. Phua, E. C. Roberson, G. Garcia, 3rd, M. Abedin, S. Schurmans, T. Inoue, and J. F. Reiter. 2015. 'Phosphoinositides Regulate Ciliary Protein Trafficking to Modulate Hedgehog Signaling', *Dev Cell*, 34: 400-09.
- Garcia-Gonzalo, Francesc R., and Jeremy F. Reiter. 2017. 'Open Sesame: How Transition Fibers and the Transition Zone Control Ciliary Composition', *Cold Spring Harbor Perspectives in Biology*, 9: a028134.
- Gaudet, Muriel, Anna-Giulia Fara, Isacco Beritognolo, and Maurizio Sabatti. 2009. 'Allele-Specific PCR in SNP Genotyping.' in Anton A. Komar (ed.), *Single Nucleotide Polymorphisms: Methods and Protocols* (Humana Press: Totowa, NJ).
- Geng, L., D. Okuhara, Z. Yu, X. Tian, Y. Cai, S. Shibazaki, and S. Somlo. 2006. 'Polycystin-2 traffics to cilia independently of polycystin-1 by using an N-terminal RVxP motif', *J Cell Sci*, 119: 1383-95.
- Gigante, Eduardo D., Megan R. Taylor, Anna A. Ivanova, Richard A. Kahn, and Tamara Caspary. 2020. 'ARL13B regulates Sonic hedgehog signaling from outside primary cilia', *Elife*, 9: e50434.
- Goebbels, S., I. Bormuth, U. Bode, O. Hermanson, M. H. Schwab, and K. A. Nave. 2006. 'Genetic targeting of principal neurons in neocortex and hippocampus of NEX-Cre mice', *Genesis*, 44: 611-21.
- Gorivodsky, Marat, Mahua Mukhopadhyay, Michaela Wilsch-Braeuninger, Matthew Phillips, Andreas Teufel, Changmee Kim, Nasir Malik, Wieland Huttner, and Heiner Westphal. 2009. 'Intraflagellar transport protein 172 is essential for primary cilia formation and plays a vital role in patterning the mammalian brain', *Dev Biol*, 325: 24-32.
- Gotthardt, K., M. Lokaj, C. Koerner, N. Falk, A. Giessl, and A. Wittinghofer. 2015. 'A G-protein activation cascade from Arl13B to Arl3 and implications for ciliary targeting of lipidated proteins', *Elife*, 4.

- Green, Warren W., Cedric R. Uytingco, Kirill Ukhanov, Zachary Kolb, Jordan Moretta, Jeremy C. McIntyre, and Jeffrey R. Martens. 2018. 'Peripheral Gene Therapeutic Rescue of an Olfactory Ciliopathy Restores Sensory Input, Axonal Pathfinding, and Odor-Guided Behavior', *The Journal of neuroscience : the official journal of the Society for Neuroscience*, 38: 7462-75.
- Guadiana, Sarah M., Susan Semple-Rowland, Daniel Daroszewski, Irina Madorsky, Joshua J. Breunig, Kirk Mykytyn, and Matthew R. Sarkisian. 2013. 'Arborization of dendrites by developing neocortical neurons is dependent on primary cilia and type 3 adenylyl cyclase', *The Journal of neuroscience : the official journal of the Society for Neuroscience*, 33: 2626-38.
- Gundersen, G. G., S. Khawaja, and J. C. Bulinski. 1987. 'Postpolymerization detyrosination of alpha-tubulin: a mechanism for subcellular differentiation of microtubules', *J Cell Biol*, 105: 251-64.
- Guo, D. F., and K. Rahmouni. 2011. 'Molecular basis of the obesity associated with Bardet-Biedl syndrome', *Trends Endocrinol Metab*, 22: 286-93.
- Guo, J., J. M. Otis, S. K. Suci, C. Catalano, L. Xing, S. Constable, D. Wachten, S. Gupton, J. Lee, A. Lee, K. H. Blackley, T. Ptacek, J. M. Simon, S. Schurmans, G. D. Stuber, T. Caspary, and E. S. Anton. 2019. 'Primary Cilia Signaling Promotes Axonal Tract Development and Is Disrupted in Joubert Syndrome-Related Disorders Models', *Dev Cell*, 51: 759-74 e5.
- Guo, Jiami, Holden Higginbotham, Jingjun Li, Jackie Nichols, Josua Hirt, Vladimir Ghukasyan, and E. S. Anton. 2015. 'Developmental disruptions underlying brain abnormalities in ciliopathies', *Nat Commun*, 6: 7857.
- Hagemann, Anja, and Steffen Scholpp. 2012. 'The Tale of the Three Brothers – Shh, Wnt, and Fgf during Development of the Thalamus', *Frontiers in Neuroscience*, 6.
- Hallahan, Andrew R., Joel I. Pritchard, Stacey Hansen, Mark Benson, Jennifer Stoeck, Beryl A. Hatton, Thomas L. Russell, Richard G. Ellenbogen, Irwin D. Bernstein, Phillip A. Beachy, and James M. Olson. 2004. 'The SmoA1 Mouse Model Reveals That Notch Signaling Is Critical for the Growth and Survival of Sonic Hedgehog-Induced Medulloblastomas', *Cancer Research*, 64: 7794.
- Hammond, Gerald R. V., Michael J. Fischer, Karen E. Anderson, Jon Holdich, Ardita Koteci, Tamas Balla, and Robin F. Irvine. 2012. 'PI4P and PI(4,5)P₂ Are Essential But Independent Lipid Determinants of Membrane Identity', *Science*, 337: 727.
- Hammond, Gerald R. V., Matthias P. Machner, and Tamas Balla. 2014. 'A novel probe for phosphatidylinositol 4-phosphate reveals multiple pools beyond the Golgi', *Journal of Cell Biology*, 205: 113-26.
- Han, Young-Goo, Hong Joo Kim, Andrzej A. Dlugosz, David W. Ellison, Richard J. Gilbertson, and Arturo Alvarez-Buylla. 2009. 'Dual and opposing roles of primary cilia in medulloblastoma development', *Nature Medicine*, 15: 1062-65.
- Haycraft, C. J., B. Banizs, Y. Aydin-Son, Q. Zhang, E. J. Michaud, and B. K. Yoder. 2005. 'Gli2 and Gli3 localize to cilia and require the intraflagellar transport protein polaris for processing and function', *PLoS Genet*, 1: e53.
- Hazen, Virginia, Madeline Andrews, L. Umans, E. Bryan Crenshaw, An Zwijsen, and S. J. Butler. 2012. 'BMP receptor-activated Smads confer diverse functions during the development of the dorsal spinal cord', *Dev Biol*, 367: 216-27.

- He, K., X. Ma, T. Xu, Y. Li, A. Hodge, Q. Zhang, J. Torline, Y. Huang, J. Zhao, K. Ling, and J. Hu. 2018. 'Axoneme polyglutamylation regulated by Joubert syndrome protein ARL13B controls ciliary targeting of signaling molecules', *Nat Commun*, 9: 3310.
- Heydemann, Ahlke, Linh-Chi Nguyen, and E. Bryan Crenshaw Iii. 2001. 'Regulatory regions from the Brn4 promoter direct LACZ expression to the developing forebrain and neural tube', *Developmental Brain Research*, 128: 83-90.
- Higginbotham, H., T. Y. Eom, L. E. Mariani, A. Bachleda, J. Hirt, V. Gukassyan, C. L. Cusack, C. Lai, T. Caspary, and E. S. Anton. 2012a. 'Arl13b in primary cilia regulates the migration and placement of interneurons in the developing cerebral cortex', *Dev Cell*, 23: 925-38.
- Higginbotham, Holden, Tae-yeon Eom, Laura E. Mariani, Amelia Bachleda, Joshua Hirt, Vladimir Gukassyan, Corey L. Cusack, Cary Lai, Tamara Caspary, and E.S. Anton. 2012b. 'Arl13b in Primary Cilia Regulates the Migration and Placement of Interneurons in the Developing Cerebral Cortex', *Dev Cell*, 23: 925-38.
- Higginbotham, Holden, Jiami Guo, Yukako Yokota, Nicole L Umberger, Chen-Ying Su, Jingjun Li, Nisha Verma, Joshua Hirt, Vladimir Ghukasyan, Tamara Caspary, and E S Anton. 2013. 'Arl13b-regulated cilia activities are essential for polarized radial glial scaffold formation.', *Nature neuroscience*, 16: 1000-7.
- Hildebrandt, Friedhelm, Thomas Benzing, and Nicholas Katsanis. 2011. 'Ciliopathies', *The New England journal of medicine*, 364: 1533-43.
- Hoon, Jing-Ling, Wai-Keung Wong, and Cheng-Gee Koh. 2012. 'Functions and regulation of circular dorsal ruffles.', *Molecular and cellular biology*, 32: 4246-57.
- Hopp, Katharina, Christina M. Heyer, Cynthia J. Hommerding, Susan A. Henke, Jamie L. Sundsbak, Shail Patel, Priyanka Patel, Mark B. Consugar, Peter G. Czarnecki, Troy J. Gliem, Vicente E. Torres, Sandro Rossetti, and Peter C. Harris. 2011. 'B9D1 is revealed as a novel Meckel syndrome (MKS) gene by targeted exon-enriched next-generation sequencing and deletion analysis', *Human Molecular Genetics*, 20: 2524-34.
- Horner, V. L., and T. Caspary. 2011. 'Disrupted dorsal neural tube BMP signaling in the cilia mutant Arl13b hnn stems from abnormal Shh signaling', *Dev Biol*, 355: 43-54.
- Huangfu, D., and K. V. Anderson. 2005. 'Cilia and Hedgehog responsiveness in the mouse', *Proc Natl Acad Sci U S A*, 102: 11325-30.
- Huangfu, D., A. Liu, A. S. Rakeman, N. S. Murcia, L. Niswander, and K. V. Anderson. 2003. 'Hedgehog signalling in the mouse requires intraflagellar transport proteins', *Nature*, 426: 83-7.
- Humbert, M. C., K. Weihbrecht, C. C. Searby, Y. Li, R. M. Pope, V. C. Sheffield, and S. Seo. 2012. 'ARL13B, PDE6D, and CEP164 form a functional network for INPP5E ciliary targeting', *Proc Natl Acad Sci U S A*, 109: 19691-6.
- Ikegami, K., M. Mukai, J. Tsuchida, R. L. Heier, G. R. Macgregor, and M. Setou. 2006. 'TTLL7 is a mammalian beta-tubulin polyglutamylase required for growth of MAP2-positive neurites', *J Biol Chem*, 281: 30707-16.
- Ingham, P. W., and A. P. McMahon. 2001. 'Hedgehog signaling in animal development: paradigms and principles', *Genes Dev*, 15: 3059-87.
- Ishikawa, H., and W. F. Marshall. 2017. 'Intraflagellar Transport and Ciliary Dynamics', *Cold Spring Harb Perspect Biol*, 9.
- Ishikawa, Takashi. 2017. 'Axoneme Structure from Motile Cilia', *Cold Spring Harbor Perspectives in Biology*, 9: a028076.

- Ivanova, A. A., T. Caspary, N. T. Seyfried, D. M. Duong, A. B. West, Z. Liu, and R. A. Kahn. 2017. 'Biochemical characterization of purified mammalian ARL13B protein indicates that it is an atypical GTPase and ARL3 guanine nucleotide exchange factor (GEF)', *J Biol Chem*, 292: 11091-108.
- Janke, C., and M. Kneussel. 2010. 'Tubulin post-translational modifications: encoding functions on the neuronal microtubule cytoskeleton', *Trends Neurosci*, 33: 362-72.
- Jbabdi, Saad, and Heidi Johansen-Berg. 2011. 'Tractography: where do we go from here?', *Brain connectivity*, 1: 169-83.
- Jessell, T. M. 2000. 'Neuronal specification in the spinal cord: inductive signals and transcriptional codes', *Nat Rev Genet*, 1: 20-9.
- Jiang, Si-Tse, Yuan-Yow Chiou, Ellian Wang, Yi-Lin Chien, Hua-Hui Ho, Fang-Ju Tsai, Chun-Yu Lin, Shu-Ping Tsai, and Hung Li. 2009. 'Essential role of nephrocystin in photoreceptor intraflagellar transport in mouse', *Human Molecular Genetics*, 18: 1566-77.
- Kenney, A. M., and D. H. Rowitch. 2000. 'Sonic hedgehog promotes G(1) cyclin expression and sustained cell cycle progression in mammalian neuronal precursors', *Molecular and cellular biology*, 20: 9055-67.
- Kim, H., H. Xu, Q. Yao, W. Li, Q. Huang, P. Outeda, V. Cebotaru, M. Chiaravalli, A. Boletta, K. Piontek, G. G. Germino, E. J. Weinman, T. Watnick, and F. Qian. 2014. 'Ciliary membrane proteins traffic through the Golgi via a Rabep1/GGA1/Arl3-dependent mechanism', *Nat Commun*, 5: 5482.
- Kobayashi, Tetsuo, and Brian D. Dynlacht. 2011. 'Regulating the transition from centriole to basal body', *J Cell Biol*, 193: 435-44.
- Komada, Munekazu. 2012. 'Sonic hedgehog signaling coordinates the proliferation and differentiation of neural stem/progenitor cells by regulating cell cycle kinetics during development of the neocortex', *Congenital Anomalies*, 52: 72-77.
- Konishi, Yoshiyuki, and Mitsutoshi Setou. 2009. 'Tubulin tyrosination navigates the kinesin-1 motor domain to axons', *Nature neuroscience*, 12: 559-67.
- Kumamoto, Natsuko, Yan Gu, Jia Wang, Stephen Janoschka, Ken-Ichi Takemaru, Joel Levine, and Shaoyu Ge. 2012. 'A role for primary cilia in glutamatergic synaptic integration of adult-born neurons', *Nature neuroscience*, 15: 399-S1.
- Lan, Yu, and Rulang Jiang. 2009. 'Sonic hedgehog signaling regulates reciprocal epithelial-mesenchymal interactions controlling palatal outgrowth', *Development (Cambridge, England)*, 136: 1387-96.
- Lancaster, Madeline A., Dipika J. Gopal, Joon Kim, Sahar N. Saleem, Jennifer L. Silhavy, Carrie M. Louie, Bryan E. Thacker, Yuko Williams, Maha S. Zaki, and Joseph G. Gleeson. 2011. 'Defective Wnt-dependent cerebellar midline fusion in a mouse model of Joubert syndrome', *Nature Medicine*, 17: 726-31.
- Larkins, C. E., G. D. Aviles, M. P. East, R. A. Kahn, and T. Caspary. 2011. 'Arl13b regulates ciliogenesis and the dynamic localization of Shh signaling proteins', *Mol Biol Cell*, 22: 4694-703.
- Lee, J. E., J. L. Silhavy, M. S. Zaki, J. Schroth, S. L. Bielas, S. E. Marsh, J. Olvera, F. Brancati, M. Iannicelli, K. Ikegami, A. M. Schlossman, B. Merriman, T. Attie-Bitach, C. V. Logan, I. A. Glass, A. Cluckey, C. M. Louie, J. H. Lee, H. R. Raynes, I. Rapin, I. P. Castroviejo, M. Setou, C. Barbot, E. Boltshauser, S. F. Nelson, F. Hildebrandt, C. A. Johnson, D. A.

- Doherty, E. M. Valente, and J. G. Gleeson. 2012. 'CEP41 is mutated in Joubert syndrome and is required for tubulin glutamylation at the cilium', *Nat Genet*, 44: 193-9.
- Lee, J. H., and J. G. Gleeson. 2010. 'The role of primary cilia in neuronal function', *Neurobiol Dis*, 38: 167-72.
- Lepelletier, Léa, Sébastien D. Langlois, Christopher B. Kent, Kristy Welshhans, Steves Morin, Gary J. Bassell, Patricia T. Yam, and Frédéric Charron. 2017. 'Sonic Hedgehog Guides Axons via Zipcode Binding Protein 1-Mediated Local Translation', *The Journal of Neuroscience*, 37: 1685-95.
- Lipinski, Robert J., Chihwa Song, Kathleen K. Sulik, Joshua L. Everson, Jerry J. Gipp, Dong Yan, Wade Bushman, and Ian J. Rowland. 2010. 'Cleft lip and palate results from Hedgehog signaling antagonism in the mouse: Phenotypic characterization and clinical implications', *Birth defects research. Part A, Clinical and molecular teratology*, 88: 232-40.
- Liu, A., B. Wang, and L. A. Niswander. 2005. 'Mouse intraflagellar transport proteins regulate both the activator and repressor functions of Gli transcription factors', *Development*, 132: 3103-11.
- Long, Fanxin, Xiaoyan M. Zhang, Seth Karp, Yingzi Yang, and Andrew P. McMahon. 2001. 'Genetic manipulation of hedgehog signaling in the endochondral skeleton reveals a direct role in the regulation of chondrocyte proliferation', *Development*, 128: 5099.
- Magiera, M. M., S. Bodakuntla, J. Ziak, S. Lacomme, P. Marques Sousa, S. Leboucher, T. J. Hausrat, C. Bosc, A. Andrieux, M. Kneussel, M. Landry, A. Calas, M. Balastik, and C. Janke. 2018. 'Excessive tubulin polyglutamylation causes neurodegeneration and perturbs neuronal transport', *EMBO J*, 37.
- Magiera, Maria M., Puja Singh, Sudarshan Gadadhar, and Carsten Janke. 2018. 'Tubulin Posttranslational Modifications and Emerging Links to Human Disease', *Cell*, 173: 1323-27.
- Mandelkow, Eckhard, and Eva-Maria Mandelkow. 1994. 'Microtubule structure', *Current Opinion in Structural Biology*, 4: 171-79.
- Mariani, L. E., M. F. Bijlsma, A. I. Ivanova, S. K. Suci, R. A. Kahn, and T. Caspary. 2016. 'Arl13b regulates Shh signaling from both inside and outside the cilium', *Mol Biol Cell*.
- Martínez, Constanza, Víctor Hugo Cornejo, Pablo Lois, Tammy Ellis, Natalia P. Solis, Brandon J. Wainwright, and Verónica Palma. 2013. 'Proliferation of Murine Midbrain Neural Stem Cells Depends upon an Endogenous Sonic Hedgehog (Shh) Source', *PLoS One*, 8: e65818.
- May, Scott R, Amir M Ashique, Mattias Karlen, Baolin Wang, Yiguo Shen, Kostantinos Zerbali, Jeremy Reiter, Johan Ericson, and Andrew S Peterson. 2005. 'Loss of the retrograde motor for IFT disrupts localization of Smo to cilia and prevents the expression of both activator and repressor functions of Gli', *Dev Biol*, 287: 378-89.
- Miertzschke, M., C. Koerner, M. Spoerner, and A. Wittinghofer. 2014. 'Structural insights into the small G-protein Arl13B and implications for Joubert syndrome', *Biochem J*, 457: 301-11.
- Mitchison, T.J. 1993. 'Localization of an exchangeable GTP binding site at the plus end of microtubules', *Science*, 261: 1044-47.
- Motoyama, Jun, Ljiljana Milenkovic, Mizuho Iwama, Yayoi Shikata, Matthew P. Scott, and Chichung Hui. 2003. 'Differential requirement for Gli2 and Gli3 in ventral neural cell fate specification', *Dev Biol*, 259: 150-61.

- Mukhopadhyay, Saikat, Hemant B. Badgandi, Sun-hee Hwang, Bandarigoda Somatilaka, Issei S. Shimada, and Kasturi Pal. 2017. 'Trafficking to the primary cilium membrane', *Mol Biol Cell*, 28: 233-39.
- Mukhopadhyay, Saikat, Xiaohui Wen, Navneet Ratti, Alexander Loktev, Linda Rangell, Suzie J Scales, and Peter K Jackson. 2013. 'The Ciliary G-Protein-Coupled Receptor Gpr161 Negatively Regulates the Sonic Hedgehog Pathway via cAMP Signaling', *Cell*, 152: 210-23.
- Nachury, M. V., A. V. Loktev, Q. Zhang, C. J. Westlake, J. Peranen, A. Merdes, D. C. Slusarski, R. H. Scheller, J. F. Bazan, V. C. Sheffield, and P. K. Jackson. 2007. 'A core complex of BBS proteins cooperates with the GTPase Rab8 to promote ciliary membrane biogenesis', *Cell*, 129: 1201-13.
- Nachury, M. V., E. S. Seeley, and H. Jin. 2010. 'Trafficking to the ciliary membrane: how to get across the periciliary diffusion barrier?', *Annu Rev Cell Dev Biol*, 26: 59-87.
- Nguyen, Vien, Khalida Sabeur, Emin Maltepe, Kurosh Ameri, Omer Bayraktar, and David H. Rowitch. 2018. 'Sonic Hedgehog Agonist Protects Against Complex Neonatal Cerebellar Injury', *Cerebellum (London, England)*, 17: 213-27.
- Nogales, Eva, Michael Whittaker, Ronald A. Milligan, and Kenneth H. Downing. 1999. 'High-Resolution Model of the Microtubule', *Cell*, 96: 79-88.
- Nolan-Stevaux, Olivier, Janet Lau, Morgan L. Truitt, Gerald C. Chu, Matthias Hebrok, Martin E. Fernández-Zapico, and Douglas Hanahan. 2009. 'GLI1 is regulated through Smoothed-independent mechanisms in neoplastic pancreatic ducts and mediates PDAC cell survival and transformation', *Genes Dev*, 23: 24-36.
- O'Hagan, R., B. P. Piasecki, M. Silva, P. Phirke, K. C. Nguyen, D. H. Hall, P. Swoboda, and M. M. Barr. 2011. 'The tubulin deglutamylase CCPP-1 regulates the function and stability of sensory cilia in *C. elegans*', *Curr Biol*, 21: 1685-94.
- Okada, A., F. Charron, S. Morin, D. S. Shin, K. Wong, P. J. Fabre, M. Tessier-Lavigne, and S. K. McConnell. 2006. 'Boc is a receptor for sonic hedgehog in the guidance of commissural axons', *Nature*, 444: 369-73.
- Onimaru, Hiroshi, Yuko Kumagawa, and Ikuo Homma. 2006. 'Respiration-Related Rhythmic Activity in the Rostral Medulla of Newborn Rats', *Journal of Neurophysiology*, 96: 55-61.
- Otto, E. A., K. Tory, M. Attanasio, W. Zhou, M. Chaki, Y. Paruchuri, E. L. Wise, M. T. F. Wolf, B. Utsch, C. Becker, G. Nürnberg, P. Nürnberg, A. Nayir, S. Saunier, C. Antignac, and F. Hildebrandt. 2009. 'Hypomorphic mutations in meckelin (MKS3/TMEM67) cause nephronophthisis with liver fibrosis (NPHP11)', *Journal of medical genetics*, 46: 663.
- Parisi, M. A. 2019. 'The molecular genetics of Joubert syndrome and related ciliopathies: The challenges of genetic and phenotypic heterogeneity', *Transl Sci Rare Dis*, 4: 25-49.
- Parisi, M. A., D. Doherty, P. F. Chance, and I. A. Glass. 2007. 'Joubert syndrome (and related disorders) (OMIM 213300)', *Eur J Hum Genet*, 15: 511-21.
- Pasqualato, Sebastiano, Louis Renault, and Jacqueline Cherfils. 2002. 'Arf, Arl, Arp and Sar proteins: a family of GTP-binding proteins with a structural device for 'front-back' communication', *EMBO reports*, 3: 1035-41.
- Pastrana, Erika, Li-Chun Cheng, and Fiona Doetsch. 2009. 'Simultaneous prospective purification of adult subventricular zone neural stem cells and their progeny', *Proceedings of the National Academy of Sciences*, 106: 6387-92.

- Pathak, Narendra, Tomoko Obara, Steve Mangos, Yan Liu, and Iain A. Drummond. 2007. 'The zebrafish fleer gene encodes an essential regulator of cilia tubulin polyglutamylation', *Mol Biol Cell*, 18: 4353-64.
- Pazour, G. J., C. G. Wilkerson, and G. B. Witman. 1998. 'A dynein light chain is essential for the retrograde particle movement of intraflagellar transport (IFT)', *J Cell Biol*, 141: 979-92.
- Pedersen, Lotte B., Johanne B. Mogensen, and Søren T. Christensen. 2016. 'Endocytic Control of Cellular Signaling at the Primary Cilium', *Trends in Biochemical Sciences*, 41: 784-97.
- Pedersen, Lotte B., Panteleimon Rompolas, Søren T. Christensen, Joel L. Rosenbaum, and Stephen M. King. 2007. 'The lissencephaly protein Lis1 is present in motile mammalian cilia and requires outer arm dynein for targeting to *Chlamydomonas* flagella', *Journal of cell science*, 120: 858-67.
- Peng, Jimmy, Pierre J. Fabre, Tiphaine Dolique, Shannon M. Swikert, Laëtitia Kermasson, Tomomi Shimogori, and Frédéric Charron. 2018. 'Sonic Hedgehog Is a Remotely Produced Cue that Controls Axon Guidance Trans-axonally at a Midline Choice Point', *Neuron*, 97: 326-40.e4.
- Persson, M., D. Stamatakis, P. te Welscher, E. Andersson, J. Bose, U. Ruther, J. Ericson, and J. Briscoe. 2002. 'Dorsal-ventral patterning of the spinal cord requires Gli3 transcriptional repressor activity', *Genes Dev*, 16: 2865-78.
- Petralia, R. S., Y. X. Wang, M. P. Mattson, and P. J. Yao. 2012. 'Subcellular distribution of patched and smoothed in the cerebellar neurons', *Cerebellum*, 11: 972-81.
- Poretti, A., E. Boltshauser, T. Loenneker, E. M. Valente, F. Brancati, K. Il'Yasov, and Thierry A G M Huisman. 2007. 'Diffusion tensor imaging in Joubert syndrome', *American Journal of Neuroradiology*, 28: 1929-33.
- Poretti, A., T A G M Huisman, I. Scheer, and E Boltshauser. 2011a. 'Joubert Syndrome and Related Disorders: Spectrum of Neuroimaging Findings in 75 Patients', *American Journal of Neuroradiology*, 32: 1459-63.
- Poretti, A., T. A. Huisman, I. Scheer, and E. Boltshauser. 2011b. 'Joubert syndrome and related disorders: spectrum of neuroimaging findings in 75 patients', *AJNR Am J Neuroradiol*, 32: 1459-63.
- Qin, J., Y. Lin, R. X. Norman, H. W. Ko, and J. T. Eggenschwiler. 2011. 'Intraflagellar transport protein 122 antagonizes Sonic Hedgehog signaling and controls ciliary localization of pathway components', *Proc Natl Acad Sci U S A*, 108: 1456-61.
- Raffel, C., R. B. Jenkins, L. Frederick, D. Hebrink, B. Alderete, D. W. Fults, and C. D. James. 1997. 'Sporadic medulloblastomas contain PTCH mutations', *Cancer Res*, 57: 842-5.
- Rafiullah, R., A. B. Long, A. A. Ivanova, H. Ali, S. Berkel, G. Mustafa, N. Paramasivam, M. Schlesner, S. Wiemann, R. C. Wade, E. Bolthausen, M. Blum, R. A. Kahn, T. Caspary, and G. A. Rappold. 2017. 'A novel homozygous ARL13B variant in patients with Joubert syndrome impairs its guanine nucleotide-exchange factor activity', *Eur J Hum Genet*, 25: 1324-34.
- Ramsbottom, Simon A., Peter E. Thelwall, Katrina M. Wood, Gavin J. Clowry, Laura A. Devlin, Flora Silbermann, Helena L. Spiewak, Shirlee Shril, Elisa Molinari, Friedhelm Hildebrandt, Meral Gunay-Aygün, Sophie Saunier, Heather J. Cordell, John A. Sayer, and Colin G. Miles. 2020. 'Mouse genetics reveals Barttin as a genetic modifier of Joubert syndrome', *Proceedings of the National Academy of Sciences*, 117: 1113.

- Reed, Nathan A., Dawen Cai, T. Lynne Blasius, Gloria T. Jih, Edgar Meyhofer, Jacek Gaertig, and Kristen J. Verhey. 2006. 'Microtubule Acetylation Promotes Kinesin-1 Binding and Transport', *Current Biology*, 16: 2166-72.
- Reiner, O., and T. Sapir. 1998. 'Abnormal cortical development; towards elucidation of the LIS1 gene product function (review)', *Int J Mol Med*, 1: 849-53.
- Roberson, Elle C., William E. Dowdle, Aysegul Ozanturk, Francesc R. Garcia-Gonzalo, Chunmei Li, Jan Halbritter, Nadia Elkhartoufi, Jonathan D. Porath, Heidi Cope, Allison Ashley-Koch, Simon Gregory, Sophie Thomas, John A. Sayer, Sophie Saunier, Edgar A. Otto, Nicholas Katsanis, Erica E. Davis, Tania Attié-Bitach, Friedhelm Hildebrandt, Michel R. Leroux, and Jeremy F. Reiter. 2015. 'TMEM231, mutated in orofacioidigital and Meckel syndromes, organizes the ciliary transition zone', *J Cell Biol*, 209: 129-42.
- Rocha, Cecilia, Laura Papon, Wulfran Cacheux, Patricia Marques Sousa, Valeria Lascano, Olivia Tort, Tiziana Giordano, Sophie Vacher, Benedicte Lemmers, Pascale Mariani, Didier Meseure, Jan Paul Medema, Ivan Bièche, Michael Hahne, and Carsten Janke. 2014. 'Tubulin glycosylases are required for primary cilia, control of cell proliferation and tumor development in colon', *The EMBO journal*, 33: 2247-60.
- Rohatgi, R., L. Milenkovic, and M. P. Scott. 2007. 'Patched1 regulates hedgehog signaling at the primary cilium', *Science*, 317: 372-6.
- Romano, S., N. Boddaert, I. Desguerre, L. Hubert, R. Salomon, D. Seidenwurm, N. Bahi-Buisson, R. Nabbout, P. Sonigo, S. Lyonnet, F. Brunelle, A. Munnich, and P. de Lonlay. 2006. 'Molar tooth sign and superior vermian dysplasia: a radiological, clinical, and genetic study', *Neuropediatrics*, 37: 42-5.
- Rosenbaum, J. L., and G. B. Witman. 2002. 'Intraflagellar transport', *Nat Rev Mol Cell Biol*, 3: 813-25.
- Sanchez-Arrones, L., F. Nieto-Lopez, C. Sanchez-Camacho, M. I. Carreres, E. Herrera, A. Okada, and P. Bovolenta. 2013. 'Shh/Boc signaling is required for sustained generation of ipsilateral projecting ganglion cells in the mouse retina', *J Neurosci*, 33: 8596-607.
- Satir, Peter, and Søren Tvorup Christensen. 2007. 'Overview of Structure and Function of Mammalian Cilia', *Annual Review of Physiology*, 69: 377-400.
- Schrack, J. J., P. Vogel, A. Abuin, B. Hampton, and D. S. Rice. 2006. 'ADP-ribosylation factor-like 3 is involved in kidney and photoreceptor development', *Am J Pathol*, 168: 1288-98.
- Schwab, M. H., A. Bartholomae, B. Heimrich, D. Feldmeyer, S. Druffel-Augustin, S. Goebbels, F. J. Naya, S. Zhao, M. Frotscher, M. J. Tsai, and K. A. Nave. 2000. 'Neuronal basic helix-loop-helix proteins (NEX and BETA2/Neuro D) regulate terminal granule cell differentiation in the hippocampus', *J Neurosci*, 20: 3714-24.
- Shaheen, Ranad, Katarzyna Szymanska, Basudha Basu, Nisha Patel, Nour Ewida, Eissa Fageih, Amal Al Hashem, Nada Derar, Hadeel Alsharif, and Mohammed A Aldahmesh. 2016. 'Characterizing the morbid genome of ciliopathies', *Genome Biol*, 17: 242.
- Sheen, Volney L. 2012. 'Periventricular Heterotopia: Shuttling of Proteins through Vesicles and Actin in Cortical Development and Disease', *Scientifica*, 2012: 480129-29.
- Sirajuddin, Minhajuddin, Luke M. Rice, and Ronald D. Vale. 2014. 'Regulation of microtubule motors by tubulin isotypes and post-translational modifications', *Nature cell biology*, 16: 335-44.
- Srour, Myriam, Fadi F. Hamdan, Jeremy A. Schwartzentruber, Lysanne Patry, Luis H. Ospina, Michael I. Shevell, Valérie Désilets, Sylvia Dobrzeniecka, Géraldine Mathonnet, Emmanuelle Lemyre, Christine Massicotte, Damian Labuda, Dina Amrom, Eva

- Andermann, Guillaume Sébire, Bruno Maranda, Forge Canada Consortium, Guy A. Rouleau, Jacek Majewski, and Jacques L. Michaud. 2012. 'Mutations in *TMEM231* cause Joubert syndrome in French Canadians', *Journal of medical genetics*, 49: 636.
- Stevens, M. C., A. H. Cameron, K. R. Muir, S. E. Parkes, H. Reid, and H. Whitwell. 1991a. 'Descriptive epidemiology of primary central nervous system tumours in children: a population-based study', *Clin Oncol (R Coll Radiol)*, 3: 323-9.
- Stevens, M. C. G., A. H. Cameron, K. R. Muir, S. E. Parkes, H. Reid, and H. Whitwell. 1991b. 'Descriptive epidemiology of primary central nervous system tumours in children: A population-based study', *Clinical Oncology*, 3: 323-29.
- Stottmann, R. W., P. V. Tran, A. Turbe-Doan, and D. R. Beier. 2009. 'Ttc21b is required to restrict sonic hedgehog activity in the developing mouse forebrain', *Dev Biol*, 335: 166-78.
- Su, C.-Y., S. N. Bay, L. E. Mariani, M. J. Hillman, and T. Caspary. 2012a. 'Temporal deletion of *Arl13b* reveals that a mispatterned neural tube corrects cell fate over time', *Development*, 139: 4062-71.
- Su, Chen-Ying, Sarah N. Bay, Laura E. Mariani, Michael J. Hillman, and Tamara Caspary. 2012b. 'Temporal deletion of *Arl13b* reveals that a mispatterned neural tube corrects cell fate over time', *Development (Cambridge, England)*, 139: 4062-71.
- Sun, Z., A. Amsterdam, G. J. Pazour, D. G. Cole, M. S. Miller, and N. Hopkins. 2004. 'A genetic screen in zebrafish identifies cilia genes as a principal cause of cystic kidney', *Development*, 131: 4085-93.
- Tadenev, Abigail L. D., Heather M. Kulaga, Helen L. May-Simera, Matthew W. Kelley, Nicholas Katsanis, and Randall R. Reed. 2011. 'Loss of Bardet-Biedl syndrome protein-8 (BBS8) perturbs olfactory function, protein localization, and axon targeting', *Proc Natl Acad Sci U S A*, 108: 10320-25.
- Taschner, Michael, and Esben Lorentzen. 2016. 'The Intraflagellar Transport Machinery', *Cold Spring Harbor Perspectives in Biology*, 8: a028092.
- Theiss, C., M. Napirei, and K. Meller. 2005. 'Impairment of anterograde and retrograde neurofilament transport after anti-kinesin and anti-dynein antibody microinjection in chicken dorsal root ganglia', *Eur J Cell Biol*, 84: 29-43.
- Thomas, Sophie, Vincent Cantagrel, Laura Mariani, Valérie Serre, Ji-Eun Lee, Nadia Elkhartoufi, Pascale de Lonlay, Isabelle Desguerre, Arnold Munnich, Nathalie Boddart, Stanislas Lyonnet, Michel Vekemans, Steven N. Lisgo, Tamara Caspary, Joseph Gleeson, and Tania Attié-Bitach. 2015. 'Identification of a novel *ARL13B* variant in a Joubert syndrome-affected patient with retinal impairment and obesity', *European Journal of Human Genetics*, 23: 621-27.
- Toro-Tapia, Gabriela, and Raman M. Das. 2020. 'Primary cilium remodeling mediates a cell signaling switch in differentiating neurons', *Science Advances*, 6: eabb0601.
- Treweek, Jennifer B., Ken Y. Chan, Nicholas C. Flytzanis, Bin Yang, Benjamin E. Deverman, Alon Greenbaum, Antti Lignell, Cheng Xiao, Long Cai, Mark S. Ladinsky, Pamela J. Bjorkman, Charless C. Fowlkes, and Viviana Gradinaru. 2015. 'Whole-body tissue stabilization and selective extractions via tissue-hydrogel hybrids for high-resolution intact circuit mapping and phenotyping', *Nature Protocols*, 10: 1860-96.
- Uzquiano, Ana, Carmen Cifuentes-Diaz, Ammar Jabali, Delfina M. Romero, Anne Houllier, Florent Dingli, Camille Maillard, Anne Boland, Jean-François Deleuze, Damarys Loew,

- Grazia M. S. Mancini, Nadia Bahi-Buisson, Julia Ladewig, and Fiona Francis. 2019. 'Mutations in the Heterotopia Gene *Eml1* Severely Disrupt the Formation of Primary Cilia', *Cell Reports*, 28: 1596-611.e10.
- Vaisse, Christian, Jeremy F. Reiter, and Nicolas F. Berbari. 2017. 'Cilia and Obesity', *Cold Spring Harbor Perspectives in Biology*, 9: a028217.
- Valenstein, Max L., and Antonina Roll-Mecak. 2016. 'Graded Control of Microtubule Severing by Tubulin Glutamylation', *Cell*, 164: 911-21.
- Valente, E. M., R. O. Rosti, E. Gibbs, and J. G. Gleeson. 2014. 'Primary cilia in neurodevelopmental disorders', *Nat Rev Neurol*, 10: 27-36.
- Valente, Enza Maria, Francesco Brancati, and Bruno Dallapiccola. 2008. 'Genotypes and phenotypes of Joubert syndrome and related disorders', *European Journal of Medical Genetics*, 51: 1-23.
- Valente, Enza Maria, Clare V. Logan, Soumaya Mougou-Zerelli, Jeong Ho Lee, Jennifer L. Silhavy, Francesco Brancati, Miriam Iannicelli, Lorena Travaglini, Sveva Romani, Barbara Illi, Matthew Adams, Katarzyna Szymanska, Annalisa Mazzotta, Ji Eun Lee, Jerlyn C. Tolentino, Dominika Swistun, Carmelo D. Salpietro, Carmelo Fede, Stacey Gabriel, Carsten Russ, Kristian Cibulskis, Carrie Sougnez, Friedhelm Hildebrandt, Edgar A. Otto, Susanne Held, Bill H. Diplas, Erica E. Davis, Mario Mikula, Charles M. Strom, Bruria Ben-Zeev, Dorit Lev, Tally Lerman Sagie, Marina Michelson, Yuval Yaron, Amanda Krause, Eugen Boltshauser, Nadia Elkhartoufi, Joelle Roume, Stavit Shalev, Arnold Munnich, Sophie Saunier, Chris Inglehearn, Ali Saad, Adila Alkindy, Sophie Thomas, Michel Vekemans, Bruno Dallapiccola, Nicholas Katsanis, Colin A. Johnson, Tania Attié-Bitach, and Joseph G. Gleeson. 2010. 'Mutations in TMEM216 perturb ciliogenesis and cause Joubert, Meckel and related syndromes', *Nature Genetics*, 42: 619-25.
- Wang, Juan, and Maureen M. Barr. 2018. 'Cell-cell communication via ciliary extracellular vesicles: clues from model systems', *Essays in Biochemistry*, 62: 205-13.
- Wang, Juan, Malan Silva, Leonard A Haas, Natalia S Morsci, Ken C Q. Nguyen, David H Hall, and Maureen M Barr. 2014. '*C. elegans* Ciliated Sensory Neurons Release Extracellular Vesicles that Function in Animal Communication', *Current Biology*, 24: 519-25.
- Wang, V. Y., and H. Y. Zoghbi. 2001. 'Genetic regulation of cerebellar development', *Nat Rev Neurosci*, 2: 484-91.
- Ward, Heather H., Ursa Brown-Glaberman, Jing Wang, Yoshiko Morita, Seth L. Alper, Edward J. Bedrick, Vincent H. Gattone, Dusanka Deretic, and Angela Wandinger-Ness. 2011. 'A conserved signal and GTPase complex are required for the ciliary transport of polycystin-1', *Mol Biol Cell*, 22: 3289-305.
- Waters, A. M., and P. L. Beales. 2011. 'Ciliopathies: an expanding disease spectrum', *Pediatr Nephrol*, 26: 1039-56.
- Webster, D R, G G Gundersen, J C Bulinski, and G G Borisy. 1987. 'Assembly and turnover of deetyrosinated tubulin in vivo', *Journal of Cell Biology*, 105: 265-76.
- Wechsler-Reya, Robert J., and Matthew P. Scott. 1999. 'Control of Neuronal Precursor Proliferation in the Cerebellum by Sonic Hedgehog', *Neuron*, 22: 103-14.
- Wen, X., C. K. Lai, M. Evangelista, J. A. Hongo, F. J. de Sauvage, and S. J. Scales. 2010. 'Kinetics of hedgehog-dependent full-length Gli3 accumulation in primary cilia and subsequent degradation', *Mol Cell Biol*, 30: 1910-22.

- Wheatley, D. N., A. M. Wang, and G. E. Strugnell. 1996. 'Expression of primary cilia in mammalian cells', *Cell Biol Int*, 20: 73-81.
- Willaredt, Marc A., Kerstin Hasenpusch-Theil, Humphrey A. R. Gardner, Igor Kitanovic, Vera C. Hirschfeld-Warneken, Christian P. Gojak, Karin Gorgas, C. Lulu Bradford, Joachim Spatz, Stefan Wöfl, Thomas Theil, and Kerry L. Tucker. 2008. 'A Crucial Role for Primary Cilia in Cortical Morphogenesis', *The Journal of Neuroscience*, 28: 12887-900.
- Wloga, Dorota, Danielle M. Webster, Krzysztof Rogowski, Marie-Hélène Bré, Nicolette Levilliers, Maria Jerka-Dziadosz, Carsten Janke, Scott T. Dougan, and Jacek Gaertig. 2009. 'TTLL3 Is a Tubulin Glycine Ligase that Regulates the Assembly of Cilia', *Dev Cell*, 16: 867-76.
- Wong, Sunny Y., Allen D. Seol, Po-Lin So, Alexandre N. Ermilov, Christopher K. Bichakjian, Ervin H. Epstein, Jr., Andrzej A. Dlugosz, and Jeremy F. Reiter. 2009. 'Primary cilia can both mediate and suppress Hedgehog pathway-dependent tumorigenesis', *Nature Medicine*, 15: 1055-61.
- Wu, Xu, John Walker, Jie Zhang, Sheng Ding, and Peter G. Schultz. 2004. 'Purmorphamine Induces Osteogenesis by Activation of the Hedgehog Signaling Pathway', *Chemistry & Biology*, 11: 1229-38.
- Yachnis, A T, and L B Rorke. 1999. 'Neuropathology of Joubert syndrome.', *Journal of child neurology*, 14: 655-9; discussion 69-72.
- Yam, P. T., C. B. Kent, S. Morin, W. T. Farmer, R. Alchini, L. Lepelletier, D. R. Colman, M. Tessier-Lavigne, A. E. Fournier, and F. Charron. 2012. '14-3-3 proteins regulate a cell-intrinsic switch from sonic hedgehog-mediated commissural axon attraction to repulsion after midline crossing', *Neuron*, 76: 735-49.
- Yam, P. T., S. D. Langlois, S. Morin, and F. Charron. 2009. 'Sonic hedgehog guides axons through a noncanonical, Src-family-kinase-dependent signaling pathway', *Neuron*, 62: 349-62.
- Yogev, S., R. Cooper, R. Fetter, M. Horowitz, and K. Shen. 2016. 'Microtubule Organization Determines Axonal Transport Dynamics', *Neuron*, 92: 449-60.
- Zhang, X. M., M. Ramalho-Santos, and A. P. McMahon. 2001. 'Smoothed mutants reveal redundant roles for Shh and Ihh signaling including regulation of L/R symmetry by the mouse node', *Cell*, 106: 781-92.
- Zhu, J., H. T. Wang, Y. R. Chen, L. Y. Yan, Y. Y. Han, L. Y. Liu, Y. Cao, Z. Z. Liu, and H. A. Xu. 2020. 'The Joubert Syndrome Gene *arl13b* is Critical for Early Cerebellar Development in Zebrafish', *Neurosci Bull*.